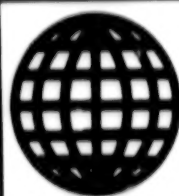


JPRS-UMS-92-016
13 November 1992



**FOREIGN
BROADCAST
INFORMATION
SERVICE**

JPRS Report

Science & Technology

***Central Eurasia:
Materials Science***

Science & Technology

Central Eurasia: Materials Science

JPRS-UMS-92-016

CONTENTS

13 November 1992

Analysis, Testing

Temperature Dependence of Breaking Stress for Molybdenum in Transition Range (Above Cold-Shortness Point) [V.F. Moiseyev, A.N. Sherban; <i>PROBLEMY PROCHNOSTI</i> , No 6, Jun 92]	1
Method of Design Calculation for Flywheel Made of Fibrous Composite with Binder [A.M. Mokeyev, S.G. Sidorov; <i>PROBLEMY PROCHNOSTI</i> , No 6, Jun 92]	1
Phase and Structural Transformations in Rhombohedral BN Under High Pressures [V.F. Britun, A.V. Kurdyumov, et al.; <i>SVERKHTVERDYIE MATERIALY</i> , No 4 (79), Jul-Aug 92]	1
Raman Scattering Spectra of Diamond Condensate Deposited From Vapor Phase Onto Diamond Powder Compacts [V.D. Andreyev, V.A. Semenov, et al.; <i>SVERKHTVERDYIE MATERIALY</i> , No 4 (79), Jul-Aug 92] ..	1
Study of Diamond Solubility in Multicomponent Metal Melts Under Thermodynamic Stability Conditions [S.A. Ivakhnenko, A.V. Andreyev, et al.; <i>SVERKHTVERDYIE MATERIALY</i> , No 4 (79), Jul-Aug 92] ...	2
Catalyst Alloys With Metastable Structure [V.V. Sobolev, V.Ya. Slobodskoy, et al.; <i>SVERKHTVERDYIE MATERIALY</i> , No 4 (79), Jul-Aug 92]	2
Effect of Point Defects on Thermal Conductivity of Diamonds [T.D. Ositinskaya, A.P. Podoba, et al.; <i>SVERKHTVERDYIE MATERIALY</i> , No 4 (79), Jul-Aug 92]	2
Geometric Parameter Behavior of Reemers From Composite 01 During Wear [G.S. Zhelezov, S.A. Singeyev; <i>SVERKHTVERDYIE MATERIALY</i> , No 4 (79), Jul-Aug 92]	3
Laws Governing the Change in Metals' Electric Resistance Due to Impurities [B.N. Aleksandrov; <i>VYSOKOCHISTYYE VESHCHESTVA</i> , No 4, Jul-Aug 92]	3
The Properties of Zinc Selenide Produced From $Zn(inf2H_3)_2$ and H_2Se [G.G. Devyatykh, V.A. Sidorov, et al.; <i>VYSOKOCHISTYYE VESHCHESTVA</i> , No 4, Jul-Aug 92]	3
Layer-by-Layer Determination of Ga in Cadmium Telluride and Cadmium-Mercury Telluride by the Atomic Absorption Method With Electrothermal Atomization [I.G. Yudelevich, N.I. Petrova, et al.; <i>VYSOKOCHISTYYE VESHCHESTVA</i> , No 4, Jul-Aug 92]	4
Chemical-Atomic Emission Analysis of High-Purity Selenium With the Use of Autoclave Dissolution of the Sample [N.V. Yerykalina, M.I. Krylova, et al.; <i>VYSOKOCHISTYYE VESHCHESTVA</i> , No 4, Jul-Aug 92]	4
An Investigation of the Distribution of Impurities in Thin ZnO Films Produced by the MOCVD Method [A.N. Moiseyev, Yu.M. Saglanskiy, et al.; <i>VYSOKOCHISTYYE VESHCHESTVA</i> , No 4, Jul-Aug 92]	5
Analysis of Low-Melting Point Metals on a Spark-Source Mass Spectrometer [A.I. Saprykin, G.G. Sikharulidze; <i>VYSOKOCHISTYYE VESHCHESTVA</i> , No 4, Jul-Aug 92]	5
Prediction of Inelastic Straining and Fracture of Laminated Composites [V.E. Vildeman, Yu.V. Sokolov, et al.; <i>MEKHANIKA KOMPOSITNYKH MATERIALOV</i> , No 3, May-Jun 92]	5
Strength and Fatigue Resistance of Fabric-Based Composites Under Combined Effect of Static Shear Stresses and Cyclical Compressive Stresses [V.A. Limonov, A.F. Razin, et al.; <i>MEKHANIKA KOMPOSITNYKH MATERIALOV</i> , No 3, May-Jun 92]	6
Effect of Plied Roving Length Difference on Fiber-Rupture Stress Realized in Organic Composite and Load-Carrying Capacity of Pressure Vessels [S.P. Yakunin, L.A. Yegorov; <i>MEKHANIKA KOMPOSITNYKH MATERIALOV</i> , No 3, May-Jun 92] ...	6
Structural Characteristics of $AlN + Y_2O_3$ Ceramics [M.A. Kuznetsova, O.A. Shevchenko, et al.; <i>POROSHKOVAYA METALLURGIYA</i> , No 8 (356), Aug 92]	7
Simulation of Fe-Zr Melts' Paramagnetic Susceptibility [O.Yu. Sidorov, O.Ye. Shlokhina, et al.; <i>METALLY</i> , No 4, Jul-Aug 92]	7

Coatings

Modification of Magnetite Films by Complexonates [Yu.I. Kuznetsov, T.I. Bardasheva; ZASHCHITA METALLOV, No 4, Jul-Aug 92]	8
A Set of Methods To Evaluate Anticorrosion Coatings for Equipment Used To Store and Transport Petroleum Products [N.N. Zakharova, G.T. Vigant, et al.; ZASHCHITA METALLOV, No 4, Jul-Aug 92]	8
The Corrosion and Protective Properties of Coating Made With an Amorphous Chromium-Phosphorus Alloy [Ye.G. Vinokurov, V.N. Kudryavtsev, et al.; ZASHCHITA METALLOV, No 4, Jul-Aug 92]	9
Producing Protective Zinc Coatings by a Programmable Pulse Current [V.A. Zabludovskiy, V.I. Kaptanovskiy, et al.; ZASHCHITA METALLOV, No 4, Jul-Aug 92]	9
Electrodeposition of Bright Tin-Lead Alloy Coatings [K.M. Tyutina, A.N. Popov, et al.; ZASHCHITA METALLOV, No 4, Jul-Aug 92]	10
Role of Diamond Ultrasonic Hardening-Finishing Treatment in Shaping Surface-Layer Quality [G.A. Iskhakova, V.P. Gileta; FIZIKA I KHIMIYA OBRABOTKI MATERIALOV, No 4, Jul-Aug 92]	10
Effect of Mechanical Alloying on Structure and Properties of Plasma Sprayed Coats of NiCr-ZrO ₂ x Y ₂ O ₃ Powder [L.K. Kondratenko, S.V. Chernyakov, et al.; METALLY, No 4, Jul-Aug 92]	11

Composite Materials

Cubic Boron Nitride-Based Composite Oxidation [E.I. Golovko, V.S. Neshpor, et al.; POROSHKOVAYA METALLURGIYA, No 8 (356), Aug 92]	12
Structure and Atomic Dislocation Mechanisms of Al-Al ₃ Co ₂ Composite Fracture [V.A. Yermishkin, R.M. Sofronova, et al.; METALLY, No 4, Jul-Aug 92]	12

Corrosion

Corrosion and Electrochemical Behavior of Titanium Silicides in Acid Solutions [V.I. Kolotyркиn, V.M. Knyazheva, et al.; ZASHCHITA METALLOV, No 4, Jul-Aug 92]	13
A Study of the Kinetics of Anodic Film Formation on Titanium in Perchlorate Alcohol Media [O.N. Nechayeva, V.P. Grigoryev, et al.; ZASHCHITA METALLOV, No 4, Jul-Aug 92]	13
The Dissolution of Binary Alloys of Titanium With Tungsten [A.I. Shcherbakov, I.V. Kasatkina, et al.; ZASHCHITA METALLOV, No 4, Jul-Aug 92]	13
The Role of Ion-Exchange Reactions in the Passivation and Local Corrosion of Metals [A.P. Nazarov, M.A. Petrunin, et al.; ZASHCHITA METALLOV, No 4, Jul-Aug 92]	14
The Water Permeability of Carbon Steel in Acidic Hydrogen Sulfide-Containing Media [M.N. Fokin, M.B. Lopatina, et al.; ZASHCHITA METALLOV, No 4, Jul-Aug 92]	14
Hydrogen Absorption by 65Mn Steel During Corrosion in Hydrogen Sulfide-Containing Media [T.Z. Akhmetov, G.A. Beysembayeva, et al.; ZASHCHITA METALLOV, No 4, Jul-Aug 92]	15
The Corrosion and Electrochemical Properties of 03Cr25Ni9MoCuTiL Steel [A.S. Zuyeva, V.A. Kalinichenko, et al.; ZASHCHITA METALLOV, No 4, Jul-Aug 92]	15

Nonferrous Metals, Alloys, Brazes, Solders

Filtering of Liquid Smelting Products Through Blast Furnace Tuyere Zones [W. Sabala, R. Budzik; IZVESTIYA VYSSHIKH UCHEBNYKH ZAVEDENIY: CHERNAYA METALLURGIYA, No 7, Jul 92]	17
Effect of Liquid Stirring on Temperature Distribution in Continuously Cast Ingot [V.V. Stulov; IZVESTIYA VYSSHIKH UCHEBNYKH ZAVEDENIY: CHERNAYA METALLURGIYA, No 7, Jul 92]	17
Steel Creep During Bainite Transformation [V.G. Leshkovtsev, A.M. Pokrovskiy; IZVESTIYA VYSSHIKH UCHEBNYKH ZAVEDENIY: CHERNAYA METALLURGIYA, No 7, Jul 92]	17
Increasing Resistance of Dies by Substituting Steel 3Kh3M3F With Steel 40Kh With Diffuse Aluminum Layer on its Surface [N.V. Temnogorova, S.A. Vodennikov, et al.; IZVESTIYA VYSSHIKH UCHEBNYKH ZAVEDENIY: CHERNAYA METALLURGIYA, No 7, Jul 92]	18
Filtration Refining of Steel To Remove Dissolved Oxygen [E.B. Ten; IZVESTIYA VYSSHIKH UCHEBNYKH ZAVEDENIY: CHERNAYA METALLURGIYA, No 7, Jul 92]	18

On Possibility of Nitrogen Oxidation by Air's Oxygen During Sinter Cooling [T.V. Detkova, A.R. Zhak; <i>IZVESTIYA VYSSHIKH UCHEBNYKH ZAVEDENIY: CHERNAYA METALLURGIYA</i> , No 7, Jul 92]	18
Improving Range of Mechanical Properties of High-Strength Maraging Steels N15F6M5K10 and N12M6K12Kh4T by Ausforming [T.R. Lapteva, V.G. Prokoshkina, et al.; <i>IZVESTIYA VYSSHIKH UCHEBNYKH ZAVEDENIY: CHERNAYA METALLURGIYA</i> , No 7, Jul 92]	18
Increasing Electrical Equipment Fire Safety at Nonferrous Metallurgy Enterprises [V.L. Ivannikov, A.K. Merzlyakov; <i>IZVESTIYA VYSSHIKH UCHEBNYKH ZAVEDENIY: CHERNAYA METALLURGIYA</i> , No 8, Aug 92]	19
Increasing Fire Safety System Efficiency at Metallurgical Enterprises [N.G. Topolskiy, V.L. Ivannikov, et al.; <i>IZVESTIYA VYSSHIKH UCHEBNYKH ZAVEDENIY: CHERNAYA METALLURGIYA</i> , No 8, Aug 92]	19
On Preventing Breakage of Electrodes Thrust Into Nonconducting Charge [V.K. Butorin, O.I. Ulanov, et al.; <i>IZVESTIYA VYSSHIKH UCHEBNYKH ZAVEDENIY: CHERNAYA METALLURGIYA</i> , No 8, Aug 92]	19
Temperature Diagnostics of Supersonic Flares Developing During Converter Smelting [V.G. Lisiyenko, O.E. Shlik, et al.; <i>IZVESTIYA VYSSHIKH UCHEBNYKH ZAVEDENIY: CHERNAYA METALLURGIYA</i> , No 8, Aug 92]	20
Computer-Aided System for Controlling In-Line Plate Mill Quench-Hardening Unit [S.S. Popyanov, Yu.A. Makagonov; <i>IZVESTIYA VYSSHIKH UCHEBNYKH ZAVEDENIY: CHERNAYA METALLURGIYA</i> , No 8, Aug 92]	20
On Sulfide Inclusion Formation in Steels [A.P. Serbin, V.Ye. Sokolov, et al.; <i>METALLY</i> , No 4, Jul-Aug 92]	20
Mechanism of REM Effect on Isothermal High-Temperature Strength of Fe- and Ni-Based Alloys [A.G. Nikolayev, T.F. Titova, et al.; <i>METALLY</i> , No 4, Jul-Aug 92]	20
Effect of Structural State on High-Temperature Ductility of Lead-Doped Steel 08Kh20N9G7T [S.A. Zinchenko, D.B. Titorov; <i>METALLY</i> , No 4, Jul-Aug 92]	21
Effect of Thermomechanical and Mechanical Treatment on Fatigue Strength of WTi3-1 Titanium Alloy [O.M. Ivasishin, P.Ye. Markovskiy, et al.; <i>PROBLEMY PROCHNOSTI</i> , No 6, Jun 92]	22
Refractory Rare Metals—Sputtering Targets for Microelectronics [A.V. Yelyutin, L.I. Voronenko, et al.; <i>TSVETNYYE METALLY</i> , No 4, Apr 92]	22
Likely Mechanisms of Metal Reduction From Oxide Films by Gaseous Reagents [Yu.V. Spichkin; <i>METALLY</i> , No 4, Jul-Aug 92]	22
Investigation of REM Effect on Carbide Structure of Ni-Based Superalloys [V.V. Sidorov, V.A. Vertogradskiy, et al.; <i>METALLY</i> , No 4, Jul-Aug 92]	23
Texture of Thin VT23 Titanium Alloy Sheets [I.V. Egiz, A.A. Babareko, et al.; <i>METALLY</i> , No 4, Jul-Aug 92]	23
Carbide Hardened Powder Molybdenum Alloys [K.B. Povarova, Ye.K. Zavarzina, et al.; <i>METALLY</i> , No 4, Jul-Aug 92]	23
Structural Conditions for Maximizing Strength and Ductility of Two-Phase Be-Y and Be-Al Materials [A.A. Chevychelov, B.A. Movchan; <i>METALLY</i> , No 4, Jul-Aug 92]	24
Stationary Potentials and Redox Transitions of Gallium and Its Alloys With Silver [A.V. Chanturia, V.Ye. Vigdergauz, et al.; <i>TSVETNYYE METALLY</i> , No 8, Aug 92]	24
Copper-Bearing Industrial Product Treatment Using Sulfur Dioxide From Pyrometallurgical Production [O.A. Lyumet, L.M. Bogacheva, et al.; <i>TSVETNYYE METALLY</i> , No 8, Aug 92]	24
SO ₂ Utilization as ZnSO ₄ in Industrial Flue Gas Treatment [V.V. Govorov, I.N. Ivanina, et al.; <i>TSVETNYYE METALLY</i> , No 8, Aug 92]	25

Nonmetallic Materials

Capillary Stability of Primary Sprayed Concrete Layer [V.A. Deryabin; <i>OGNEUPORY</i> , No 7-8, Jul-Aug 92]	26
Effect of Ferric and Ferrous Oxides on Periclase Spinel Product Resistance [Ye.S. Borisovskiy, G.I. Kuznetsov, et al.; <i>OGNEUPORY</i> , No 7-8, Jul-Aug 92]	26
Self-Propagating High-Temperature Synthesis: General Premises [V.I. Sumin, Yu.N. Makurin; <i>OGNEUPORY</i> , No 7-8, Jul-Aug 92]	26
Production of Fireclay Light-Weight Refractories [T.M. Sandutsa, L.A. Dergaputskaya; <i>OGNEUPORY</i> , No 7-8, Jul-Aug 92]	26
Cracking Resistance and Strength of End Sections of Prestressed Structural Concrete Parts With Wire-Rope Reinforcement [N.A. Markarov, R.Sh. Sharipov, et al.; <i>BETON I ZHELEZOBETON</i> , No 5, May 92]	27

Effect of Dispersible in Water Film-Forming Clogging Compounds on Quality of Protective Pipe Jacket [G.V. Topilskiy, V.I. Melikhov, et al.; <i>BETON I ZHELEZOBETON</i> , No 5, May 92]	27
Effect of Additives on Corrosion Resistance of Building Mortars in Technogenic Media [V.V. Goncharov, A.M. Rozhanskaya; <i>BETON I ZHELEZOBETON</i> , No 5, May 92]	27
Life Expectancy of Reinforced-Concrete Cover Plates for Railroad Buildings [V.P. Chirkov, A.N. Kardangushev; <i>BETON I ZHELEZOBETON</i> , No 5, May 92]	28
Electrical Resistance of Oxide Film Coatings on Glass [A.B. Atkarskaya, V.I. Borulko, et al.; <i>STEKLO I KERAMIKA</i> , No 5, May 92]	28
Elasticity of Si_3N_4 -Base Ceramic [V.N. Yakovkin, V.A. Kuzmenko; <i>STEKLO I KERAMIKA</i> , No 5, May 92]	28
Some Technological Problems in Enamel-Coating of Cast Iron Products [P.G. Pauksch; <i>STEKLO I KERAMIKA</i> , No 5, May 92]	29
Crystallization of "Biosital" Glass-Ceramic during Radiation Heating [S.T. Suleymenov, A.A. Mirzakhodzhaev, et al.; <i>STEKLO I KERAMIKA</i> , No 5, May 92]	29
Stability of Quartz Glass Slurries [A.M. Akhyan; <i>STEKLO I KERAMIKA</i> , No 5, May 92]	30
Use of Porcelain Collet as Filler Material [B.U. Barshchevskiy, V.M. Loginov; <i>STEKLO I KERAMIKA</i> , No 5, May 92]	30
Effect of Pressing Force on $\text{YBa}_2\text{Cu}_3\text{O}_{7-x}$ Powder Structure and T_c [V.F. Shamray, Yu.V. Yefimov, et al.; <i>FIZIKA I KHIMIYA OBRABOTKI MATERIALOV</i> , No 4, Jul-Aug 92]	30
Fibers and Fibrous Materials for Reinforcing Composites With Extreme Characteristics [K.Ye. Perepelkin; <i>MEKHANIKA KOMPOSITNYKH MATERIALOV</i> , No 3, May-Jun 92]	31
Mechanical Properties of Polyethylene- and Thermally Exfoliated Graphite-Based Composite Materials [L.S. Semko, I.G. Chernysh, et al.; <i>MEKHANIKA KOMPOSITNYKH MATERIALOV</i> , No 3, May-Jun 92]	31
Stressed State of Polycrystalline Diamond Compacts Under Thermal and Force Load in High Pressure Machines [A.M. Anisin; <i>SVERKHTVERDYIE MATERIALY</i> , No 2 (77), Mar-Apr 92]	31
Determining Wear Resistance of Polycrystalline Diamond Compacts by Acoustic Emission Method [S.L. Udovik, B.A. Oleynikov, et al.; <i>SVERKHTVERDYIE MATERIALY</i> , No 2 (77), Mar-Apr 92]	32
Structure Formation in Diamond-Bearing Foil [O.A. Katrus, E.E. Mitrova, et al.; <i>SVERKHTVERDYIE MATERIALY</i> , No 2 (77), Mar-Apr 92]	32
TiB_2 Structural Transformations at High Pressures and Temperatures [G.S. Oleynik, Yu.I. Lezhnenko, et al.; <i>SVERKHTVERDYIE MATERIALY</i> , No 2 (77), Mar-Apr 92]	32
Effect of Static Magnetic Field on Electrodeposition of Diamond-Bearing Composite Coats [G.N. Znamenskiy, I.A. Tsisar, et al.; <i>SVERKHTVERDYIE MATERIALY</i> , No 2 (77), Mar-Apr 92]	33
Formation of Graphite With Corrugated Layers During Diamond Graphitization [V.D. Andreyev, Yu.I. Sozin, et al.; <i>SVERKHTVERDYIE MATERIALY</i> , No 3 (78), May-Jun 92]	33
Effect of Glow Discharge Parameters and Heat Treatment on Synthetic Diamond Single Crystal Metallization [Ya.L. Potapenko, N.A. Paskal, et al.; <i>SVERKHTVERDYIE MATERIALY</i> , No 3 (78), May-Jun 92]	33
Wear Resistance of Si_3N_4 -TiN Ceramics Under Friction Against Diamond Abrasive [Yu.G. Gogotsi, A.M. Kovalchenko, et al.; <i>SVERKHTVERDYIE MATERIALY</i> , No 3 (78), May-Jun 92]	34
Effect of Nickel and Manganese Sulfates on Chromium Sulfate Solution Recovery in Synthetic Diamond Production [V.V. Putivlskiy, A.A. Milner, et al.; <i>SVERKHTVERDYIE MATERIALY</i> , No 3 (78), May-Jun 92]	34
Selecting Methods of Efficient Nonfired High-Alumina Ceramic Product Machining [V.P. Lepetukha, I.M. Sova; <i>SVERKHTVERDYIE MATERIALY</i> , No 3 (78), May-Jun 92]	34
Superfinishing of Carbide- and Nitride-Based Engineering Ceramics [A.A. Orap, Ya.A. Kryl, et al.; <i>SVERKHTVERDYIE MATERIALY</i> , No 3 (78), May-Jun 92]	35
Electric Conductivity of BN_{sph} Polycrystals Produced by Direct Phase Transition From Pyrolytic BN [N.A. Shishonok, V.B. Shipilo; <i>POROSHKOVAYA METALLURGIYA</i> , No 8 (356), Aug 92]	35
β -BN Oxidation Mechanism [A.P. Garshin, V.Ye. Shvayko-Shvaykovskiy; <i>POROSHKOVAYA METALLURGIYA</i> , No 8 (356), Aug 92]	36
Postradiation Defects in Neutron-Irradiated Pyrolytic BN [A.V. Kabyshev, V.M. Ketskalo, et al.; <i>POROSHKOVAYA METALLURGIYA</i> , No 8 (356), Aug 92]	36

Preparations

Higher Strength and Cold Resistance of Structural Steels Will Advance Machine Building and Construction [N. P. Lyakishev, S. I. Tishayev; <i>STAL</i> , No 5, May 92]	37
Ways of Saving Titanium in Alloying of Converter Steel [V. P. Kirilenko, P. I. Yugov, et al.; <i>STAL</i> , No 5, May 92]	37
Modernization of a Converter Automated Control System [S. M. Chumakov, V. D. Kuleshov, et al.; <i>STAL</i> , No 5, May 92]	37
Silicon in Low-Carbon Rimmed and Semikilled Steel [B. A. Burdonov, I. K. Ibrayev, et al.; <i>STAL</i> , No 5, May 92]	38
Higher Assimilation of Titanium in Ladle Treatment and Teeming of Corrosion-Resistant Chromium-Nickel Steel [M. A. Filimonov, A. F. Kolosov, et al.; <i>STAL</i> , No 5, May 92]	38
Production of White Synthetic Corundum Powders With Isometric Grit Shape [S.M. Uman, Yu.N. Nikitin, et al.; <i>SVERKHTVERDYIE MATERIALY</i> , No 4 (79), Jul-Aug 92]	38
Optimization of Diamond and Mechanochemical Polishing of Semiconductor Wafers [B.G. Zakharov, V.V. Rogov, et al.; <i>SVERKHTVERDYIE MATERIALY</i> , No 4 (79), Jul-Aug 92]	39
Standardization Principles of Complex Shaped Items Made by Powder Metallurgy Methods [Yu.G. Dorofeyev, A.Ye. Kushchevskiy, et al.; <i>POROSHKOVAYA METALLURGIYA</i> , No 8 (356), Aug 92]	39

Treatments

Stressed State of Thin-Walled Tubes During Multicycle Deformation by Drawing [Yu.A. Tsekhanov; <i>PROBLEMY PROCHNOSTI</i> , No 6, Jun 92]	40
A Process for Producing Getter Powders for Ultrapurification of Gases [M.L. Kotsar, V.M. Azhazha, et al.; <i>VYSOKOCHISTYYE VESHCHESTVA</i> , No 4, Jul-Aug 92]	40
Neutron Effect and Environmental Aspects of Using Iron in Nuclear Fission and Fusion Reactors [Ye.V. Demina, V.V. Ivanov, et al.; <i>FIZIKA I KHIMIYA OBRABOTKI MATERIALOV</i> , No 4, Jul-Aug 92]	40
Graphite Materials' Size Behavior Under Irradiation and Their Serviceability Criterion [Yu.S. Virgilyev; <i>FIZIKA I KHIMIYA OBRABOTKI MATERIALOV</i> , No 4, Jul-Aug 92]	41
Structure and Property Behavior of Carbon Fibers Under High-Temperature Neutron Irradiation [Ye.N. Kurolenkin, Yu.S. Virgilyev, et al.; <i>FIZIKA I KHIMIYA OBRABOTKI MATERIALOV</i> , No 4, Jul-Aug 92]	41
Investigation of Martensitic Steels' Temperature Conditions Under High-Fluence Ion Implantation [V.G. Abdrashitov, V.V. Ryzhov, et al.; <i>FIZIKA I KHIMIYA OBRABOTKI MATERIALOV</i> , No 4, Jul-Aug 92]	41
Radiation-Induced Insulator Electrization for Fusion Reactor's Superconducting Magnetic System [A.I. Akishin, A.I. Tyutrin, et al.; <i>FIZIKA I KHIMIYA OBRABOTKI MATERIALOV</i> , No 4, Jul-Aug 92]	42
Interaction of Thin Copper Films With Sulfur Under Pulse Laser Irradiation [F.A. Piskunov, A.S. Podoltsev, et al.; <i>FIZIKA I KHIMIYA OBRABOTKI MATERIALOV</i> , No 4, Jul-Aug 92]	42
Decomposition and Property Behavior of α -Al ₂ O ₃ Single Crystals Under Multiple Exposure to 1.06 μ m Pulse Laser Radiation [A. Chmel, S.B. Yeronko, et al.; <i>FIZIKA I KHIMIYA OBRABOTKI MATERIALOV</i> , No 4, Jul-Aug 92]	42
Reversible and Irreversible Structure Defect Formation on Silicon Surface Under Laser Pulse Effect [A.F. Banishev, L.V. Novikova; <i>FIZIKA I KHIMIYA OBRABOTKI MATERIALOV</i> , No 4, Jul-Aug 92]	43
Al-Cu Alloy Zone Melting Experiment Under Normal Gravity and in Weightlessness Using Mirror-Beam Furnace' Unit [S.A. Maslyayev, V.N. Pimenov, et al.; <i>FIZIKA I KHIMIYA OBRABOTKI MATERIALOV</i> , No 4, Jul-Aug 92]	43
Structural Characteristics of Laser-Doped Layers on VT-6 Alloy Produced Using Boron Powder Injection [A.M. Bernshteyn, Ye.M. Yandimirkin; <i>FIZIKA I KHIMIYA OBRABOTKI MATERIALOV</i> , No 4, Jul-Aug 92]	43
Protecting YBa ₂ Cu ₃ O _{7-δ} Ceramics From Degradation in Water Vapors [V.L. Arbutov, O.M. Bakunin, et al.; <i>FIZIKA I KHIMIYA OBRABOTKI MATERIALOV</i> , No 4, Jul-Aug 92]	44

Effect of High Pressure on Hard Alloy Properties [A.V. Gerasimovich, N.M. Grigoryev; <i>SVERKHTVERDYIE MATERIALY</i> , No 2 (77), Mar-Apr 92]	44
Laser Heat Treatment of Powder Iron-Graphite Materials [P.A. Vityaz, V.S. Ivashko, et al.; <i>POROSHKOVAYA METALLURGIYA</i> , No 8 (356), Aug 92]	44

Welding, Brazing, Soldering

Long-Term Strength and Creep of Molybdenum Alloy Welds at High Temperatures [V.V. Bukhanovskiy, V.K. Kharchenko, et al.; <i>AVTOMATICHESKAYA SVARKA</i> , No 2 (467), Feb 92]	46
On Mechanism of Heat Affected Zone Crack Prevention During Hardenable Steel Welding Using Austenitic Materials [Yu.N. Gotalskiy, D.P. Novikova; <i>AVTOMATICHESKAYA SVARKA</i> , No 2 (467), Feb 92]	46
Narrow Gap Welding of Steels and Alloys Sensitive to Thermal Cycle [V.I. Kulik, V.A. Kazakov, et al.; <i>AVTOMATICHESKAYA SVARKA</i> , No 2 (467), Feb 92]	46
Electron Beam Control in Electron Beam Vaporization and Remelting Units [V.P. Mishchenko (deceased); <i>AVTOMATICHESKAYA SVARKA</i> , No 2 (467), Feb 92]	47
Electron Beam Sweep Generators for Welding and Heat Treatment [Yu.N. Lankin, Ye.N. Bayshtuk; <i>AVTOMATICHESKAYA SVARKA</i> , No 2 (467), Feb 92]	47
Capacitor Discharge Stud Welding Under Water [D.M. Kaleko, N.A. Chvertko, et al.; <i>AVTOMATICHESKAYA SVARKA</i> , No 2 (467), Feb 92]	47
Low-Temperature Vacuum Soldering Practices of Lattice Girder Structure Joints From Aluminum Alloys [V.F. Khorunov, V.F. Lapchinskiy, et al.; <i>AVTOMATICHESKAYA SVARKA</i> , No 2 (467), Feb 92]	47

Extractive Metallurgy, Mining

Radiometric Ore Enrichment [V.A. Mokrousov; <i>RAZVEDKA I OKHRANA NEDR</i> , No 4, Apr 92]	49
Quantitative Rock and Ore Analysis for Mineral Content [V.S. Gaydukova, V.V. Golubnichiy, et al.; <i>RAZVEDKA I OKHRANA NEDR</i> , No 4, Apr 92]	49
Protection of Environment During Preparation of Hydrogenous Mineral Deposits for Industrial Utilization by Underground Leaching Ore Deposits in Preparation for Industrial Processing [K.G. Brovin; <i>RAZVEDKA I OKHRANA NEDR</i> , No 4, Apr 92]	49
Principles of Developing and Results of Testing BS20 and BS36 Diamond Drill Bits [V.I. Opolskiy, R.K. Bogdanov, et al.; <i>RAZVEDKA I OKHRANA NEDR</i> , No 4, Apr 92]	50
Drill Bits With Tungstenless Matrix for Effective Rock Blasting [A.M. Isonkin; <i>RAZVEDKA I OKHRANA NEDR</i> , No 4, Apr 92]	50
The Experience of Operating a Dump Leaching Shop at the Kounradskiy Ore Mine [M.Yu. Radzhibayev, N.Ye. Plaksa, et al.; <i>TSVETNYYE METALLY</i> , No 4, Apr 92]	50
Conditioning Copper Heap Leaching Solutions From Oxidized Ore of the Kounradskiy Ore Mine Deposit [A.V. Shubinok; <i>TSVETNYYE METALLY</i> , No 4, Apr 92]	51
Change in the Material Composition of Balanced Copper-Porphyric Ores of the Dumps of the Kounradskiy Ore Mine During the Leaching Process [S.I. Druzhinina, L.D. Sheveleva, et al.; <i>TSVETNYYE METALLY</i> , No 4, Apr 92]	51
The Potentials of Geotechnology in Processing Oxidized Copper Ores [G.A. Pavlichenko, B.M. Rogov, et al.; <i>TSVETNYYE METALLY</i> , No 4, Apr 92]	52
Mechanism of the Bacterial-Chemical Leaching of Pyritic Ores [L.D. Sheveleva, O.B. Krushkol, et al.; <i>TSVETNYYE METALLY</i> , No 4, Apr 92]	52
Preparing an Ore Mass for Underground Copper Leaching by the Hole-Slit Method [B.V. Dyakov, S.N. Popov, et al.; <i>TSVETNYYE METALLY</i> , No 4, Apr 92]	52
The Possibility of Geotechnological Extraction of Molybdenum Based on Hypochlorite and Sulfuric Acid Leaching [G.M. Yashina; <i>TSVETNYYE METALLY</i> , No 4, Apr 92]	53
A Biohydrometallurgical Process for Processing Gold-Pyrite Concentrate [R.Ya. Aslanukov, G.V. Sedelnikova, et al.; <i>TSVETNYYE METALLY</i> , No 4, Apr 92]	53
The Use of Bioactive Wastes From Antibiotics Production in Hydrometallurgy [B.N. Laskorin, G.I. Karavayko, et al.; <i>TSVETNYYE METALLY</i> , No 4, Apr 92]	54
Protecting Underground Waters During the Geotechnological Processing of Nonferrous Metal Ores [A.M. Roygbaum, L.D. Sheveleva, et al.; <i>TSVETNYYE METALLY</i> , No 4, Apr 92]	54

Miscellaneous

Decreasing Discharges When Emptying Dust Precipitators [A.M. Kasimov, Ye.S. Makarenko, et al.; TSVETNYYE METALLY, No 8, Aug 92]	56
Water Defluorination Electrocoagulation Unit [B.L. Prisyazhnyuk; TSVETNYYE METALLY, No 8, Aug 92]	56
Investigation of Municipal Sewer Sediment Dewatering Using Titanium Production Waste [V.S. Proshkin, N.N. Stremilova; TSVETNYYE METALLY, No 8, Aug 92]	56

Temperature Dependence of Breaking Stress for Molybdenum in Transition Range (Above Cold-Shortness Point)

927D0246B Kiev PROBLEMY PROCHNOSTI in Russian No 6, Jun 92 (manuscript received 22 May 91) pp 20-25

[Article by V.F. Moiseyev and A.N. Sherban, Institute of Materials Science at Ukrainian Academy of Sciences, Kiev; UDC 539.345:539.4:669.1:669.28:536.98]

[Abstract] The temperature dependence of the breaking stress for molybdenum is analyzed theoretically by considering the plastic deformation process during relaxation prior to fracture as well as the specifics of brittle fracture without subcritical crack growth under load. A physical model is constructed that describes transition to fracture with spalling and to the temperature range above the cold-shortness point. A mathematical model of this process is then constructed which deals essentially with scales of dimensional changes from microcracks to macrocracks in accordance with dislocation theory and including the Burgers vector, particular importance being assigned to the tip of a macrocrack or notch and the decrease of its radius of curvature. In the cold-shortness range after inception of a macroyield, interaction of microcracks with the initial crack or notch can lead to its becoming much sharper and lead to fracture in accordance with the stress criterion. As the yield strength decreases with rising temperature, at some temperature it ceases to be an adequate criterion of fracture with spalling, and strain begins to play the principal role. Simultaneous strain hardening of the metal and its deformation at the tip of a crack produce a change in the crack dimensions (length l and tip radius r), thus also a change in the magnitude of the stress concentration factor $c_1 = 2(l/r)^{1/2}$. This theoretical analysis is supplemented with experimental data, tests having been performed on specimens of the Mo - 6 Zr alloy. Three kinds of specimens with three different stress concentration factors were tested: 1) specimens notched by means of an electric spark ($c_1 = 8$); 2) flat ground specimens ($c_1 = 2.5$); 3) electrolytically polished specimens ($c_1 = 1.5$). Figures 4; references 13.

Method of Design Calculation for Flywheel Made of Fibrous Composite with Binder

927D0246D Kiev PROBLEMY PROCHNOSTI in Russian No 6, Jun 92 (manuscript received 20 Mar 90) pp 39-41

[Article by A.M. Mokeyev and S.G. Sidorov, Kazan Institute of Chemical Technology; UDC 678:2.001:621]

[Abstract] A method of design calculation for structures made of a fibrous composite is proposed which takes into account the strength and stiffness characteristics of the binder. The method is based on net theory and is demonstrated on a chordally wound flywheel. The corresponding system of differential equations in strains is, with the aid of an appropriate approximating difference scheme, converted into a system of difference equations in displacements with a small parameter. This nonlinear

system is then solved by Newton's method for the radial distribution of interlayer shear stress. A specific example is considered an isotropic flywheel consisting of two disks with different mechanical characteristics and with a hole through both. With the highest-order (second) derivative multiplied by a trimming factor, the system of equations is solved numerically for the general case of unequal fiber and binder displacements as well as asymptotically for the limiting case of equal fiber and binder displacements. Figures 1; references 2.

Phase and Structural Transformations in Rhombohedral BN Under High Pressures

927D0247A Kiev SVERKHTVERDYIE MATERIALY in Russian No 4 (79), Jul-Aug 92 pp 3-7

[Article by V.F. Britun, A.V. Kurdyumov, I.A. Petrusha, A.A. Svirid, Institute of Materials Science Problems and Superhard Materials Institute at the Ukrainian Academy of Sciences, Kiev; UDC 548.33]

[Abstract] The differences in the phase and structural transformations of various boron nitride modifications are discussed, and the crystallographic patterns of phase transformations and fine structure evolution under static pressure in rhombohedral BN within a broad temperature range are examined by the transmission electron microscopy methods. To this end, highly textured pyrolytic BN containing 80 percent of the rhombohedral modification and up to 20 percent of highly disordered hexagonal modification is compressed in a toroidal cell under a 7-8 GPa pressure within a 25 to 2,600°C temperature range. The [001] sample texture axis is oriented along the compression axis. The electron microscopy study is carried out using samples thinned by the ion spraying method. An analysis shows that the rhombohedral/adwurtzite phase transition occurs by the longitudinal layer bending mechanism starting at about 300°C through an intermediate graphite-like ADAD structure while the phase transformation is preceded by twinning in the rhombohedral structure; at a 1,500-2,00°C, a wurtzite/adsphalerite transformation accompanied by the 4H intermediate structure formation is observed. Recrystallization processes are observed in sphalerite at above 2,300°C. Figures 3; references 10; 6 Russian, 4 Western.

Raman Scattering Spectra of Diamond Condensate Deposited From Vapor Phase Onto Diamond Powder Compacts

927D0247B Kiev SVERKHTVERDYIE MATERIALY in Russian No 4 (79), Jul-Aug 92 pp 8-10

[Article by V.D. Andreyev, V.A. Semenov, T.A. Nachalnaya, A.F. Goncharov, Superhard Materials Institute at the Ukrainian Academy of Sciences and Crystallography Institute at Russia's Academy of Sciences, Moscow; UDC 621.762.02]

[Abstract] Production of diamond, adamantane, and amorphous carbon phases by condensation and the dependence of the resulting product structure and properties on the substrate properties and structure are discussed, and vapor phase deposition of the diamond phase onto diamond is investigated due to the need to establish the process parameters and examine the properties of the resulting condensate. To this end, diamond film is synthesized by the gas phase activation with glow discharge plasma; the films are deposited onto diamond powder compacts with various structural defects. The films are then examined by Raman light scattering (KRS) spectroscopy so as to ascertain the structure and phase composition of the material. To this end, Raman spectra are excited by an Ar-laser at $\lambda=48.0$ and 514.5 nm and measured by the DFS-24 double monochromator. Raman spectra of standard materials and the films deposited on a diamond single crystal as well as Raman scattering spectra characterized by a varying degree of shift relative to the standard diamond line position are plotted. The substrate spectrum shifts considerably toward the low-frequency region but as the film thickness increases, it moves closer to the characteristic $1,332\text{ cm}^{-1}$ line and disappears, while only the deposited film line remains. This phenomenon is attributed to the fact that during the vapor phase deposition, the diamond condensate structure may differ greatly from the base structure. Figures 3; references 5: 4 Russian, 1 Western.

Study of Diamond Solubility in Multicomponent Metal Melts Under Thermodynamic Stability Conditions

927D0247C Kiev SVERKHTVERDYIE MATERIALY in Russian No 4 (79), Jul-Aug 92 pp 11-16

[Article by S.A. Ivakhnenko, A.V. Andreyev, I.S. Belousov, Superhard Materials Institute at the Ukrainian Academy of Sciences, Kiev; UDC 669.017.324.74.784:666.233]

[Abstract] Current practices of growing large diamond crystals on seed by carbon recrystallization through a metal melt at a temperature gradient and a lack of published empirical data on this subject necessitated a study of the diamond solubility and its temperature coefficient in various metal solvents; the difficulties of experimental measurements of these parameters which have hindered research thus far are discussed. The diamond solubility in metal melts is determined by a method based on measuring the mass loss of diamond crystals in contact with a metal sample at a pressure and temperature which ensure that the process occurs within the area of diamond's thermodynamic stability. A schematic diagram of the experiment is cited and the dependence of the diamond solubility logarithm in metal melts on the reciprocal value of temperature is plotted. The chemical composition of four sample melts, the diamond solubility in metal melts in the thermodynamic stability region, the diamond dissolution heat in metal melts under a 6.0 GPa pressure at high temperatures, and the chemical potential difference of graphite and diamond

and the carbon oversaturation in metal melts under a 6.0 GPa pressure at high temperatures are summarized. Two out of the four melts are identified as suitable for growing large crystals. The findings make it possible to control the diamond growth process while the temperature coefficient of solubility and carbon supersaturation may serve as tentative criteria for selecting the melts for diamond seed growth by the temperature gradient method. Figures 2; tables 4; references 8: 6 Russian, 2 Western.

Catalyst Alloys With Metastable Structure

927D0247D Kiev SVERKHTVERDYIE MATERIALY in Russian No 4 (79), Jul-Aug 92 pp 16-20

[Article by V.V. Sobolev, V.Ya. Slobodskoy, S.I. Gubenko, A.D. Sharabura, A.A. Udoyev, Dnepropetrovsk Mining Institute and Poltava Synthetic Diamond and Diamond Tool Plant; UDC 539.216+620.18+666.233]

[Abstract] The use of catalytic media and the effect of the carbon concentration in it on the diamond crystal size as well as the properties of the newly designed Ni-Mn catalysts with a metastable structure (KMS) produced by rapid uniaxial quenching are discussed. A schematic diagram of the alloy quenching unit is cited, and the parameters of the quenching process conducted in an inert atmosphere are outlined. Catalyst plates produced in the unit are crushed and ground to the necessary size without waste. The microstructure of the new catalyst is examined under a Neophot-21 optical microscope, and the phase composition is measured by qualitative X-ray phase diffraction analysis in a DRON-2M diffractometer in FeK radiation using an Mn filter. The chemical composition of the KMS catalyst is determined by a JMS-T330 scanning electron microscope with an XR 200/300 attachment by Link, while the bulk density and specific surface are measured by a Pore-Sizer 9300 pore meter. The average element distribution in the KMS plate thickness is plotted without indicating the line strength or reflection angles, and the phase composition of KMS plates and a commercial catalyst and the initial synthesis mixture composition and synthesis results are summarized. The strength of diamonds produced in the presence of the KMS catalyst exceeds that stipulated by GOST by an average of 25 percent. Crystals with a higher graininess have a poor strength, but this situation can be remedied by electromagnetic field treatment. Diamonds with the 160/63 fraction have the best compressive strength. Figures 2; tables 4; references 3.

Effect of Point Defects on Thermal Conductivity of Diamonds

927D0247E Kiev SVERKHTVERDYIE MATERIALY in Russian No 4(79), Jul-Aug 92 pp 27-31

[Article by T.D. Ositinskaya, A.P. Podoba, S.V. Shmegeera, Superhard Materials Institute at the Ukrainian Academy of Sciences, Kiev; UDC 536.2:666.233]

[Abstract] The effect of phonon-phonon coupling and phonon scattering by the crystal structure irregularities on the thermal conductivity of dielectric solids and the contribution of various types of defects at various temperature are discussed, and the process of phonon scattering by the nitrogen impurity atoms and vacancies in diamonds are considered. Impurity nitrogen found in the single crystal lattice of natural and synthetic diamonds forms several types of defects; of these, attention is focused on point defects formed by isolated N atoms which isomorphically substitute carbon in the diamond lattice (the so-called C-defects). The experimental and analytical temperature dependence of thermal conductivity of natural diamonds and synthetic diamonds grown by spontaneous crystallization is plotted and then calculated in Debye's approximation for diamonds with various C-defect and vacancy concentrations using published data. The theoretical and experimental data are rather consistent if the additional vacancy contribution to the phonon scattering process is taken into account. Charge material inclusions in crystals do not lead to noticeable scattering. It is speculated that first N-V, then N-V-N (where V is vacancy) complexes form in diamonds; this is confirmed indirectly by the results of photoluminescence spectroscopy. Figures 2; references 18: 8 Russian, 10 Western.

Geometric Parameter Behavior of Reamers From Composite 01 During Wear

927D0247H Kiev *SVERKHTVERDYIE MATERIALY* in Russian No 4 (79), Jul-Aug 92 pp 53-56

[Article by G.S. Zheleznov, S.A. Singeyev, Syzran Branch of the Samara Polytechnic Institute; UDC 621.951.025.7]

[Abstract] The unsteady behavior of reamers with cutting inserts from composite 01 during the machining of hardened steels prompted a study of the reamer insert behavior during the machining of bearing raceways from steel ShKh15 hardened to HRC 62-65 using six-edge reamers with a 35 mm diameter with 01 composite inserts soldered to the body. The wear of the cutting inserts during the machining at a 1.5-2.5 m/s cutting speed and a 0.1-0.3 mm/rev feed with a 0.1-0.3 mm depth is examined under an UIM-21 toolmaker's microscope, a MIM-7 metallographic microscope, and an optical comparator. The cutting insert edge after the sharpening and honing and after machining to a 0.3 mm wear as well as the cutting tip rounding and beveling during the reamer wear are shown. The likely mechanisms of cutting tip wear are discussed, and the edge radii and angles are measured: the edge radius increases while the plan approach angle decreases. The wear vs. radius and plan approach angle vs. edge radius correlations are established. Figures 3; references 4.

Laws Governing the Change in Metals' Electric Resistance Due to Impurities

927D0248A Moscow *VYSOKOCHISTYYE VESHCHESTVA* in Russian No 4, Jul-Aug 92 (manuscript received 14 Nov 91) pp 35-46

[Article by B.N. Aleksandrov, Low-Temperature Physics Engineering Institute, Kharkov; UDC 536.543]

[Abstract] One of the most important quantitative indicators of the degree of a high-purity metal's "electronic" purity is relative residual resistivity ($\delta_0 = \rho_0/\rho_{293}$, where ρ_0 and ρ_{293} indicate the given specimen's resistivity at about 0 and 293 K). Different impurities can have very different effects on a metal's electric resistance, with the difference often reaching one or two orders of magnitude. In view of this fact, the author of the study reported herein has studied the laws governing the change in different metals' electric resistance when subjected to the effects of different impurities. Specifically, he has examined the change ($\Delta\rho/c$) in the residual electric resistance of 34 different metal matrices when different types of impurities with a concentration c of about 1 percent or less are dissolved in them. The impurities considered are each located in one of three long periods of the periodic table of elements, and the behaviors of transition and nontransition metals are each covered separately. In the final section of this review, the author turns his attention to the those impurities that are most "harmful" to nontransition and transition metals. Specifically, S, Se, Te, P, As, Sb, and Bi impurities are the most harmful in univalent, bivalent, and trivalent nontransition metals, while S, Se, and Te impurities are the most "harmful" impurities in tetravalent nontransition metals. Na, K, Rb, Cs, Ca, Sr, and Ba impurities are to be considered "harmful" for Ti and Pb. In view of the similarities between the electron structure of Cu, Ag, and Au, it may be assumed that all of the impurities specified as being "harmful" in Cu and Ag will also be "harmful" in Au. As far as transition metals are concerned, impurities from groups 4, 5, and 6 should also be considered "harmful." Figures 7, tables 3; references 26: Russian, Western.

The Properties of Zinc Selenide Produced From $Zn(\text{inf}2H_3)_2$ and H_2Se

927D0248B Moscow *VYSOKOCHISTYYE VESHCHESTVA* in Russian No 4, Jul-Aug 92 (manuscript received 10 Mar 92) pp 54-59

[Article by G.G. Devyatykh, V.A. Sidorov, Ye.M. Gavrilshchuk, and A.N. Moiseyev, High-Purity Substances Chemistry Institute, Russian Academy of Sciences, Nizhny Novogorod; UDC 535.34.537.226]

[Abstract] The authors of the study reported herein examined the properties of zinc selenide produced by using the MOCVD [metal-organic chemical vapor deposition] method. ZnSe layers were grown in a horizontal-type continuous reactor on substrates of polished quartz glass at temperatures ranging from 250 to 510°C and pressures ranging from 1.5×10^{-1} to 3 torr. Wafers

measuring 70 x 100 mm² and up to 15 mm thick were grown. The deposition rate in the vicinity of the maximum thickness ranged from 20 to 800 $\mu\text{m/h}$. The resultant material had a polycrystalline structure with clear signs of a [111] axial texture. In the planes parallel to the base, the crystal boundaries were irregular and had a multitude of curvilinear segments, with the grains themselves oriented in a chaotic manner. In the planes normal to the base the grains were elongated along the direction of their growth. The grain increased in size farther out from the substrate. Another striking feature of the study specimens' crystalline structure was the presence in each individual crystallite of a systems of short parallel lines at angles close to 45° in relation to the normal. An analysis of the effect of growth conditions on the study crystals' properties revealed that increasing the precipitation temperature facilitated the formation of a columnar structure and resulted in an intensification of the cracking of the layers. Cracking was found to be especially intensive at temperatures of 400 to 450°C and attenuated at temperatures above 450°C. Reducing the process temperature was found to result in more intensely colored crystals. At 250°C, the material lost its transparency in the optical range of the spectrum and turned from orange-brown to brown. Increasing the temperature and reducing the precipitation rate, on the other hand, resulted in a material with increased transparency; however, the shading with a preponderance of orange tones was maintained all the way up to temperatures of 510°C and growth rates of 20 $\mu\text{m/h}$. The color of the study specimens turned out to be insensitive to changes in the ratios of the reagents' flow speeds. Significant changes were also discovered in the infrared range of the spectrum as well. Laser calorimetry was used to measure the absorption factors of a number of MOC-hybrid ZnSe specimens. The MOC-hybrid material was found to be far inferior to monocrystalline and zinc-hydride zinc selenide (the MOC specimens had typical absorption factors of 1 to 5 x 10⁻² cm⁻¹ versus the values reported elsewhere for monocrystalline and zinc-hydride zinc selenide (1 x 10⁻³ and 4 x 10⁻⁴ cm⁻¹, respectively). The experiments performed indicated that despite the fact that the MOCVD-ZnSe produced under the study conditions possesses high mechanical characteristics, they are still inferior to monocrystalline CVD-ZnSe from the standpoint of their optical properties. Figures 3; references 17: 8 Russian, 9 Western.

Layer-by-Layer Determination of Ga in Cadmium Telluride and Cadmium-Mercury Telluride by the Atomic Absorption Method With Electrothermal Atomization

927D0248D Moscow VYSOKOCHISTYYE
VESHCHESTVA in Russian No 4, Jul-Aug 92
(manuscript received 5 Feb 92) pp 128-131

[Article by I.G. Yudelevich, N.I. Petrova, and L.M. Buyanova, Inorganic Chemistry Institute, Siberian Department, Russian Academy of Sciences, Novosibirsk; UDC 543.422:539.23]

[Abstract] The authors of the study reported herein have developed a new technique for layer-by-layer determination of gallium impurities in cadmium telluride and cadmium-mercury telluride by the atomic absorption method with electrothermal atomization. During their work to develop the new method, the researchers used a Hitachi Z-8000 atomic absorption spectrometer with Zeeman background correction; ultrapure HCl, HBr, and HNO₃; chemically pure bromine that had been distilled twice; and KU-2 cationite and AV-17 anionite. A standard 1 mg/ml gallium solution was prepared along with working comparison solutions with concentrations of 10 and 0.1 $\mu\text{g/ml}$. The studies performed to determine the best procedure for atomic absorption determination of gallium in a graphite furnace by using a Hitachi Z-8000 established the following conditions as optimal: wavelength, 287.6 nm; initial drying temperature, 80°C; final drying temperature, 120°C; cineration temperature, 300°C; atomization temperature, 2,800°C, drying and cineration time, 30 seconds; and atomization time, 5 seconds. The working range of gallium concentrations was found to be between 0.002 to 0.03 $\mu\text{g/l}$. A polishing etching agent of 2.5 percent Br₂ in 4 N HBr was to used for separate analysis of the layers. A lower detection threshold of 2.4 x 10¹⁷ atoms of gallium per cm³ was achieved with a layer thickness of 0.3 μm . Figures 3; references 9: 7 Russian, 2 Western.

Chemical-Atomic Emission Analysis of High-Purity Selenium With the Use of Autoclave Dissolution of the Sample

927D0248E Moscow VYSOKOCHISTYYE
VESHCHESTVA in Russian No 4, Jul-Aug 92
(manuscript received 14 Jan 92) pp 137-140

[Article by N.V. Yerykalina, M.I. Krylova, R.V. Pakhomov, A.N. Tumanova, and Ye.I. Filatova, Chemistry Scientific Research Institute, Nizhniy Novogorod State University, Nizhniy Novogorod; UDC 543.42]

[Abstract] A new method has been developed for atomic emission spectral determination of impurities in high-purity selenium. In order to decrease the lower detection thresholds of the method, the researchers used the technique of autoclave dissolution of the sample and distillation of the base in the form of SeO₂. Nitric acid vapors were used to transform elemental selenium into SeO₂. During the course of the distillation process, the impurities are concentrated in a graphite powder collector. An STE-1 spectrograph was used to photograph the emission spectra on type 2 photographic plates. A three-lens communication system was used to design a 2-mm discharge interval for the spectrograph's slit. A discharge current of 10 A was used to excite the spectrum. The interval between the electrodes was kept constant during the discharge process. The conventional procedure was used to expose the photographic plates. The new atomization spectral determination method is capable of detecting impurities in amounts ranging from $n \times 10^{-6}$ to $n \times 10^{-8}$ percent (mass) depending on the nature of the element. The random error of the determinations was

found for an impurity concentration 5- to 10-fold higher than the detection thresholds. It was characterized by a relative standard deviation of 0.28 to 0.35. Tables 2; references 17: 9 Russian, 8 Western.

An Investigation of the Distribution of Impurities in Thin ZnO Films Produced by the MOCVD Method

927D0248F Moscow VYSOKOCHISTYYE
VESHCHESTVA in Russian No 4, Jul-Aug 92
(manuscript received 19 Feb 92) pp 141-144

[Article by A.N. Moiseyev, Yu.M. Saglanskiy, L.G. Ryabov, and D.A. Raldugin, High-Purity Substances Chemistry Institute, Russian Academy of Sciences, Nizhny Novogorod; UDC 543.7:539.216:661.847.92]

[Abstract] The authors of the study reported herein examined the distribution of impurities in thin zinc oxide films produced by the metal-organic chemical vapor deposition [MOCVD] method. The zinc films were precipitated from a gaseous phase at atmospheric pressure by oxidation of high-purity diethyl zinc by diethyl ether in a stream of argon. The diethyl zinc was fed in at a rate of 4×10^{-5} mol/min, and the diethyl ether was fed in at a rate of 4 to 6×10^{-3} mol/min with a total argon stream of 1 to 1.2 l/min. The temperature of the substrate during the deposition process ranged from 325 to 445°C. An RNI-545A scanning Auger spectrometer was used to study the composition profile of the ZnO layers at a residual pressure of 1×10^{-7} Pa. The electron sounding beam had an energy of 3 keV and current of 1.6×10^{-5} A. The electron beam's diameter was on the order of 100 μ m. A current density of 50 μ A/cm² was used during the ion sputtering by a beam of Ar⁺ ions with an energy of 1 keV. Under these conditions, the zinc oxide was sputtered at a rate on the order of 80 angstroms/min. The studies performed demonstrated that the carbon impurity present in zinc oxide films produced at the optimal temperature by the MOCVD method has a surface origin. The thickness of the carbon-contaminated layer does not exceed 0.1 μ m. When the synthesis temperature is decreased below 350°C, however, the concentration of carbon impurity in the bulk of the ZnO films may reach several percentage points. This thickness of the transition layer at the film-substrate interface was found to depend on the substrate material. For the specific synthesis conditions studied, the thickness of this transition layer was determined to range from 0.11 μ m for a silicon substrate to 0.25 μ m for a gallium arsenide substrate. A Specord-M80 IR spectroscopy was also used to determine the carbon-containing substances in the ZnO films. The results obtained by the Auger spectrometry studies were found to be constant with those of the IR spectroscopy studies. Figures 2; references 14: 2 Russian, 12 Western.

Analysis of Low-Melting Point Metals on a Spark-Source Mass Spectrometer

927D0248G Moscow VYSOKOCHISTYYE
VESHCHESTVA in Russian No 4, Jul-Aug 92
(manuscript received 28 Oct 91) pp 145-150

[Article by A.I. Saprykin and G.G. Sikharulidze, Inorganic Chemistry Institute, Novosibirsk, Siberian Department, Russian Academy of Sciences, and Problems of the Technology of Microelectronics and High-Purity Substances Institute, Russian Academy of Sciences, Chernogolovka, Moscow Oblast; UDC 543.51]

[Abstract] The authors of this article have proposed a spark-source mass spectrometry-based method of analyzing low-melting point metals. The new method is based on a combination of presparking the analysis samples until they reach the melting point and vaporization and ionization of the molten specimen by the voltage of a spark generator. The charge composition of the plasma is shown to correspond to the composition of the plasma of molten-metal ion sources operating in a cathode mode, whereas the energy distribution of the ions is shown to correspond to a sparking distribution. The high stability of the ionic current makes it possible to greatly simplify the set of exposures required to determine impurities at concentration levels of 10^{-3} to 10^{-8} percent (mass) and to improve the reproducibility of the impurity concentrations determined by a factor of 3 to 5. The validity of the proposed analysis method was checked by the "add-and-find" method on specimens of gallium and indium to which impurities ranging in concentration from 10^{-3} to 10^{-4} percent (mass) had been added. The results of this "add-and-find" check confirmed that the new method is free of systematic error. Next, the results achieved by using the new spark-source spectrometry technique were compared with independently obtained results from a chemical-atomic emission analysis. Although the numerical values obtained by both methods only coincided for 4 of the 34 impurities analyzed, the authors interpreted the comparison results as evidence that the two independent analysis methods are in generally good agreement with one another. The authors conclude by stating that standard specimens of high-purity tin produced in 1991 (which contain impurities at concentration levels of 10^{-3} - 10^{-6} and 10^{-4} - 10^{-7}) may be used to calibrate spark-source mass spectrometers so that they may be used to perform analyses in a molten-metal ion source mode. Figures 2, tables 2; references 12: 9 Russian, 3 Western.

Prediction of Inelastic Straining and Fracture of Laminated Composites

937D0009C Riga MEKHANIKA KOMPOSITNYKH
MATERIALOV in Russian No 3, May-Jun 92
pp 315-322

[Article by V.E. Vildeman, Yu.V. Sokolov, A.A. Tashkinov, Perm Polytechnic Institute; UDC 539.3:678.067]

[Abstract] The origins of the nonlinear relationship of the composite materials' stress and strain are discussed, and mathematical models of the composites' straining and fracture are developed; in addition, new features of their mechanical behavior related to the joint operation of structural members are addressed. To this end, a structural phenomenological model of composite materials is developed by expanding the function of state and introducing the vulnerability function in the form of fourth rank tensors. A stochastic boundary problem is formulated, and the characteristics of mechanical behavior of composites under active straining, residual stresses, and deformation and structural failure processes are examined. The dependence of the macrostress tensor invariants on the macrodeformation tensor invariants, the straining and loading paths of structural members under simple composite straining, the hydrostatic compression of laminated composites, the residual structural stresses and deformations of Al and Mg layers and macrodeformations after relieving the load, and composite strain diagrams and local load relief under structural failure conditions are plotted. An analysis of the curves shows that if a laminated composite consists of isotropic layers with identical shear moduli and coinciding vulnerability functions, its stress and strain at the macrolevel correspond to stress and strain at the structural level. It is shown that the residual stresses and strain in the composite under complex loading depend on preloading. The results of a numerical computer analysis of the inelastic straining process and fracture of a metal-polymer and laminated metallic composite are discussed. Figures 5; references 12.

Strength and Fatigue Resistance of Fabric-Based Composites Under Combined Effect of Static Shear Stresses and Cyclical Compressive Stresses

937D0009D Riga MEKHANIKA KOMPOSITNYKH MATERIALOV in Russian No 3, May-Jun 92
pp 332-340

[Article by V.A. Limonov, A.F. Razin, M.Ya. Mikelsons, Central Scientific Research Institute of Special Machine Building, Moscow oblast, and Polymer Mechanics Institute at the Latvian Academy of Sciences, Riga; UDC 539.3:678.067]

[Abstract] The behavior of composite materials under the combined effect of static and cyclic loads is discussed, and the need for taking these factors into account at the composite design stage is stressed. The study centers on similar types of composite structures such as thin-walled rods, pipes, and shafts operating under static and cyclic shear and compression stresses while the stresses developing in the material may be reduced to an equivalent system of tension-shear and compression-shear. The strength characteristics under static uniaxial and combined loading and the effect of static shear stresses on the endurance strength of fiber-based glass plastics under compression are examined experimentally in tubular samples made from a glass plastic and an epoxy binder. The shape and dimensions of the samples

are shown, and the uni- and biaxial proportionate static compression axes are shown. The static strength surface of samples as measured in tubular samples under three loading paths, material axes and effective stress diagram under combined loading, complex loading conditions of tubular samples under static shear and cyclic compression, fatigue diagrams under cyclic asymmetric compressions with static shear, and the dependence of static compressive stresses on the static shear are plotted. An analysis shows that application of the static shear component decreases the tensile and compressive strength relative to the strength behavior under uniaxial pressure. The resulting strength characteristics may be used in strength, rigidity, and stability analyses of thin-walled shells, shafts, and rods from cloth-based glass plastics. Figures 7; tables 2; references 7.

Effect of Plied Roving Length Difference on Fiber-Rupture Stress Realized in Organic Composite and Load-Carrying Capacity of Pressure Vessels

937D0009E Riga MEKHANIKA KOMPOSITNYKH MATERIALOV in Russian No 3, May-Jun 92
pp 418-422

[Article by S.P. Yakunin, L.A. Yegorov, St. Petersburg Mechanics Institute; UDC 678.027]

[Abstract] The effect of the filament length difference in the organic composite plied rovings used for making pressure vessels is discussed, and the probabilistic interrelation of the reinforcement fiber characteristics and the composite strength properties is examined on the basis of a statistical study of such reinforcement properties as the filament-length difference, moisture content, and linear density. An experimental study aimed at finding the effect of the length-difference on the fiber-breaking stress development in plied rovings is carried out in annular samples made from SVM plied rovings with a linear density of 1,000 mg/m and EDT-10 epoxy binder at various reinforcement tensions. According to statistical data, the mean length difference of this material is 0.97 mm/m with a 17 percent variance. The behavior of the composite and fiber-rupture stress as a function of the specific reinforcement tension at several length-difference values, the feasible domain of fiber-rupture stress realized in a unidirectional composite at a 0.997 confidence level, and the dependence of the pressure vessel's load-carrying capacity on the plied roving-length variation and linear density are plotted. A decrease in the filament-length difference increases the fiber rupture stress and composite breaking stress. The findings show that the length difference is the characteristic which significantly affects the pressure vessel's load-carrying capacity at a unit stress in the reinforcing material realized during the winding of up to 0.25 N x m/mg. Figures 3; references 5.

Structural Characteristics of AlN + Y₂O₃ Ceramics

937D0017A Kiev POROSHKOVAYA
METALLURGIYA in Russian No 8 (356), Aug 92
pp 11-14

[Article by M.A. Kuznetsova, O.A. Shevchenko, I.F. Fesenko, Superhard Materials Institute and Institute of Materials Science Problems at the Ukrainian Academy of Sciences, Kiev; UDC 621.762]

[Abstract] The methods of increasing the heat conduction of AlN-based polycrystal materials used for making integrated circuit substrates, primarily by increasing the dissolved oxygen concentration or using sintering activation additions, such as Y₂O₃, are discussed, and it is noted that the structure of the highly conducting AlN + Y₂O₃ materials is still poorly known. Thus, polycrystalline samples produced from an AlN powder made by plasma chemical (PKhS) and furnace (PS) synthesis and from commercial yttrium oxide (5 percent) and sintered at 1,850°C in a nitrogen medium or compacted at 1,700-1,900°C at a 25 MPa pressure in graphite molds are investigated. The sample thermal conductivity is measured at room temperature using Ni and Cu standards for calibration, microstructural studies are carried out by transmission electron microscopy using thin foils and replicas, and an X-ray diffraction analysis is conducted. Pure and activated AlN hot compaction curves are plotted. An analysis shows that addition of the activator increases the sintering rate under hot compaction; a liquid phase forms above 1,800°C according to the diagram. The ceramic structure depends on the origin of the original AlN powder and sintering duration. A liquid phase forms during both types of synthesis at 1,800°C. An increase in the grain size at a 90 min exposure and the presence of fine grains in the liquid phase areas attests that structural transformations occur through the liquid phase by the recrystallization mechanism whereby large grains fracture and the small ones

grow. AlN powder made by furnace synthesis is suggested for producing ceramics with a 180 W/m x K thermal conductivity; ultradisperse ceramic powders are also recommended. Figures 4; references 3: 2 Russian, 6 Western.

Simulation of Fe-Zr Melts' Paramagnetic Susceptibility

937D0019B Moscow METALLY in Russian No 4,
Jul-Aug 92 pp 36-39

[Article by O.Yu. Sidorov, O.Ye. Shlokhina, E.A. Pastukhov, Yekaterinburg; UDC 669.15:537.6]

[Abstract] The lack of sufficient experimental data on the magnetic properties of solid and liquid alloys with transition *d*-metals and the uncertainty of theoretical studies of the temperature-concentration behavior of the magnetic susceptibility of reciprocal *d*-metal alloys prompted an attempt to describe analytically the concentration dependence of magnetic susceptibility of liquid Fe-Zr alloys using information about their electronic and atomic structure. Experimental and theoretical isothermal curves of the magnetic susceptibility and chemical short-range order parameter of liquid Fe-Zr alloys at various temperatures are plotted, and formulae are derived for calculating the paramagnetic susceptibility of *d*-metals. The electronic structure is modeled using the continued fraction method which makes it possible to take into account the principal characteristics of the atomic and electronic structure of transition *d*-metals and alloy formation; to this end, a self-consistent tight coupling model is used. It is speculated that the proposed approach may serve as an adequate basis for developing a model for assessing the concentration dependence of magnetic and thermodynamic properties of reciprocal melts of *d*-metals in the framework of their atomic and electronic structure. Figures 1; tables 1; references 18: 14 Russian, 4 Western.

Modification of Magnetite Films by Complexonates

927D0257E Moscow ZASHCHITA METALLOV
in Russian No 4, Jul-Aug 92 (manuscript received
5 Aug 91) pp 586-592

[Article by Yu.I. Kuznetsov and T.I. Bardasheva, Physical Chemistry Institute, Russian Academy of Sciences; UDC 620.193.01:553.311]

[Abstract] The authors of the study reported herein studied the formation of magnetite layers on the surface of low-carbon steels in neutral ammonium nitrate electrolytes containing complexonate-type inhibitors. Their primary objective in so doing was to find a way of replacing the conventional alkaline bluing of steel that is generally conducted in concentrated solutions and that is thus undesirable from an ecological standpoint. To produce the oxide (magnetite) coatings for the studies, the researchers used cylindrical specimens of St3 steel with an area of 10 cm². The specimens were cleaned with emery paper, degreased in ethanol, and immersed into an oxidizing bath so that the ratio of the unmixed solution to its surface was between 6.0 and 6.5. The temperature of the nitrate solutions ranged from 95 to 98°, while that of the nitrate-alkaline solution ranged from 130 to 140°. In most of the experiments, the oxidation lasted 40 minutes. The oxidized specimens were rinsed in distilled water, dried with filter paper, kept for at least 16 hours in an exciter over calcium chloride, and then weighed. The protective properties of the resultant coatings were evaluated visually and based on the mass loss incurred by each specimen after eight hours of testing on an Oka corrosion meter. The protective properties of the oxide coatings were also determined by immersing the specimens into a copper sulfate solution (20 g/l) for 30 seconds, rinsing them, drying them, and checking for the presence of released copper on their surface. The thickness of the magnetite films was estimated by the mass loss incurred by each specimen after removal in an acetone solution of HCl. The potentials were measured relative to saturated a silver chloride electrode, and the polarization curves were taken in a borate buffer solution with a pH of 7.4 with and without an additive of 0.005 M sodium chloride and corrosion inhibitor (nitrite or sodium phenylanthranilate). Polarization of the electrodes (0.2 mV/s) was begun after a quasi-stationary potential had been reached, which was 15 to 20 minutes after the electrode had been immersed into the study solution. The oxide coatings produced in the three study solutions (solution 1 = 5 g/l NH₄NO₃; solution 2 = 1.5 g/l Al(NO₃)₃; solution 3 = 750 g/l NaOH and 150 g/l NaNO₃) and differed markedly from the standpoint of protective properties and film thickness. The thickest films (1.7 to 1.9 μm) were formed in an acidic (pH 4.0) aluminum nitrate solution, but their protective properties were rather weak. As expected, the films produced by alkaline bluing (in solution 3) had the best protective properties even though the thickness of the magnetite layer did not exceed 0.85 μm. From an ecological standpoint, the best

alternative is oxidation of steel in a neutral, relatively diluted (5 g/l) solution of NH₄NO₃ containing small amounts of zinc oxyethylidene diphosphonate to increase coatings' protective properties. The complexonate-modified oxide coating tested was found to also manifest improved corrosion resistance when subjected to the activating effect of chlorides. When oxidized steel will likely come into contact with chloride solutions, it is best to add the inhibitor not only to the oxidizing solution, but also to the corrosive solution. Figures 4; references 8; Russian

A Set of Methods To Evaluate Anticorrosion Coatings for Equipment Used To Store and Transport Petroleum Products

927D0257H Moscow ZASHCHITA METALLOV
in Russian No 4, Jul-Aug 92 (manuscript received
23 Nov 90) pp 654-658

[Article by N.N. Zakharova, G.T. Vigant, and V.A. Mityagin; UDC 620.193]

[Abstract] The authors of this article have proposed a set of methods that is adequate for making an aggregate evaluation of the set of indicators characterizing the suitability of an organic anticorrosion coating for use in contact with petroleum products. The currently used set of test methods for equipment designed for use with petroleum products (as stipulated in All-Union State Standard [GOST] 9.409-88) calls for the standard tests to determine a) resistance to the effect of petroleum products and climate factors of regions with a tropical, moderate, or cold climate; b) resistance to the effects of detergents; and c) resistance to the effects of steam. It is the contention of the authors that despite the positive aspects of the aforesaid standard methods, they cannot give a complete picture of the behavior of coatings when they are used on the inner surface of tanks designed to hold petroleum products. Because such coatings must withstand the simultaneous effects of each of the elements in the three-phase system consisting of fuel, tank-bottom water, and a gas-and-air phase, the authors have proposed that coatings for equipment used to store and/or transport petroleum products also be subjected to special tests that would make it possible to estimate their protective properties when subjected to a steam-and-gas atmosphere, a petroleum product, or tank-bottom water in cases of a temperature differential ranging from +60° to -25°. The main evaluation criterion in the proposed set of methods is a summary quantitative estimate of the change in coatings' protective properties in accordance with GOST 9.407-84 that considers the relative weight of each of the following types of destruction: dissolution, crumbling, cracking, peeling, appearance of bubbles, appearance of foci of corrosion damage on a surface, and appearance of under-film damage. In addition to this evaluation criterion, the proposed set of methods also calls for determination of the coating's capacitance-resistance characteristic and for a determination of changes in the coating's adhesion, elasticity, and impact strength. The mutual effect of coatings and fuels is

determined experimentally by estimating the change in the amount of free film by using the indicators "swelling" and "washoff" as evidence of the sorption-desorption processes at work in coatings. A method of evaluating the performance properties of fuels after contact with a coating applied to a metal surface has also been included in the set of evaluation methods as a way of predicting permissible times for which fuels may be stored in tanks with given test coatings. The given fuel's chemical and thermal stability, its accumulation of metal and mechanical impurities, and its conductivity and stability are determined. After describing their proposed comprehensive set of testing methods, the authors present tables detailing the results of tests of coatings stability when exposed to the effects of corrosive media and the effects of coatings on RT jet fuel. Examples illustrating the implementation of the proposed coating evaluation procedure are also presented. Tables 2; references 6: Russian

The Corrosion and Protective Properties of Coating Made With an Amorphous Chromium-Phosphorus Alloy

927D02571 Moscow ZASHCHITA METALLOV
in Russian No 4, Jul-Aug 92 (manuscript received
20 Jun 91) pp 659-664

[Article by Ye.G. Vinokurov, V.N. Kudryavtsev, V.V. Bondar, and Ye. Borsh, Moscow Chemical Technology Institute imeni D.I. Mendeleev; UDC 621.357.7:669.268]

[Abstract] The authors of the study reported herein conducted X-ray phase and thermographic analyses of an electrolytic chromium-phosphorus alloy in order to determine the bounds of the stability of its amorphous state. Specifically, they studied the amorphicity, protective properties, and corrosion resistance of coatings of a chromium-phosphorus alloy that had been electrodeposited onto a steel (08kp) substrate with a roughness of about 0.4 to 0.5 μm . The electrolyte used in the studies contained chromium, aluminum, and sodium sulfates along with carbamide and sodium hypophosphate. The electrolysis was performed at a temperature of 35°, the electrolyte had a pH of 1.4, and the current density equaled 45 A/dm². A ceramic diaphragm separated the cathodic and anodic spaces. The chromium-phosphorus alloy's tendency toward passivation was determined by anodic polarization potentiodynamic (5 mV/s) curves obtained in a 0.5-M sulfuric acid solution at room temperature. The study alloy's corrosion resistance was determined on the basis of its rate of dissolution in a 1-M solution of hydrochloric acid. The alloy's rate of dissolution was calculated by the change in the concentration of Cr³⁺ ions in the solution by the atomic absorption method. Each of the study specimens was held for 500 to 700 hours. A Philips X-ray diffractometer was used for the X-ray phase analysis, and a Jeol ISM-50 scanning electron microscope was used to determine microporosity and the micropores' characteristics. The studies performed established that highly corrosion resistant

amorphous chromium-phosphorus alloy coatings are microporous (10^5 to 10^6 cm⁻²) and have a protective ability of about 70 percent even though data regarding relative microporosity would lead one to expect them to have a protective ability between 90 and 95 percent. An analysis of the macroporosity, corrosion potentials, and protective ability of the study coatings reveals that they are all dependent on coating thickness, which is in turn dictated by the formation of cracks in the coating. Further analysis of the data obtained regarding the surface morphology, micro- and macroporosity, and protective ability of chromium-phosphorus alloy coatings confirmed that the latter is dictated mainly by macroporosity and the presence of cracks in the coating. The cracks found to form in the study coatings were deemed the result of the inclusion of hydroxo chromium compounds in the coating. Coating thicknesses of 0.7 to 1.5 μm were found to be optimal from the standpoint of protective ability. A nickel substrate was recommended as a way of increasing the study coatings' protective ability. Figures 5, table 1; references 5: Russian

Producing Protective Zinc Coatings by a Programmable Pulse Current

927D0257J Moscow ZASHCHITA METALLOV
in Russian No 4, Jul-Aug 92 (manuscript received
13 Feb 91) pp 669-674

[Article by V.A. Zabludovskiy, V.I. Kaptanovskiy, A.A. Zabludovskiy, and V.I. Kagan, Dnepropetrovsk Railroad Transport Engineers Institute; UDC 621.357.7:539.2]

[Abstract] The authors of the study reported herein examined the effect that the concentration of the additives DKhTI-102A and DKhTI-104B in a standard ammoniate zinc-plating electrolyte and pulsed electrolysis modes has on the cathode polarization, structure, and protective properties of zinc coatings. The researchers used a standard electrolyte that contained the following (g/l): zinc sulfate, crystalline hydrate, 80 to 100; ammonium chloride, 180 to 200; boric acid, 20 to 25; DKhTI-102A, 80 to 100; and DKhTI-104B, 5 to 10. The pH was varied from 4.5 to 6, and the process temperature was varied between 15 and 30°. The electrodeposition was conducted on different substrates (copper, steel, brass, etc.) in thicknesses ranging from 6 to 30 μm . The process was conducted with a direct current by using 1) the existing technology; 2) a reversing-pulse current with control of the parameters of the forward and reverse pulse bursts and with variation of the reversal parameter from 3 to 10 seconds; and 3) with a programmable pulse current with "pulse width" modulation of the polarizing current. A P-5827M potentiostat was used to record potentiodynamic polarization curves with speeds of 2 to 20 mV/s, and type S1-18 and S1-83 electronic oscillographs were used to take the polarization measurements. An Epiquant microscope was used to study the surface structure of the coatings produced, and a DRON-UM-1 X-ray diffractometer was used to determine the fine structure and crystalline

lattice periods. The studies performed established that increasing the concentration of DKhTI-102A and DKhTI-104B results in a shift in the polarization curves of the resultant coatings to the negative range (from -1.0 to -1.32 V). Increasing the concentration of the two additives, on the other hand, was found to result in a decrease in the threshold current: In an electrolyte without either of the two additives the threshold current reached 4 A/dm²; in a standard electrolyte containing the DKhTI additives, the threshold current ranged from 1.2 to 1.5 A/dm². When the concentration of the DKhTI additives was reduced by an order of magnitude, the threshold current reached 2.5 to 3.5 A/cm². Studies performed by using a pulsed unipolar current established that increasing the pulse-following frequency from 10 to 1000 Hz reduces polarization and raises the threshold current somewhat. Studies of the zinc current efficiency demonstrated that increasing the average direct-current density from 1 to 3 A/dm² results in a decrease in current efficiency from 90 to 55 percent in a standard electrolyte and in a slight worsening of the coatings' external appearance. The use of a programmable pulse current was found to make it possible to reduce the concentration of scarce DKhTI additives required in zinc-plating electrolytes, increase the corrosion resistance of coatings, reduce coatings' porosity in thin layers, and increase the rate at which zinc coatings may be applied. Figures 3, table 1; references 7: Russian

Electrodeposition of Bright Tin-Lead Alloy Coatings

927D0257L Moscow ZASHCHITA METALLOV in Russian No 4, Jul-Aug 92 (manuscript received 4 Feb 91) pp 678-681

[Article by K.M. Tyutina, A.N. Popov, V.A. Zonin, Ye.V. Shurikova, and L.A. Rogovaya, Moscow Chemical Technology Institute imeni D.I. Mendeleyev; UDC 541:138.3:621.357]

[Abstract] The authors of this concise report worked to improve the process characteristics of electrolytes used for electrodeposition of bright tin-lead (POS-50) coatings, which are used as metal-resists in the production of printed circuit boards by the subtractive process. The researchers' primary objectives in conducting the study were to reduce the overall cost of producing the coatings and the amount of scarce brighteners required for the process, simplify the process of synthesizing the coatings, and make it easier to correct and control the electrolyte. Four different versions of the brightener KOSLA-A2, i.e., KOSLA-A2MPP, KOSLA-A2, KOSLA-A2D, and KOSLA-A3, were tested to determine the feasibility of using them in the electrodeposition of POS-60 coatings. The researchers' interest in KOSLA-A2 as opposed to other brighteners generally used to produce bright coatings (ALSOK, MKHTI-M4, BOS-MKHTI) was dictated by the fact that electrolytes based on KOSLA-A2 can be prepared by simply pouring the starting components together without any special equipment and because the synthesis and properties of KOSLA-A2 are not sensitive to either the purity of the raw materials or their

length and conditions of storage. The electrodeposition was performed on copper specimens measuring 2 x 2.5 x 0.2 cm. The current efficiency was determined by a copper coulometer. The distribution of the coating on printed circuit boards was determined by the polished microsection method, the coatings' solderability was determined in accordance with All-Union State Standard 9.302-79, and the stability of the coatings in etching agent was determined by Branch Standard [OST] 107.460092.004.01-86 and visually. The printed circuit board specimens were all found to meet GOST 237552-79. Each of the four brighteners tested resulted in coatings that maintained their solderability with acid-free fluxes without corrosion-proofing for more than 18 months, and the solderability of all of the coatings tested conformed to the requirements stipulated in GOST 9.302 79. All of the coatings maintained their brightness at pH levels above 9.5. When exposed to a copper-ammonium solution, all of the coatings darkened when the pH was below 9.0, but all could be brightened once again in a solution of CS(NH₂)₂ + HBF₄ at 50°. All of the coatings also maintained their brightness in solutions of sodium chlorite, sodium bromate, or solutions based on ammonium persulfate. The electrolytes to which KOSLA-A2MPP, KOSLA-A2, or KOSLA-A2D had been added could be corrected by adding KOSLA-A2 after 30 to 40 A-h/l after a loss of brightness began by adding 0.2 ml/l KOSLA-A2 every 1.5 A-h/l. The electrolyte containing the KOSLA-A3 could be similarly corrected by adding KOSLA-A3 in the same amount at the same intervals. In cases of low current density, the composition of the alloy coating electrodeposited in the electrolytes containing KOSLA-A2MPP and KOSLA-A2 was found to be little dependent on cathodic current density, and the current efficiency of coatings produced in the electrolyte to which KOSLA-A2D had been added was practically independent of the cathodic current density. The lead content of the latter electrolyte even increased somewhat as the cathodic current density increased. A comparison of the cathodic polarization curves recorded when Sn was precipitated from electrolytes containing the additives ALSOK, KOSLA-A2, and STANEX-3N3 revealed that KOSLA-A2 is significantly less effective from the standpoint of inhibiting the cathode process than is STANEX-3N3. On the basis of the said polarization curves, both ALSOK and KOSLA-A2 and ALSOK were classified as only weakly inhibitive brighteners. Figures 3, table 1; references 4: 3 Russian, 1 Western.

Role of Diamond Ultrasonic Hardening-Finishing Treatment in Shaping Surface-Layer Quality

937D0008J Moscow FIZIKA I KHIMIYA OBRABOTKI MATERIALOV in Russian No 4, Jul-Aug 92 pp 112-117

[Article by G.A. Iskhakova, V.P. Gileta, Novosibirsk; UDC 539.89+681.8]

[Abstract] The importance of improving the serviceability of mechanical parts by ensuring an optimum combination of geometric parameters and physical and mechanical properties of the surface prompted the development of diamond ultrasonic hardening-finishing treatment

(AUZO) which forms a principally new layer characterized by a regular micro- and submicrogeometry and a specific structural state which determines its improved performance. The kinematic and dynamic dependence of DUST parameters are considered and an attempt is made to ascertain their role in shaping the quality of the hardened layer. The basic patterns of the DUST process are examined assuming that the ultrasonic tool performs harmonic oscillations, and a formula is derived for describing the tool edge displacement. The kinematic and dynamic characteristics of DUST are interpreted graphically, and the dependence of the static load and hardening depth during DUST on the initial material microhardness and the behavior of the mechanical characteristics of the hardened layer of steel 45 during DUST are plotted. An analysis shows that the total contact load, the magnitude and direction of the relative contacting surface velocity, and the tool feed are the principal factors affecting the DUST process parameters. The relationship between the strength properties and the number of ultrasonic tool impacts per unit of hardened surface is established, and it is recommended that for steel 45, DUST be conducted at an 18 kHz frequency and a part velocity of 70-110 m/min in order to maximize the hardening effect. As the tool frequency increases, the output of the process increases without a decrease in the hardening effect. Figures 3; references 6.

Effect of Mechanical Alloying on Structure and Properties of Plasma Sprayed Coats of $\text{NiCr-ZrO}_2 \times \text{Y}_2\text{O}_3$ Powder

937D0019K Moscow METALLY in Russian No 4,
Jul-Aug 92 pp 209-217

[Article by L.K. Kondratenko, S.V. Chernyakov, V.V. Kudinov, P.Yu. Pekshev, V.F. Shamray, Moscow; UDC 669.245'26+669.296'794'787]

[Abstract] Increasing uses of plasma spraying technology for producing multicomponent high-temperature coats on gas turbine engine parts are noted, and the effect of mechanical alloying on structure and properties of plasma sprayed $\text{NiCr-ZrO}_2 \times \text{Y}_2\text{O}_3$ powder coats is examined. To this end, a model alloy containing 20 percent Cr and 30 percent ZrO_2 which is a prototype of the composite powders or mechanical mixtures used for making single-layer multicomponent and multilayer metal ceramic coats is analyzed. The research procedure involves a radiographic and metallographic analysis and optical and electron microscopy. The X-ray study is carried out in a DRON-3.0 diffractometer in CuK filtered radiation. The samples for the study are produced by mechanical alloying in a planetary Pulverizette-5 ball mill by Fritsch GmbH and plasma spraying using a Plasma-Technik AG unit. All calculations, including coherent scattering area (OKR) analyses, are made by approximations. The effect of the ball mill treatment duration on the substructural features of Ni-Cr alloy in the powder material and in the coat is summarized, and the crystal lattice constant variations of individual components as a function of the milling duration and diffraction patterns of the coats made from powders milled for two and eight hours are plotted. The study confirms that the Ni-Cr alloy lattice constant increase with the milling duration is due to the oxygen diffusion into the Ni-Cr alloy solid solution and that the volume fraction of the oxide forming in the coat increases with the milling duration. Despite the large size of ZrO_2 inclusions, their homogeneous distribution ensures the high high-temperature and erosion resistance in acid media and cyclical strength. Moreover, microcrack formation in plasma sprayed coats is less intensive and the crack spread is hindered by the elastic Ni-Cr alloy matrix with a uniform fine structure. Figures 5; tables 1; references 5: 1 Russian, 4 Western.

Cubic Boron Nitride-Based Composite Oxidation

937D0017C Kiev *POROSHKOVAYA METALLURGIYA*
in Russian No 8 (356), Aug pp 18-21

[Article by E.I. Golovko, V.S. Neshpor, V.A. Ponomarenko, G.N. Makarenko, V.B. Fedorus, I.I. Timofeyeva, I.G. Donets, Institute of Materials Science Problems at the Ukrainian Academy of Sciences, Kiev; UDC 621.762]

[Abstract] Oxidation resistance of an elbor borazon-based composite with a B_4Si addition is investigated. To this end, composite material samples containing 70 percent of cubic boron nitride (elbor borazon) and 30 percent of boron silicide produced by hot compaction of a mixture of B_4Si and β -BN powders with a size of $<2 \mu m$ in an anvil-type high pressure unit at a 1,950-2,000°C temperature and 15 GPa pressure for 15 min are used. The samples have a $3.5 g/cm^3$ density at a <0.5 percent open porosity. An X-ray diffraction analysis reveals no more than 3 percent of other phases. The cutting properties of the sample are tested on steel KhVG with an HRC = 52-54 hardness at a 160 m/min cutting speed and a 0.5 mm and 0.07 mm/RPM cross feed and longitudinal feed, respectively; the wear did not exceed 0.09-0.11 mm. The oxidation resistance is examined in powdered samples produced by compact grinding and in compacted sample under static conditions. Thermogravimetric oxidation curves of the composite and its components, differential thermal and differential thermogravimetric oxidation curves, kinetic oxidation curves of BN and composite, and kinetic oxidation curves of the boron silicide addition at various temperatures are plotted. An analysis shows that oxidation commences at 840°C and is characterized by a small mass gain up to 1,050°C; the rate intensifies above 1,050°C and above 1,200°C, the loss of mass becomes dominant. The oxidation process is accompanied by the B_2O_3 , nitrogen, and nitrous oxide formation. The findings also indicate that B_4Si oxidation has a dominant effect on the oxidation process and the silicide concentration addition increases the oxidation resistance. The

borosilicate glass forming in the process increases the scaling resistance. Figures 4; references 4.

Structure and Atomic Dislocation Mechanisms of Al- Al_9Co_2 Composite Fracture

937D0019J Moscow *METALLY* in Russian No 4,
Jul-Aug 92 pp 185-190

[Article by V.A. Yermishkin, R.M. Sofronova, M.M. Golubkova, A.M. Leksovskiy, Yu.A. Fadin, Moscow; UDC 669.018-419.8]

[Abstract] The factors which determine the good mechanical properties of composites (KM) are discussed, and it is noted that the composite fracture and straining mechanisms at a deeper atomic dislocation level are still not well understood while *in situ* experiments are fraught with difficulties and require that the material under study be a microcomposite. Flaky and fibrous model composites produced by oriented crystallization of the Al-Co alloy in which the Al matrix is reinforced with Al_9Co_2 intermetallic fibers are examined by transmission electron microscopy (TEM) under a JEM-200A electron microscope at an accelerating potential of 150 kV and under a JEM-100 microscope with a 1 MeV accelerating voltage. The orientational correlations (OS) of Al and Al_9Co_2 lattices are plotted, and a coherent lattice coupling model constructed of the composite components is developed. The study shows that the flaky composite has a layered epitaxial heterostructure. Straining and fracture tests of composite microsamples helped to identify the role of the structural factors in the development of deformation and rupture. It is shown that the dislocation shear mechanism of metallic single crystals is universal and extends to intermetallic compounds while the fracture mechanisms are determined by the character of processes in the matrix and the geometric features of the reinforcing phase distribution. The considerably higher strength of microsamples over macrosamples is attributed to the effect of the scaling factor. Figures 4; references 11: 9 Russian, 2 Western.

Corrosion and Electrochemical Behavior of Titanium Silicides in Acid Solutions

927D0257A Moscow ZASHCHITA METALLOV
in Russian No 4, Jul-Aug 92 (manuscript received
4 Jul 91) pp 545-552

[Article by V.I. Kolotyarkin, V.M. Knyazheva, O.S. Yurchenko, Yu.P. Kolosvetov, V.B. Kozhevnikov, and T.N. Stoyanovskaya, Physical Chemistry Scientific Research Institute imeni L.Ya. Karpov and Kiev State Pedagogical Institute imeni A.M. Gorkiy; UDC 620.193.41:546.821.281]

[Abstract] The authors of the study reported herein examined the distinctive features of the corrosion and electrochemical behavior of compact specimens of the titanium silicides Ti_3Si_3 , $TiSi$, and $TiSi_2$ in H_2SO_4 , HCl , and HNO_3 solutions. The titanium silicides were all manufactured by hot-molding the respective powders that were in turn obtained by direct synthesis from the respective elements in a vacuum of 0.133 Pa at temperatures of 1,200 to 1,500°C. A DRON-1 diffractometer was used to control the phase composition of both the powders and compact silicide specimens. The methods of atomic-absorption spectrometry, photocolormetry, and X-ray photoelectron spectroscopy were used to study the aforesaid compounds in the cases of potentiodynamic and potentiostatic polarization. The studies performed established that all of the titanium silicides studied are more corrosion resistant than titanium in the range of potentials of its active dissolution and active-passive transition. $TiSi_2$ was found to manifest an especially high level of corrosion resistance. The good corrosion resistance of all of the silicides tested was attributed to the high strength of the covalent Ti-Si and Si-Si bonds. The study titanium silicides were found to manifest a high tendency toward passivation and passive-state stability in acid solutions (including in the presence of chloride ions). The principal anodic process in the potential range studied was determined to be that of dissolution of the titanium from the $TiSi_2$ metal sublattice. $TiSi_2$ (titanium disilicide) was found to be an especially promising corrosion-resistant material for use in acidic oxidation- and reduction-type media. The only drawback of the titanium silicides studied that was discovered is their elevated brittleness. The authors conclude by stating that this brittleness may be reduced by using the study titanium silicides in the form of a composite with a plastic corrosion-resistant metallic interlayering. The titanium silicides studied were also recommended for use as anticorrosion surface layers on substrates of plastic building material. Figures 3, tables 2; references 17: 14 Russian, 3 Western.

A Study of the Kinetics of Anodic Film Formation on Titanium in Perchlorate Alcohol Media

927D0257B Moscow ZASHCHITA METALLOV
in Russian No 4, Jul-Aug 92 (manuscript received
15 May 91) pp 553-558

[Article by O.N. Nechayeva, V.P. Grigoryev, and A.A. Popova, Rostov State University and Physical and

Organic Chemistry Scientific Research Institute, Rostov State University; UDC 620.193.47]

[Abstract] The authors of the study reported herein examined the kinetics of the formation of anodic films on titanium in perchlorate alcohol media. For their studies, the researchers used 0.1 M solutions of $LiClO_4$ in methanol, ethanol, propanol, and butanol. Chemically pure anhydrous $LiClO_4$ solutions were dried in a vacuum cabinet at 120°. Their potentiodynamic curves (5 mV/s) were taken on a PI-50-1 pulse potentiostat with a PDP-4.002 two-coordinate potentiometer. A P-5827M potentiostat with a KSP-4 potentiometer was used to take the chronoamperograms. A saturated silver chloride electrode referenced to a standard hydrogen electrode served as the standard electrode. The disk electrode's rotation frequency was varied from 830 to 3,900 rpm. Before the polarization measurements were taken, the titanium (VT1-0) electrodes (area, 1 cm²) were treated in a 1:2 mixture of concentrated HF and HNO_3 , rinsed with bidistilled water, and dried with filter paper. The measurements were taken at a temperature of 25°. The potentiodynamic curves recorded for the titanium are characteristic of easily passivated metals. The linear correlation of $lg i$ in different potential ranges with the Taft constant σ^* characterizing electron density in the reaction center of the functional group was taken as evidence of the applicability of the principle of a linear relationship between the free energies and the study processes. The inverse proportionality of the logarithm of the current density to the dielectric constant was taken as an indication of a link between the characteristics of anodic dissolution and the electrostatic properties of the medium. A study of the dependence of i and τ at different potentials demonstrated that a decrease in the current over the time characterizing the development of a passive state on the electrode's surface is also observed when E is more negative than the critical potential on the potentiodynamic curve. The range $E < E_{cr}$ was thus found to correspond to a conditionally active, or to be more exact, conditionally passive state that is strengthened during anodic polarization, which is reflected by the continuous decrease in current. The kinetics of the formation of films was, as in aprotic media, found to depend on the location of the alcohol in the homologous series. The critical passivation potential decreased from methanol to butanol, whereas the rate of film propagation along the electrode surface increased, and the transition from a logarithmic to a parabolic film formation law was found to accelerate in the process. Figures 4, tables 3; references: Russian

The Dissolution of Binary Alloys of Titanium With Tungsten

927D0257C Moscow ZASHCHITA METALLOV
in Russian No 4, Jul-Aug 92 (manuscript received
19 Mar 91) pp 559-563

[Article by A.I. Shcherbakov, I.V. Kasatkina, N.D. Tomashov, G.M. Plavnik, and T.P. Puryayeva, Physical Chemistry Institute, Russian Academy of Sciences; UDC 620.193.01:546.821]

[Abstract] The authors of the study reported herein examined the kinetics of the active dissolution of the system Ti-W. Alloys of titanium and tungsten that contained 1, 3, 5, and 10 percent (mass) tungsten in the charge were studied in a poured state in a solution of 5 N H_2SO_4 that had been deaerated with argon for 0.5 hours before and during the entire course of the experiment. The amount of titanium dissolved was determined by photocolorimetric analysis of the solution. The analysis method had a sensitivity of 10^{-7} g/cm³. The rates of dissolution of titanium from the study alloys were investigated at two fixed potentials, -0.25 and -0.4 V in relation to the potentials at 3, 50, and 70°. Preliminary studies established that for pure titanium, a potential of 0.4 V corresponds to active dissolution of titanium and -0.25 V is the critical passivation potential. The sample alloys studied all had an α -structure. The studies performed established that the mechanism of active dissolution of Ti-W alloys is as follows. In the first few minutes, the surface of the alloy becomes enriched with tungsten atoms thanks to the predominance of titanium dissolution. Next, a dynamic equilibrium is established between the amount of tungsten atoms moved to the surface (but still bound with the alloy lattice by electrons) and the number of atoms crystallized on the alloy's surface into a powder tungsten-rich phase. This phase appears in the form of a dark loose layer on the surface and has no noticeable effect on the rate at which the alloy dissolves. The kinetics of the alloys' dissolution are determined primarily by the ratio of surface concentrations of titanium and tungsten that have not lost their electronic contact with the base. The rate at which the study alloys underwent active dissolution was found to decrease as their tungsten content increased. This was explained in terms of the blocking effect of the tungsten atoms. Figures 2; references 6: 5 Russian, 1 Western.

The Role of Ion-Exchange Reactions in the Passivation and Local Corrosion of Metals

927D0257D Moscow ZASHCHITA METALLOV
in Russian No 4, Jul-Aug 92 (manuscript received
30 Jan 91) pp 564-574

[Article by A.P. Nazarov, M.A. Petrunin, and Yu.N. Mikhaylovskiy, Physical Chemistry Institute, Russian Academy of Sciences; UDC 620.193.01]

[Abstract] The authors of the study reported herein examined the role of ion-exchange reactions in processes of the passivation and local corrosion of metals. A999 aluminum, MG90 magnesium, and St3 carbon steel were used in the studies. The surfaces of all of the study specimens were modified by silanes. The researchers' primary objective was to determine the effect of an electrolyte's anionic composition on the electrochemical behavior of the study specimens. The electrochemical and corrosion studies performed established that the presence of negatively charged groups in an electrolyte results in inhibition of the metals' depassivation, whereas the presence of positively charged groups results

in activation of depassivation. The charge and ion-exchange properties of the metal surface were also found to play a role in depassivation processes. Specifically, an analysis of the effect of the charge of the metal surface on pitting formation indicated that inhibiting depassivation requires the creation of surface hydrolytically stable phases carrying a negative charge and possessing cation-exchange properties. On the basis of the studies performed, the researchers developed a model of depassivation of metal due to the migration of L^{-n} anions through an oxide-hydroxide metal film (in other words, an ion-exchange mechanism of absorption and migration through an anion-exchange membrane to the Me/MeO_n interface). Figures 6; references 42: 9 Russian, 33 Western.

The Water Permeability of Carbon Steel in Acidic Hydrogen Sulfide-Containing Media

927D0257F Moscow ZASHCHITA METALLOV
in Russian No 4, Jul-Aug 92 (manuscript received
7 Aug 90) pp 615-619

[Article by M.N. Fokin, M.B. Lopatina, and T.P. Purveyeva, Physical Chemistry Institute, Russian Academy of Sciences; UDC 620.194.2]

[Abstract] The authors of the study reported herein examined the water permeability of U8A carbon steel in 1 M hydrogen sulfide-containing sulfuric acid during controlled cathodic and anodic polarization. The experiments were performed in a two-chamber Devanathan cell into whose diffusion section 1 M of an alkaline solution had been poured. The diffusion side of the membrane was coated with a layer of palladium, and its potential in the alkali relative to the saturated silver chloride electrode was kept at +0.2 V. After a constant background current (not exceeding 0.05 A/m²) had been established, the hydrogen sulfide-saturated acid solution was poured into the polarization chamber until the required concentration was achieved. The change in polarization current over time on both sides of the membrane was recorded during potentiostatic polarization of the working side of the membrane. At a potential of -0.2 V, the addition of 5 mM H_2S to the solution delayed the establishment of a stationary water permeability regimen somewhat; however, the stationary flow of hydrogen through the membrane increased eightfold. A further decrease in the potential resulted in a shortening of the incubation period; however, the stationary flow of hydrogen increased by yet another factor of 1.5 at a potential of -0.25 V. The fact that it did not increase further was explained in terms of the fact that the threshold of the increase in activity of the adsorbed hydrogen on the working surface of the membrane had been reached. When cathode polarization of an electrode in acidic solutions without hydrogen sulfide is increased, the hydrogen penetration rate generally increases. In the hydrogen sulfide-containing sulfuric acid solutions studied, however, the flow of hydrogen through the membrane was found to not depend on the amount of the cathode potential shift, which means that it did not

depend on the hydrogen ion discharge current either. This was found to be the case all the way to -0.8 V. In a solution containing 4 mM hydrogen sulfide, the threshold stationary hydrogen flow was reached beginning at the free-corrosion potential (-0.25 V), and in the case of an H_2S concentration of 60 mM it was reached at even more positive potentials. Within the framework of the series of experiments conducted with different hydrogen sulfide concentrations (5 to 70 mM) in a 1-M sulfuric acid solution, the researchers were able to demonstrate that in U8A steel at the free-corrosion potential, hydrogen sulfide begins to act as a stimulator of microvolumetric selective corrosion beginning at a concentration of 10 mM, which is to say that it is a progressively effective promoter of hydrogen absorption. A linear correlation was discovered between a high rate of high penetration of hydrogen into steel and susceptibility of the said steel to embrittlement during low anodic shifts in electrode potential. Figures 4; references 3; Western

Hydrogen Absorption by 65Mn Steel During Corrosion in Hydrogen Sulfide-Containing Media

927D0257G Moscow ZASHCHITA METALLOV
in Russian No 4, Jul-Aug 92 (manuscript received
27 Feb 91; after revision 27 May 91) pp 620-624

[Article by T.Z. Akhmetov, G.A. Beysembayeva, D.S. Mukanov, and N.G. Krapivnyy, Kazakh State University, Alma-Ata, and Dnepropetrovsk Chemical Technology Institute; UDC 620.193]

[Abstract] The authors of this article worked to develop a mathematical model of hydrogen absorption by 65Mn steel during corrosion in hydrogen sulfide-containing media. In order to develop their model, the researchers conducted an experiment to study the effect of selected inhibitors on the process of hydrogen absorption by steel in a hydrogen sulfide medium. The experiments were performed in a two-section electrochemical cell with a horizontal membrane. The cell's cathode space was filled with corrosive medium, and the diffusion space was filled with alkali solution. The diffusion side of the membrane operated in a potentiostatic hydrogen ionization mode, and the ionization current characterized the rate of diffusion penetration of the absorbed hydrogen. The membrane had an area of 20 cm², a thickness of 0.05 cm, and was made of 65Mn steel. A 3 percent NaCl solution saturated with H_2S under a pressure of 0.1 mPa was used as the corrosive medium. In some of the individual experiments, the H_2S concentration was varied and controlled iodometrically. Polydimethyldiallyl ammonium chloride and Sever 1 (a commercial hydrogen sulfide corrosion inhibitor representing a mixture of polyalkylpyridines) were used as inhibitors. The experiments performed established that increasing the hydrogen sulfide concentration resulted in an increase in penetration speed and in stationary ionization current (confirming that the threshold surface hydrogen saturation on the incoming surface of the membrane had been reached). The experiments were found to be consistent with existing theory. Thanks to the fact that they made it

possible to switch from relative units to dimensional units, however, the experiments offered the additional benefit of giving the researchers an idea of the magnitude of i_{∞} and its dependence on rate constant. As inhibitor was added to the solution, the stationary currents of hydrogen penetration decreased in a regular fashion, thus confirming a decrease in hydrogen absorption by the incoming surface of the steel. The time required for the kinetic curve to reach a plateau was increased. This increase was attributed to a suppression of the rate at which the steel corroded. After processing the experimentally obtained dependences, the researchers were able to conclude that the main parameters characterizing the behavior of the study system are the concentration of atomic hydrogen at the membrane's inlet (C_H^0) and the constant of the rate at which the electrode surface filled with atomic hydrogen (k). The experiments performed thus enabled the researchers to consider both the kinetics of the filling of the steel's surface with atomic hydrogen and the kinetics of hydrogen diffusion in the solid phase when developing their model. The authors concluded by stating that additional information regarding the mechanism of the effect of surfactants on the process of the corrosion of steel in a hydrogen sulfide-containing medium may be obtained by comparing the relative changes in C_H^0 and k and that additional research is needed to determine the effect of other process parameters on k . Figures 2, tables 4; references 6: 4 Russian, 2 Western.

The Corrosion and Electrochemical Properties of 03Cr25Ni9MoCuTiL Steel

927D0257K Moscow ZASHCHITA METALLOV
in Russian No 4, Jul-Aug 92 (manuscript received
7 Aug 90) pp 675-678

[Article by A.S. Zuyeva, V.A. Kalinichenko, and G.P. Chernova, Physical Chemistry Institute, Russian Academy of Sciences; UDC 620.193:669.15-194]

[Abstract] The authors of this concise report compared the electrochemical behavior and corrosion resistance of the new steel 03Cr25Ni9MoCuTiL with those of the alloy EI-943L. 03Cr25Ni9MoCuTiL steel contains the following (percent by mass): 0.03 C; 25 to 26 Cr; 8-10 Ni; 2.5 to 3.0 Mo; 3.0 to 3.5 Cu; 0.5 to 0.8 Si; 0.8 to 1.0 Mn, and 0.3 to 0.7 Ti. It is classified as an austenite-ferrite steel and, for all practical purposes, contains equal parts (50 percent) of each phase. Specimens of 03Cr25Ni9MoCuTiL steel were hardened from a temperature of 1,100 to 1,150°; they were held for two hours and then cooled in water. Next, the specimens were subjected to electrochemical-corrosion studies in sulfuric acid solutions (15, 35, 70, and 93 percent) at temperatures of 60 and 80°. A P-4848 potentiostat was used to record the specimens' anodic and cathodic potentiodynamic curves (4, 0.8, and 0.2 mV/s). Unlike the alloy 06CrNi28MoCuTiL, the steel 03Cr25Ni9MoCuTiL has two active dissolution peaks in its potentiodynamic curves recorded in sulfuric acid. The presence of these two peaks is related to the steel's two-phase nature: the

first peak belongs to its ferrite phase, and the second belongs to its austenite phase. Corrosion tests conducted in 15, 35, and 93 percent sulfuric acid solutions established that 03Cr25Ni9MoCuTiL steel and the alloy EI-943L have virtually identical corrosion rates (both of which are considered acceptable for cast steels and alloys, i.e., under 0.5 mm/year). In 70 percent H_2SO_4 solutions, the new 03Cr25Ni9MoCuTiL steel was found to corrode more than the alloy 06CrNi28MoCuTiL and

should thus not be used in such solutions. The high corrosion resistance of the new steel that was observed in 15 and 35 percent H_2SO_4 solutions at 60 and 80° was attributed to its passivity. The new economically alloyed steel 03Cr25Ni9MoCuTiL was thus found to be a suitable substitute for the more costly 06CrNi28MoCuTiL (EI-943L) in most sulfuric acid solutions and may thus be used as a building material. Figures 2, table 1; references 4: 3 Russian, 1 Western.

Filtering of Liquid Smelting Products Through Blast Furnace Tuyere Zones

937D0013A Moscow IZVESTIYA VYSSHIKH UCHEBNIKH ZAVEDENIY: CHERNAYA METALLURGIYA in Russian No 7, Jul 92 pp 11-15

[Article by W. Sabela, R. Budzik, Czenstochowa Metallurgical Institute, Poland; UDC 669.162.26]

[Abstract] Existing views on the behavior of liquid smelting products in the blast furnace whereby they do not enter the coke combustion zones in front of the air tuyeres are discussed, and the concept of the dry zone above the tuyere chambers is introduced. The inconsistency of published data on the filtering of liquid melting products through the blast furnace tuyere zones prompted a study of the actual pig iron and steel filtering paths in the blast furnaces. A study of the coke combustion process in a vertical furnace with a 160 mm diameter conducted at the Gliwice Metallurgy Institute in Poland are summarized, and the experience accumulated at various ferrous metallurgy enterprises, e.g., by Kondoh, Konishi, *et al* at Chiba in Japan and by Greuel, Hillnhutter, *et al* in Germany is reviewed. Simulation studies conducted in a laboratory using stearine, which is characterized by a gradual change in viscosity with temperature, are reported. The correlation of the stearine temperature and viscosity and the temperature distribution in a model simulating a hearth at a 10 m³/h air blast rate through a tuyere with a 5 mm diameter are plotted. An analysis of experimental and cold hearth model studies shows that they fail to take into account the effect of temperature on the slag and metal melt viscosity; hot model studies as well as experiments in operating furnaces demonstrate that highly heated slag and pig iron are filtered through coke in the peripheral areas over the tuyere zones and through the combustion zones themselves despite a strong effect of the tuyere gases. The kinetic energy of the blast and the temperature distribution in the hearth are shown to be the principal factors affecting the pig iron and slag drop and jet movement in the blast furnace hearth. Thus, mass burning of the air tuyeres at the bottom may be arrested or eliminated by sloping the tuyere axes by 6° downward near the furnace axis. The burning effect is minimized in V-shaped cohesion zones. Figures 11; references: 8 Western.

Effect of Liquid Stirring on Temperature Distribution in Continuously Cast Ingot

937D0013B Moscow IZVESTIYA VYSSHIKH UCHEBNIKH ZAVEDENIY: CHERNAYA METALLURGIYA in Russian No 7, Jul 92 pp 15-17

[Article by V.V. Stulov, Dnepropetrovsk State University; UDC 621.746.51]

[Abstract] The effect of agitation on the solidification process in melts and the duration of the system's two-phase state is discussed, and the temperature distribution in the ingot under continuous casting is simulated

by pouring molten paraffin through two ladle nozzles with one opening in each whereby the ladles are shifted from the mold center toward the opposite wide sides. As a result, the liquid velocity increases in the near-wall areas and the liquid itself is stirred. In performing the paraffin simulation, the Fourier, Froude, and Bio similitude criteria equality condition is met. A schematic diagram of the experiment is cited, and the temperature distributions in the ingot under the simulated conditions and existing continuous casting practices are plotted. The findings demonstrate that casting of liquid through two ladles whereby the jet is directed along the wide ingot sides makes it possible to equalize the temperature distribution across the ingot cross section. The findings may be used in developing and designing devices with stirring in the horizontal continuous casting mold plane. Figures 3; references 4.

Steel Creep During Bainite Transformation

937D0013C Moscow IZVESTIYA VYSSHIKH UCHEBNIKH ZAVEDENIY: CHERNAYA METALLURGIYA in Russian No 7, Jul 92 pp 45-47

[Article by V.G. Leshkovtsev, A.M. Pokrovskiy, Moscow State Technical University imeni N.E. Bauman; UDC 539.374:621.771.07]

[Abstract] Structural transformations occurring during bulk hardening of bainite steel and the shear processes occurring during bainite transformations in steel under loading are discussed, and the deformation developing during the bainite transformation under load is examined in the framework of the problem of residual stressed developing during the heat treatment of steel parts. The study is carried out in an Ala-Too experimental unit (similar to the IMASH 20-75 unit). To this end, plane samples of steel 75Kh2GNMF with an elevated supercooled austenite stability with a 30x2x2.5 mm working side are loaded and examined under creep conditions during heating in a vacuum. The low lagging of the heating device makes it possible to attain a high cooling rate of 100-150K/min in order to produce supercooled austenite. Creep tests involve measuring the resistivity which serves as an indicator of the steel's bainite transformation. A formula is derived for finding the correlation between the resistivity and strain. The bainite and total creep curves, the dependence of the bainite deformation on the conversion degree at various stresses, and the tangential stress distribution in the longitudinal banding cross section are plotted. An analysis of the findings shows that a special type of structural deformation develops during bainite transformations under stress which can be described as creep flow. The creep law variables are derived for analyzing the taut strained state of parts under heat treatment and a formula is derived for finding the creep flow rate tensor components and solving the viscoelastic stress problem of parts under heat treatment. Figures 3; references 8: 6 Russian, 2 Western.

Increasing Resistance of Dies by Substituting Steel 3Kh3M3F With Steel 40Kh With Diffuse Aluminum Layer on its Surface

937D0013D Moscow IZVESTIYA VYSSHIKH UCHEBNIKH ZAVEDENIY: CHERNAYA METALLURGIYA in Russian No 7, Jul 92 pp 53-54

[Article by N.V. Temnogorova, S.A. Vodennikov, V.L. Kropachek, D.Yu. Boguslavskiy, Zaporozhye Industrial Institute; UDC 669.14.018.258:621.793]

[Abstract] The high cost and frequent failures of die parts used in die casting molds prompted an investigation into ways of extending their service life and lowering their cost. To this end, a study of various protective coats on die steel 3Kh3M3F (which itself was a replacement for steel 3Kh2V8F) is carried out showing that aluminum coats applied by diffusion deposition in a cryolite-alumina melt with calcium and magnesium fluoride additions increase the high-temperature strength and resistance of dies substantially. An X-ray diffraction analysis reveals that the up to 240 μm thick coats consist of a solid solution of Al in $\alpha\text{-Fe}$ of excess FeAl_3 phases depending on the heat treatment conditions. The protective coats have a microhardness of 5,510-8,690 MPa while the sample matrices—from 2,780 to 4,700 MPa. The good coat properties prompted a study of the possibility of substituting this steel with cheaper steel 40Kh with a diffusion Al coat. An ionic solution of sodium and aluminum fluoride and chlorides is used for diffusion saturation. X-ray diffraction and metallographic analyses show the presence of a multilayer structure on the samples: an Al-based solid solution with a 450-470 MPa microhardness, a FeAl intermetallic compound, and a diffusion Al layer under the first two, consisting of a Fe-based solid solution with a 4,120-3,400 MPa microhardness. The substitution has proven to be profitable and efficient and resulted in a marginal saving rate of 3.9 ruble/ruble. References 6.

Filtration Refining of Steel To Remove Dissolved Oxygen

937D0013E Moscow IZVESTIYA VYSSHIKH UCHEBNIKH ZAVEDENIY: CHERNAYA METALLURGIYA in Russian No 7, Jul 92 pp 54-59

[Article by E.B. Ten, Moscow Steel and Alloy Institute; UDC 669.046.552.3]

[Abstract] The refining effect accompanying steel filtering, whereby the dissolved oxygen concentration is lowered in addition to removing the nonmetal inclusions suspended in the melt, and the underlying premises of this refining action are discussed. Filtration steel refining is possible due to the fact that the filter's developed surface serves as a heterogeneous backing to which the deoxidation products precipitate from the supersaturated solution. The deoxidation reaction and its mechanism and the filter material participation in the reaction are examined, and a model of the liquid metal jet passing in the pore channel of a granular filter is cited. The effect of the process factors on

the filtration deoxidation refining efficiency is estimated, and the design and experimental values of the filtering efficiency indicators are summarized. The effect of the filter thickness and its granular element size on the change in the dissolved O_2 concentration and the effect of the filtering rate on the change in the dissolved O_2 content in filtered steel are plotted. An analysis confirms that a physical and chemical model of the melt and filter interaction can be used to develop a mathematical description of the filtration refining process. Figures 3; references 10.

On Possibility of Nitrogen Oxidation by Air's Oxygen During Sinter Cooling

937D0013F Moscow IZVESTIYA VYSSHIKH UCHEBNIKH ZAVEDENIY: CHERNAYA METALLURGIYA in Russian No 7, Jul 92 pp 74-75

[Article by T.V. Detkova, A.R. Zhak, Moscow Steel and Alloy Institute; UDC 622.785:541.122.4]

[Abstract] The urgency of lessening the environmental impact of sinter preparation and decreasing the nitrous oxide concentration in the sinter flue gas prompted a thermodynamic study of the possibility of oxidizing nitrogen with air's oxygen by circulating the air through the sinter cake. Equilibrium NO formation reaction constants, equilibrium NO concentrations, equilibrium NO_2 formation reaction constants, equilibrium NO_2 concentrations at various pressures, and the total equilibrium nitrous oxide concentration (NO_x) at various temperatures are summarized. The study confirms the possibility of oxidizing nitrogen with air's oxygen during the cooling of sinter by the air filtered through the cake layer. Tables 1; references 2.

Improving Range of Mechanical Properties of High-Strength Maraging Steels N15F6M5K10 and N12M6K12Kh4T by Ausforming

937D0013G Moscow IZVESTIYA VYSSHIKH UCHEBNIKH ZAVEDENIY: CHERNAYA METALLURGIYA in Russian No 7, Jul 92 p 78-75

[Article by T.R. Lapteva, V.G. Prokoshkina, V.V. Rusanenko, Moscow Steel and Alloy Institute; UDC 621.789:669.15-194.55-157.8]

[Abstract] The possibility of improving the range of mechanical properties of high-strength maraging steels N15F6M5K10 and N12M6K12Kh4T with the help of ausforming (VTMO) is investigated. To this end, instead of regular hardening, the steels are subjected to ausforming with a 80-150 percent straining degree and 30-50 percent cold deformation (KhD). An analysis of the treated samples with a polygonized and recrystallized structure and a refined austenite grain shows that despite the presence of 10-25 percent of γ -phase, the hardness and strength increase in the nonaged state while ductility increases somewhat. After aging by a corrected procedure after ausforming with cold deformation, the complex of mechanical properties improved compared to hardened

steel. The results of a fractographic analysis of the aged sample fractures are consistent with the outcome of mechanical tests: while hardened samples have a mixed brittle-viscous fracture character, the fracture becomes fully viscous after ausforming. Thus, the use of ausforming refines the austenite grain and martensite packets and facilitates a more disperse and uniform α -phase distribution, the development of a planar texture, and the formation of retained austenite as a result of which the hardness and strength as well as ductility and toughness increase both in the aged and nonaged state, making it possible to attain the high-strength state in the steel under study. References 1

Increasing Electrical Equipment Fire Safety at Nonferrous Metallurgy Enterprises

937D0014A Moscow IZVESTIYA VYSSHIKH
UCHEBNIKH ZAVEDENIY: CHERNAYA
METALLURGIYA in Russian No 8, Aug 92 pp 30-33

[Article by V.L. Ivannikov, A.K. Merzlyakov, Fire-Fighting Engineering Institute, Moscow; UDC 669.046:614.842.86]

[Abstract] The high energy demand of the nonferrous metals industry and its heavy reliance on extensive power networks and power equipment prompted an investigation into the fire safety of the electrical systems and cable lines used in gas scrubbing and dust removal. The study is carried out at Moscow's Fire-Fighting Engineering Institute (VIPShT); it addresses the factors which affect the breakout of fires and ignition in process facilities. The degree of fire hazard in various types of electrical equipment is summarized, and it is shown that automation is necessary for fully taking these factors into account. A modular fire safety system (MSPZ) developed at the Fire-Fighting Engineering Institute is described, and its block diagram for a leakage current protection system is cited. The shortcomings of the MSPZ system, which is capable merely of responding to threshold events without analyzing their dynamics, prompted the development of an intelligent system of preventing prefire conditions in electrical units and eventually—the development of a computer-aided system of fire safety at a production facility containing electrical units (ASOPB); the operating principle of the ASOPB system is explained, and its block diagram is cited. The proposed system is highly reliable and efficient and has great functional capabilities. It may operate both off-line and as a part of an integrated computer-aided control system at a nonferrous metallurgy production enterprise. Figures 3; references 1.

Increasing Fire Safety System Efficiency at Metallurgical Enterprises

937D0014B Moscow IZVESTIYA VYSSHIKH
UCHEBNIKH ZAVEDENIY: CHERNAYA
METALLURGIYA in Russian No 8, Aug 92 pp 33-38

[Article by N.G. Topolskiy, V.L. Ivannikov, A.K. Merzlyakov, Fire-Fighting Engineering Institute, Moscow; UDC 669.046:614.842.86]

[Abstract] The underlying principles of the fire safety measures taken at industrial enterprises, especially in the metallurgy industry and stipulated by existing requirements, are outlined; it is noted that the scope of modern metallurgical plants and the speed of metallurgical processes call for implementing a computer-aided facility fire safety system (ASPB) in order to ensure fire protection. The ASPB system is called upon to prevent fires and protect both equipment and personnel; it is an integrated system consisting of subsystems which perform their operations by built-in programs, functionally, and system-wide; each subsystem is tied to a specific controlled entity (TOU) and is open to upgrading. Structurally, the system has a distributed modular-bus architecture on the basis of local networks with distributed data processing and direct network station control functions where the stations are executed as dedicated processors. Control functions are realized by new adaptive control algorithms. A block diagram of the ASPB system is cited, and the purpose and operating principle of each functional unit is explained. The ASPB efficiency is assessed by both qualitative and quantitative indicators; the use of the system makes it possible constantly to monitor operator actions in ensuring fire safety, free personnel from routine and tedious manual labor, and increase staff readiness for action in extreme situations. The most common quantitative estimate of the system's efficiency is its survival probability under alert duty conditions (i.e., being ready for fire). Figures 1.

On Preventing Breakage of Electrodes Thrust Into Nonconducting Charge

937D0014C Moscow IZVESTIYA VYSSHIKH
UCHEBNIKH ZAVEDENIY: CHERNAYA
METALLURGIYA in Russian No 8, Aug 92 pp 40-41

[Article by V.K. Butorin, O.I. Ulanov, A.Ye. Koshelev, Kuznetsk Integrated Iron and Steel Works; UDC 669.046:621.3.035.2]

[Abstract] The breakage statistics of the arc furnace electrode are cited, and it is noted that 30 to 40 percent of all recorded breaks in DSP 100 NZA and DSP 100 I6 furnaces occur when the electrodes are thrust into a nonconducting burden. An analysis of the characteristic electrode/electrode holder system (SEE) vibrations when the electrode is thrust against a nonconducting charge shows that the vibration amplitude in the horizontal plane reflects rather accurately the arc burning characteristics while a decrease in this amplitude from the present mean value indicates an impending collapse. The amplitude begins to decrease some 20-40 s before the breakage, when it drops to zero; the reproducibility of these findings exceeds 90 percent. Thus, it is possible to predict with a high degree of certainty the moment when the electrode is thrust into the nonconducting burden and is about to break by analyzing the electrode/electrode holder system vibrations and take proper control measures to prevent the impending breakage. The 20-40 s lead time is sufficient for taking correcting measures if the process is computer-controlled. Figures 1.

Temperature Diagnostics of Supersonic Flares Developing During Converter Smelting

937D0014D Moscow IZVESTIYA VYSSHIKH UCHEBNIKH ZAVEDENIY: CHERNAYA METALLURGIYA in Russian No 8, Aug 92 pp 44-45

[Article by V.G. Lisiyenko, O.E. Shlik, P.A. Neshcheret, Urals Polytechnic Institute; UDC 669.184.662.61:536.2]

[Abstract] The interaction of the supersonic oxidant jet emerging from the tuyere nozzle in the Fe-C melt typical of converter melting and the effect of the physical and chemical processes in the flare zone on the heat and mass transfer in the steelmaking vessel as well as the effect of the temperature in and near the combustion zone on these processes are considered. One method of diagnosing the temperatures both in the mixing zone and in the flame and the surrounding area is examined. The diagnostic procedure is based on predicting the self-excited oscillatory processes developing in the jet by monitoring the acoustic signal which characterizes these vibrations. The acoustic signal generation mechanism is discussed, and the acoustic spectra of the supersonic jets emerging from the tuyere nozzles during converter smelting at various times after the start of melting at different oxygen rates are plotted. An analysis shows that the spectra have a characteristic peak within a 710-815 kHz frequency range, and it is speculated that the effective temperature which determines the speed of sound in the medium corresponds to the temperature of carbon monoxide—the principal gas liberated in the process. This makes it possible to calculate the vibration wavelength which corresponds to the temperature range in the flare. This correlation makes it possible to assess the combustion front and ambient temperature and thus control the converter process. Figures 1.

Computer-Aided System for Controlling In-Line Plate Mill Quench-Hardening Unit

937D0014E Moscow IZVESTIYA VYSSHIKH UCHEBNIKH ZAVEDENIY: CHERNAYA METALLURGIYA in Russian No 8, Aug 92 pp 45-47

[Article by S.S. Popyvanov, Yu.A. Makagonov, All-Union Scientific Research Institute of Metallurgical Thermal Engineering; UDC 621.78:658.52.011.56]

[Abstract] The reasons for installing the quench hardening units in-line in plate mills are outlined, and a full-size pilot prototype of a system for controlling the operation of the in-line plate mill quench hardening unit developed at the All-Union Scientific Research Institute of Metallurgical Thermal Engineering (VNIIMT) is described. The computer-aided process control system (ASU TP) for the in-line controlled cooling unit makes it possible to control the quench hardening process, select the temperature rate and final temperature, and monitor and control the water rate section by section. The unit serves for cooling plates and semifinished rolled stock during and after rolling in a plate mill. A block diagram of the rolling process with a controlled cooling unit and

a block diagram of the computer-aided controlled cooling unit are cited. The control system has a two-layer architecture: at the lower layer, the mean mass temperature is measured, cooling unit variables are monitored, and the actuating mechanisms are controlled using a TVSO-1 microcomputer while at the higher layer, an IBM PC/XT microcomputer collects and processes data from entities and generates control actions and information accompanying the rolled products to other kindred systems. Although the system does not solve fully all the problems expected of it (it is a pilot unit) and cannot take into account all the nuances of process situations which may arise, it makes it possible to develop future computer-aided systems for controlling quench hardening units with more versatile hardware and software built into local process control networks. Figures 2.

On Sulfide Inclusion Formation in Steels

937D0019C Moscow METALLY in Russian No 4, Jul-Aug 92 pp 80-85

[Article by A.P. Serbin, V.Ye. Sokolov, G.N. Plotnikov, Yekaterinburg; UDC 669.18:546.221]

[Abstract] The effect of sulfur and sulfide inclusions on the mechanical properties of cast and strained steels and the factors affecting the sulfide formation in structural steel are discussed; the effect of Mn, C and Al on the sulfide inclusion formation in carbon steel is examined under the same cooling conditions so as to rule out the effect of the metal solidification rate on the formation of segregation processes and sulfide phase precipitation from the melt. To this end, steel is cast into dry molds; sulfide inclusions are studied by metallographic and X-ray spectral microanalysis (RMSA). The chemical composition of the pilot smeltings and of the sulfide phase in these smeltings is summarized, and the effect of the Mn concentration in medium carbon steel on the Fe and Mn concentration in sulfides is plotted. The study demonstrates that the sulfide phase formation in steel deoxidized with Al is determined primarily by the Mn and C content; the latter expands the solidification interval, increases the sulfur activity in the melt, and accelerates its concentration buildup in the solid-liquid zone liquidus where S interacts with Mn and other sulfide-forming elements. Being a strong deoxidizer, Al removes O_2 from the solution and thus facilitates the sulfide phase formation when the melt is supersaturated with S; Al has a weak affinity for S and thus affects the sulfide phase formation itself only indirectly. Figures 2; tables 2; references 12: 8 Russian, 4 Western.

Mechanism of REM Effect on Isothermal High-Temperature Strength of Fe- and Ni-Based Alloys

937D0019D Moscow METALLY in Russian No 4, Jul-Aug 92 pp 86-93

[Article by A.G. Nikolayev, T.F. Titova, N.V. Penskiy, L.A. Kucherenko, M.M. Verklov, Moscow; UDC 669.245:782:669.017.3]

[Abstract] Current methods of increasing the high-temperature strength of alloys by microalloying and ten traditional interpretations (models) of the mechanism of increasing the high-temperature strength of Fe- and Ni-based alloys by adding small amounts of rare earth metals (RZM) are reviewed; the shortcomings and inconsistencies of these models are noted. The effect of Sc, Y, La, and Dy on the isothermal high-temperature strength of the KhN45Yu, EI652, KhN60VT, Kh20N80Yu3 alloys and NiAl intermetallic compounds within a 900-1,200°C temperature range in the air is examined. The alloys under study represent different classes of superalloys, yet REMs have an identical effect in all cases. Oxidation of the above alloys and intermetallic compound in the air at 900°C and 1,200°C as a function of REM additions is plotted. An analysis of the chemical composition of the alloy surface after heat treatment at varying conditions using thermal gravimetry analysis, optical and scanning electron microscopy, Auger spectroscopy, ESCA, and autoradiography makes it possible to conclude that an additional barrier layer forms in the surface oxide film under the interaction of REM oxides with aluminum and chromium oxides; this additional barrier layer is only 800-1,000 angstrom thick, so its direct detection is difficult and calls for additional studies. It is also speculated that the findings may be applicable to cobalt alloys. Figures 2; tables 2; references 20: 6 Russian, 14 Western.

Effect of Structural State on High-Temperature Ductility of Lead-Doped Steel 08Kh20N9G7T

937D0019G Moscow METALLY in Russian No 4,
Jul-Aug 92 pp 124-130

[Article by S.A. Zinchenko, D.B. Titorov, Izhevsk; UDC 669.1.018.8]

[Abstract] The tendency to hot cracking of stainless austenitic steels containing δ -ferrite and the negative effect of low-melting additions on the high-temperature ductility of these steels prompted an investigation into the combined effect of δ -ferrite and lead additions on the high-temperature ductility of austenitic corrosion-resistant steel 08Kh20N9G7T. To this end, model smeltings are cast into 50 kg ingots whereby the δ -ferrite amount is manipulated within 3.4-13.9 percent by changing the Cr and Mn content. A 0.0040 percent lead microaddition is introduced. The chemical composition of the five model smeltings and structural parameters of model smeltings are summarized, and Auger spectra of the austenite-ferrite interface boundary is plotted. The high-temperature ductility is determined by tensile tests and wedge rolling at the initial hot rolling temperature (1,170°C); the tensile tests are carried out in an IMASH-20-75 machine in an Ar medium. The microstructure is revealed by etching, and the fracture surface is examined under a REM-200 scanning electron microscope; local chemical analysis is conducted by an MS-46 Kameka microanalyzer and Auger spectra are plotted by a JAMP-10S microprobe on metallographic sections. A decrease in the high-temperature ductility and hot rolling corrosion resistance is due to the presence of nonmetallic titanium carbonitride crystallization additions on the ferrite/austenite interface in contact with lead particles. The high-temperature ductility drops linearly with an increase in the Sn concentration after exposure and hot working while low-temperature annealing with subsequent exposure increases the ductility compared to regular heating. New ferrite crystal grains form at the high-temperature heating stage with an interface which is free of the nonmetallic crystallization inclusions. Figures 4; tables 3; references 11: 9 Russian, 2 Western.

Effect of Thermomechanical and Mechanical Treatment on Fatigue Strength of WTi3-1 Titanium Alloy

927D0246A Kiev *PROBLEMY PROCHNOSTI* in Russian No 6, Jun 92 (manuscript received 22 May 91) pp 12-19

[Article by O.M. Ivasishin, P.Ye. Markovskiy, V.N. Dneprenko, V.A. Boguslayev, Yu.S. Nalimov, and O.N. Gerasimchuk, Institute of Metal Physics, Kiev, and Institute of Problems in Strength, Zaporozhye, at Ukrainian Academy of Sciences; UDC 669.295:539.4]

[Abstract] Forgings of the WTi3-1 Ti-W alloy and fan blades made of them were tested on an EVE20/5000 electrodynamic vibrator stand for fatigue strength after rough milling, finish milling, polishing, chemical etching, and finish polishing. They were tested in symmetric load cycles of the fundamental flexural vibration mode until the resonance frequency had dropped 1 percent with attendant formation of a macrocrack. Both structure and texture of two kinds of specimens were examined under a NEOPHOT-32 optical microscope and a JEM-100CX transmission electron microscope: specimens which had remained intact after 2×10^7 load cycles under maximum stress and specimens which had fractured during the very early stages under a stress of the same amplitude. Their crystallographic texture and phase content were examined in a special apparatus with automatic data processing built at the Institute of Metal Physics. An analysis of the S-N curves and microphotographs indicates a variety of operative deformation and cracking mechanisms, which explains the wide spread of fatigue strength and life of similarly treated specimens as well of differently treated ones. Residual compressive stresses after mechanical treatment were found to compensate the detrimental effect of appreciable surface roughness. Hydrogenation of the fresh surface after removal of the defective surface layer by etching is evidently the cause of a sharp decrease of fatigue strength, residual stresses in the new surface layer further enhancing local hydrogen buildup in that layer. Additional degassing-annealing at 720°C under a vacuum of 1 mPa for two hours was found to almost completely restore the mechanical characteristics of this alloy to their pre-etching level. Figures 7; references 6.

Refractory Rare Metals—Sputtering Targets for Microelectronics

927D0252K Moscow *TSVETNYYE METALLY* in Russian No 4, Apr 92 pp 51-54

[Article by A.V. Yelyutin, L.I. Voronenko, and O.Yu. Pasechnik, Giredmet; UDC 669.29:621.382]

[Abstract] The concept of sputtering targets for microelectronics is a comparatively new and very promising area of the use of high-purity rare refractory metals. The main factor dictating the acceptability of such sputtering targets is that they be free of toxic impurities (most notably radioactive elements, molybdenum ions, heavy metals, and gaseous impurities). Nearly all certificates

for high-purity targets made of refractory metals are based on the results of glow-discharge mass spectrometry tests. Neutron activation analysis, while far superior, is still too expensive for regular use at the present time. Available data on the impurity profiles of targets manufactured by the leading Japanese, U.S., and European firms illustrate just how big a discrepancy exists between the "ideal" requirements regarding the impurity profile of targets and the actual quality of commercially produced targets. According to the foreign literature, it is likely that acceptable levels of gaseous impurities will be achieved in the next few years under laboratory conditions but will still not be achieved under commercial conditions. In the former USSR, study of the problem of commercial production of high-purity rare metals began in 1978-1980. During the past few years, the scientific foundations for a process for deep purification of refractory metals have been developed, and process flows for producing high-purity cast metals by combined methods of preliminary and finishing refining have been proposed and implemented. High-purity niobium in the form of ingots and intermediate products for superconducting accelerating structures operating in the microwave wavelength range have come to enjoy the most widespread use. In an effort to meet the growing need for high-purity metals for the above purposes, the Giredmet has created equipment that makes it possible to produce targets in the form of plane rectangular and round ingots for electron beam melting in an oil-less vacuum with a low concentration of gaseous impurities (H, O, N, C) and alkaline and alkaline earth metals. Targets made of high-purity niobium, tantalum, and titanium that were produced on the said equipment have been used and "passed the tests" of various clients. A comparison of these targets with their foreign analogues shows that those produced at the Giredmet have a higher purity. Methods of producing ingots, sheets, and tubes of high-purity niobium (with relative resistivity ratios of 500 to 1,000) for use in creating microwave-range superconducting accelerating system resonators have been developed and assimilated on a commercial scale. The high quality of the materials produced has been confirmed by Prof. H. Padamsee of Cornell University among others. Figures 2, tables 4; references 13: 1 Russian, 12 Western.

Likely Mechanisms of Metal Reduction From Oxide Films by Gaseous Reagents

937D0019A Moscow *METALLY* in Russian No 4, Jul-Aug 92 pp 28-32

[Article by Yu.V. Spichkin, Voronezh; UDC 669.094.2]

[Abstract] The importance of metal reduction from oxide in metallurgy practices and the scarcity of data on certain characteristic features of these reactions (due to the difficulty of study methods) prompted an investigation into the effect of the nickel and copper oxide film thickness and the base conductivity on the mechanism of metal reduction from oxides with gaseous agents and the role of the electron phenomena in the oxide films in the

reduction reaction mechanism. A new interference indication method developed recently for studying both the kinetics and mechanism of a broad range of processes is complemented with ellipsometric measurements of the oxide film thickness in order to examine the reduction reaction mechanism. To this end, 35-150 nm oxide films are reduced on various metallic (Ni, Cu, and Al) and dielectric (mica and quartz) substrates with H_2 and CO. A phase analysis of the films is carried out in an EG-100M electron diffraction analyzer. The oxide deposition procedure is outlined. The study shows that reduction of nickel and copper oxide films on any dielectric base may occur by two likely mechanisms depending on the film thickness: one below the critical thickness and one above. Reduction of oxide films, regardless of the film thickness, is accompanied by the metal phase development in the outer layer, i.e., occurs by the thick film mechanism. The conclusion is drawn that thick oxide film reduction on metal and reduction of oxide metals of any thickness on dielectrics can be regarded as the outcome of the work of a large number of microgalvanic cells located in the oxide's outer layer whereby the oxide/gas interface serves as the anode and the metal phase surface forming in the outer reducing film layer serves as the cathode. The process is divided into an electron phase and an ionic (atomic) displacement phase, i.e., diffusion. The electron phenomena occurring in the oxide lead to the development of space charges and electric field which greatly affect the charged particle diffusion in the reducing oxides. Figures 3; references 10.

Investigation of REM Effect on Carbide Structure of Ni-Based Superalloys

937D0019E Moscow METALLY in Russian No 4,
Jul-Aug 92 pp 94-98

[Article by V.V. Sidorov, V.A. Vertogradskiy, Ye.A. Kuleshova, I.M. Khatsinskaya, Moscow; UDC 669.245:669.13/.15.018.44]

[Abstract] The use of small rare earth metal amounts in superalloys for additionally increasing their phase stability and improving their mechanical properties as well as modifying carbides is discussed, and it is noted that not all REMs modify carbides to the same degree. Consequently, an attempt is made to use modern research and differential thermal analysis (DTA) methods to ascertain the patterns of the carbide morphology behavior in nickel-based superalloys modified by various REMs. To this end, the ZhS6U-VI alloy with and without microadditions of Y and La are used, and the selection of the specific REMs for the study is explained. The Y concentration in the sample before and after the differential thermal analysis is examined using X-ray spectral microanalysis. A fragment of the alloy cooling DTA curves with and without 0.10 percent La and Y additions is plotted, and the chemical composition of Ti, Nb, W, and Hf carbides in the alloy with and without Y additions is summarized. An analysis of the carbide formation during the solidification of the

ZhS6U-VI Ni-based superalloy shows that globular carbides form at high temperatures while letter-shaped carbides form at lower temperatures. It is speculated that the carbides form on a substrate made up of carbides of REMs whose lattice parameters are the closest to those of the MeC carbide lattice. In other words, YC forming by a eutectic reaction at a temperature above 1,500°C serves as a seed for MeC. Figures 2; tables 1; references 13; 12 Russian, 1 Western.

Texture of Thin VT23 Titanium Alloy Sheets

937D0019F Moscow METALLY in Russian No 4,
Jul-Aug 92 pp 119-123

[Article by I.V. Egiz, A.A. Babareko, A.I. Khorev, Moscow; UDC 669.295.5-41:548.735.6]

[Abstract] The development of different crystallographic structures in the plane of rolled titanium alloy sheets, i.e., multicomponent, prismatic, and basal, and the effect of various factors and transformations on the texture formation are discussed; it is noted that the VT23 titanium alloy is in a two-phase state after various types of treatment whereby the volume of the α - and β -phases is sufficient for determining the texture of both phases, making it possible to study the processes occurring in the alloy during hot and warm straining by using both phases' characteristics. Thus, 10 mm thick sheets of the VT23 alloy are annealed at 1,000°C for one hour, cooled in the air, then rolled to a 2 mm thickness with heating to 1,000-1,500°C in 100°C steps. The study is carried out by X-ray analyses with subsequent inverse pole figure (OPF) plotting. A DRON diffractometer is used to plot the X-ray diffraction pattern in CuK radiation. The layer-by-layer behavior of the alloy phases with a shear texture and the cross section β -phase distribution, inverse pole figures of rolled alloy sheet in various cross sections, and the prismatic texture and 1124 orientation fraction texture behavior in central layers of rolled sheets as a function of temperature are plotted. An analysis of the findings reveals that plastic flow under straining with an 80 percent reduction (from 10 to 2 mm) above the polymorphous transformation temperature occurs by means of plane deformation on both surfaces and in the central layers up to 1/6 deep, while volume fractions of the α - and β -phases with a shear texture reach 70 and 90 percent, respectively. Rolling at low temperatures noticeably decreases the volume of material with a shear texture. The findings make it possible to select the rolling temperature of thin sheets of VT23 alloy in order to ensure the formation of crystallographic orientations that are optimal for operation under different conditions. Figures 3; references 2.

Carbide Hardened Powder Molybdenum Alloys

937D0019H Moscow METALLY in Russian No 4,
Jul-Aug 92 pp 139-148

[Article by K.B. Povarova, Ye.K. Zavarzina, Yu.O. Tolstobrov, S.S. Lukyanchikova, R.M. Mikhridinov, A.G. Bochvar, Moscow; UDC 669.28-492.2]

[Abstract] The lower cost and higher practicability of powder alloys vs. vacuum-melted alloys prompted a study of powder molybdenum alloys with carbide hardening in which carbon is bound in refractory stable carbides. To this end, an attempt is made to produce powder wire molybdenum alloys with carbide hardening. Nine alloy compositions are prepared from a Mo powder produced by hydrogen reduction of MoO_3 with Hf, C and B additions in various amounts. The granulometric composition and mean powder particle size are determined by photosedimentation analysis and scanning electron microscopy. The particle size distribution in the initial charge, Hf and Mo distribution in the alloys, the effect of annealing on the short-term strength, elongation, and reduction in area at room temperature, high-temperature strength of strained wire from carbide hardened alloys, and the long-term strength of wires are plotted. A study of the effect of straining on the structure and properties of alloys shows that residual porosity is virtually nonexistent while excess phases formed during sintering form two types of inclusions. An analysis reveals the possibility of partially stabilizing refractory carbides by adding a deoxidizer (B and/or C) to the burden; the alloys have an adequate ductility in the strained state and after annealing. The strength properties are determined by the phase composition; they improve with an increase in the hardening phase content. Great reserves for improving the high-temperature strength characteristics by further increasing the excess phase volume fraction and dispersivity are noted; to this end, preliminary grinding in attrition mills is necessary. Figures 6; references 10: 8 Russian, 2 Western.

Structural Conditions for Maximizing Strength and Ductility of Two-Phase Be-Y and Be-Al Materials

937D00191 Moscow *TSVETNYE METALLY* in Russian No 4, Jul-Aug 92 pp 154-157

[Article by A.A. Chevychelov, B.A. Movchan, Kiev; UDC 669.017.12:539.4.015]

[Abstract] The low ductility of Be at room and subzero temperatures and the futility of known methods of remedying this situation by modification and alloying prompted an experimental study of the dimensional-structural approach to improving the strength and ductility of two-phase inorganic materials whereby the mechanical properties of brittle materials are improved due to precise manipulation of the two-phase structure. This is accomplished by programmed addition of a specified amount of second phase. To this end, Al and Y are selected as the second components since they have a low reciprocal solubility in the solid state and form a simple eutectic system. The dependence of the mean grain size of the second phase and mean free spacing between the particles on the YBe_{13} concentration in two-phase Be- YBe_{13} systems, the effect of the two-phase Be- YBe_{13} material composition on the ultimate strength, yield strength, and elongation at rupture, and the dependence of the mechanical properties of two-phase Be-Al materials on their composition are plotted. A correlation of the structural and dimensional parameters

for maximizing the strength and ductility is established, and it is speculated that the mechanical properties may be further improved (while maintaining a high ductility) by decreasing the Be particle size. The alloys' strength properties improve and ductility decreases almost linearly with an increase in the Be content. It is noted that these relations are typical of simple eutectic systems and follow the law of mixing in a first approximation. Figures 5; references 8: 7 Russian, 1 Western.

Stationary Potentials and Redox Transitions of Gallium and Its Alloys With Silver

937D0020A Moscow *TSVETNYE METALLY* in Russian No 8, Aug 92 pp 15-17

[Article by A.V. Chanturia, V.Ye. Vigdergauz, L.S. Strizhko, Moscow Steel and Alloy Institute; UDC 669.87]

[Abstract] The behavior of a gallium electrode in water is studied by potentiometric titration and cyclical voltammetry, and the observation that this electrode is covered with oxidation products is attributed to the fact that its stationary potential falls within the thermodynamic stability range of gallium oxide. The effect of pH on the stationary potential of gallium, silver, and their alloys, cyclical voltage current diagrams of the stationary Ga and Ag-Ga electrodes in a helium atmosphere at a pH = 1.3, cyclical voltage current diagrams of a stationary Ga electrode in a He atmosphere at pH = 9.2, cyclical voltage current diagrams of stationary Ga and Ag-Ga electrodes in a He atmosphere at pH=9.2, and cyclical voltage current diagrams of stationary Ga and Ag-Ga electrodes in a He atmosphere at pH = 13 are plotted. The experimental cyclical voltage current curve (TsVA) coincides with the thermodynamic potential at $\text{pH} > 11$. An analysis of redox transitions of Ga and its alloys with Ag by the cyclical voltage current diagram method confirms that the transition activity peaks in an alkaline medium; the study is carried out using a PI-50-1 potentiostat. An examination of the anode polarization of Ga in an acid medium reveals no metal dissolution while hydrogen liberation is noted under the cathode polarization of Ga, which is consistent with published data. Active Ga dissolution during the anode polarization is observed in alkaline media whereby the presence of Ag enhances the process. An analysis of the findings attests to the absence of passivating films on Ga at $\text{pH} > 11$. The use of cathode electrochemical treatment is suggested for decreasing pH. Figures 5; tables 1; references 6.

Copper-Bearing Industrial Product Treatment Using Sulfur Dioxide From Pyrometallurgical Production

937D0020B Moscow *TSVETNYE METALLY* in Russian No 8, Aug 92 pp 17-20

[Article by O.A. Lyumet, L.M. Bogacheva, Kh.R. Ismatov, V.M. Piletskiy, Chemistry Institute at the Uzbek Academy of Sciences and Almalyk Mining and Metallurgy Works; UDC 669.33]

[Abstract] The insufficient utilization and recovery of copper-bearing industrial products which may serve as a source of Cu and Ni prompted a study of hydrometallurgical processing methods, and an attempt to develop a technology which makes it possible to maximize the Ni and Zn recovery, ensure selective Cu, Ni, and Zn precipitation in the form of commercial or semifinished products, and create practicable and closed production cycles for processing Cu-bearing products. Salt precipitation from copper, copper-nickel, and copper-zinc solutions using a flue gas with 6-12 percent SO_2 is examined in detail; a preliminary study is carried out in model solutions in order to optimize the copper recovery process. Potentiostatic copper precipitation curves, the dependence of the Cu precipitation degree on various factors, and the Cu and Zn recovery under weakly acidic leaching are plotted. Block diagrams of the Cu and Ni recovery process and copper filter cake reprocessing are cited. Optimum conditions of the Chevreuil salt precipitation from Ni- and Zn-bearing solutions are established: pH = 3.0-3.5, a 75-80°C temperature, and a 150 percent CO_2 rate relative to the theoretically necessary amount (TNK). Figures 5; references 3.

SO_2 Utilization as ZnSO_4 in Industrial Flue Gas Treatment

937D0020C Moscow TSVETNYYE METALLY in Russian
No 8, Aug 92 pp 23-25

[Article by V.V. Govorov, I.N. Ivanina, A.V. Gladkiy,
Scientific Research Institute of Waste Gas Treatment]

[Abstract] The urgency of developing a waste-free flue gas treatment technology in nonferrous metallurgy, particularly in removing sulfur dioxide from the fuming furnace waste gas at Zn-bearing material processing plants, and the scarcity of published data on such systems prompted an investigation into the liquid phase equilibria, a study of the kinetics of zinc bisulfate oxidation with oxygen of air or treated gas, and tests of the process in a pilot unit. For simplicity's sake, it is assumed that all absorbed sulfur dioxide in the solution is in the form of sulfur bisulfite and in the solid phase—in the form of poorly soluble crystal hydrate. The dependence of the equilibrium zinc bisulfite concentration in the solution on the zinc sulfate concentration at various temperatures, the dependence of the zinc bisulfite oxidation rate on the suspension pH and oxygen concentration in gas, and the dependence of the zinc bisulfite oxidation rate on the zinc sulfate content are plotted. The experiment shows that the oxidation rate is proportionate to the bisulfite ion and oxygen concentration while the presence of zinc sulfate noticeably lowers the oxidation rate. An equation is derived for calculating the oxidation process kinetics. The findings confirm the expediency of the oxidation stage at absorbent pH of close to 4.0. An analysis of tests carried out in a 500 cm^3 pilot unit at the Ryazan Nonferrous Metal Smelter shows that the process can be recommended for use in nonferrous metallurgy; the specific design should be selected depending on the gas characteristics. The process also leads to sulfuric acid savings in addition to producing zinc sulfate. Figures 3; references 6.

Capillary Stability of Primary Sprayed Concrete Layer

927D0216A Moscow OGNEUPORY in Russian, No 7-8, Jul-Aug 92 pp 3-8

V.A. Deryabin, Eastern Refractories Institute; UDC 666.762.044.24.001.4

[Abstract] The conditions ensuring the necessary properties of sprayed (air-placed) concrete lining and the adhesion of sprayed concrete particles are discussed, and the lack of adequate published sources dealing with these issues is noted. The features of capillary attachment of individual sprayed concrete particles through liquid layers and the development of the primary sprayed layer are examined. To this end, the capillary attraction forces, the mechanism of particle attachment to a rough surface, adhesive attachment of particles, and the hydrodynamic effect of the liquid layer on the attaching particle are considered in detail. The relationship between the particle size and its capillary attachment is analyzed, and the concept of critical size, i.e., the maximum particle dimension at which it attaches itself to the walls and roof of the furnace, is introduced. The study shows that the liquid layer not only causes capillary attraction, but also absorbs excess kinetic energy of the particles and prevents the gunned particles from bouncing back. Figures 8; references 9: 8 Russian, 1 Western.

Effect of Ferric and Ferrous Oxides on Periclase Spinelide Product Resistance

927D0216B Moscow OGNEUPORY in Russian No 7-8, Jul-Aug 92 pp 8-11

[Article by Ye.S. Borisovskiy, G.I. Kuznetsov, S.Z. Tsiporina, B.P. Aleksandrov, S.V. Kazakov, All-Union Refractories Institute; UDC 666.762.453.017:620.178.16]

[Abstract] The effect of ferric and ferrous oxides on the crystal phase development in periclase chromite refractories and the resulting effect of these phases on the refractory product stability is discussed, and the effect of changes in the phase composition and ferrous and ferric oxides on the properties of periclase spinelide refractories with a low SiO_2 concentration is investigated. The ferrous and ferric oxide concentration in the 3-0.5 mm fraction grains of the chromite alumina spinelide (KhGSh) is summarized, and the microstructure of various KhGSh specimens is examined. The chemical composition of iron-free KhGSh samples and the physical and chemical properties of periclase spinelide items with varying ferrous and ferric oxide concentrations are examined. The study reveals that low-silicon periclase refractory items with excess iron in the Cr-containing component are not suitable due to their vulnerability to slags while refractories containing ferrous and ferric oxides in an optimum amount for the uniform spinelide matrix formation can be used for making lining in continuous metallurgical units. In cyclically operating

units with extreme conditions, periclase spinelide refractories with a minimum ferrous and ferric oxide concentration have the best performance indicators. Figures 6; tables 2; references 3.

Self-Propagating High-Temperature Synthesis: General Premises

927D0216C Moscow OGNEUPORY in Russian No 7-8, Jul-Aug 92 pp 16-17

[Article by V.I. Sumin, Yu.N. Makurin, Central Scientific Research Institute of Materials Science and Urals Polytechnic Institute]

[Abstract] The general principles of self-propagating high-temperature synthesis (SVS)—a wave localization of self-inhibiting solid phase reactions whereby the chemical interaction between the solid disperse components occurs without fusing or gasification of the reagents or products and is localized after thermal initiation in the zone of reagents spontaneously mixing in space in the form of a combustion wave—are discussed. Refractory, abrasive, and ceramic applications of self-propagating high-temperature synthesis are outlined, and it is noted that in recent years, the concept of self-propagating high-temperature synthesis has been expanded and now includes all combustion processes which occur with the formation of substances and materials, including multicomponent systems. References 5.

Production of Fireclay Light-Weight Refractories

937D0216D Moscow OGNEUPORY in Russian No 7-8, Jul-Aug 92 pp 19-21

[Article by T.M. Sandutsa, L.A. Dergaputskaya, Urals State Scientific Research Institute of Refractories; UDC 666.762.16-127.022.69]

[Abstract] The low strength of light-weight refractory materials made with coke—a scarce material whose production is power-intensive—prompted an attempt to establish the possibility of using chemical production waste as the combustible addition for making light-weight refractories whose properties are as good as those of the ShKL-1.3 product pursuant to GOST 5040-78. To this end, KV-2 Vladimir kaolin, ShKV-2 chamotte made from this kaolin, and waste from polyethylene wax and synthetic rubber production are used as the initial products. The chemical composition of the waste products and the granular composition and bulk mass of the waste products are summarized, and the effect of the limit of grain size and addition concentration on the apparent density and compressive strength of samples roasted at a 1,380°C temperature is plotted; the mechanical properties of the refractories are tabulated. The findings demonstrate that chemical industry waste can be used for making light-weight refractories with good properties, but the process requires special purification facilities for capturing the gas being liberated during the heat treatment of the products. Figures 1; tables 2.

Cracking Resistance and Strength of End Sections of Prestressed Structural Concrete Parts With Wire-Rope Reinforcement

927D0227A Moscow *BETON I ZHELEZOBETON*
in Russian No 5, May 92 pp 13-15

[Article by N.A. Markarov, doctor of technical sciences, professor, R.Sh. Sharipov, candidate of technical sciences, and Yu.V. Petrenko, engineer, Scientific Research Institute of Reinforced Concrete; UDC 691.87:693.554:539.3/4]

[Abstract] Although an oblique lay of reinforcing wire rope ensures optimum performance of concrete parts with prestressed end sections under concentrated continuous loads and under impacts, inspection has revealed longitudinal cracks and loss of concrete-to-steel contact not only during production, but also during storage while all design and manufacturing specifications have been met within prescribed tolerances. This calls for refinement of the design procedure, by considering the maximum allowable prestress level and the appropriate cross-sectional area of that obliquely laid reinforcement. Following a theoretical analysis and an experimental study, formulas have been developed for calculation of both parameters with not only the compressive strength of an end section, but also its cracking resistance (stress) as design criteria. Specimens were designed and tested accordingly. The results confirm that without obliquely laid reinforcement longitudinal cracks lower the load capacity of concrete by 10-30 percent, while longitudinal cracks with limited mouth width in concrete end sections with obliquely laid reinforcement do not noticeably lower the strength of such sections. Figures 3; tables 1; references 4.

Effect of Dispersible in Water Film-Forming Clogging Compounds on Quality of Protective Pipe Jacket

927D0227B Moscow *BETON I ZHELEZOBETON*
in Russian No 5, May 92 pp 21-23

[Article by G.V. Topilskiy, candidate of technical sciences, and V.I. Melikhov, candidate of technical sciences, All-Union Scientific Research Institute of Reinforced Concrete, V.P. Koretskiy, candidate of technical sciences, Ukrainian Scientific Research Institute of Hydraulic Engineering and Soil Improvement; UDC 679.69:620.193.8:62:691.327]

[Abstract] Considering that the main factor causing deterioration of protective pipe jackets made of spatter concrete is desiccation of that concrete during heat treatment and its subsequent cracking, several nontoxic new film-forming clogging compounds dispersible in water have been developed at the Institute of Concrete and Reinforced Concrete. These compounds contain soft paraffins or petrolatum with melting points within the 36-44°C range and emulsifiers along with special-purpose additives (latexes, corrosion inhibitors, water repellants, or others). Impregnation of concrete with any of these compounds is more reliable as well as less

laborious and thus also less costly than impregnation with modified petrolatum according to current practice, which not only requires a higher temperature within the 85-95°C, but is also less hygienic. These new compounds were tested at the Institute of Concrete and Reinforced Concrete, at the Ukrainian Scientific Research Institute of Hydraulic Engineering and Soil Improvement, also at the Byelarusian Institute of Construction Science, for their effect on three performance key characteristics of concrete: 1) strength after 1-day, 7-day, and 3-month curing periods; 2) loss of water during heat treatment; 3) water absorption during storage in water for 1-day, 40-day, and 100-day periods. Such tests were performed on spatter concrete covering steel pipes and impregnated with: 1) VDMP soft paraffin, 2) VDPI petrolatum, 3) SKS-65GP butadiene-styrene latex, 4) VDMP + 20 percent SKS-65GP, 5) ATsF-3N acetoformaldehyde resin, 6) VDSV water suspension of slop wax + 20 percent mineral oil, 7) distillate residue of PMFS polymethyl phenolsulfonate. These tests were performed at the Institute of Concrete and Reinforced Concrete, at the Ukrainian Scientific Research Institute of Hydraulic Engineering and Soil Improvement, and at the Byelarusian Institute of Construction Science. The results confirm that addition of these film-forming clogging compounds can appreciably decrease (by a factor of 3 to 5) the permeability of a concrete jacket and thus also its water absorption at sufficiently low temperatures within the 40-60°C range without, however, increasing its strength. They are thus as effective as modified petrolatum melt. Tables 4; references 3.

Effect of Additives on Corrosion Resistance of Building Mortars in Technogenic Media

927D0227C Moscow *BETON I ZHELEZOBETON*
in Russian No 5, May 92 pp 23-25

[Article by V.V. Goncharov, candidate of technical sciences, Kiev Institute of Construction Engineering, and A.M. Rozhanskaya, candidate of biological sciences, Institute of Materials Science at Ukrainian Academy of Sciences; UDC 67969:620.193.8:627:691.327]

[Abstract] An experimental study of various building mortars was made concerning both chemical and microbiological effects on them in aggressive industrial media. Model specimens of 1:3 sand-to-cement mixtures with 0.4, 0.6, 0.8 water-to-cement ratios were prepared for this purpose. They were tested plain and separately with each of three organic cationic surface-active compounds added by injection with sealing water in concentrations of 0.1 percent, 0.55 percent, and 1 percent: 1) Catamine AB, 2) Catapin KB, 3) Polydim P. They were all tested in liquid media both aggressive toward concrete and nutritious for microorganisms, namely aqueous solutions of: A) 5 g/l meat extract + 3 g/l peptone; B) 5 g/l $\text{Na}_2\text{S}_2\text{O}_3$, 2 g/l KNO_3 + 0.5 g/l NH_4Cl + 2 g/l KH_2PO_4 (pH 7); C) 7 g/l calcium lactate + 0.5 g/l yeast hydrolyzate + 2 g/l MgSO_4 + 1 g/l NH_4Cl + 1 g/l $\text{CaSO}_4 \cdot 2\text{H}_2\text{O}$ + 0.5 g/l K_2HPO_4 (pH 7.5). The mortars were then tested again after these media had been doped with bacteria, three

groups of bacteria having been injected each into the medium most favorable for its growth: medium A with ammonifiers converting proteins to organic acids and ammonia, medium B with bacteria oxidizing thiosulfates to H_2SO_4 and sulfur, medium C with bacteria reducing sulfates to H_2S . The corrosion resistance of mortars was evaluated on the basis of flexural strength criteria: index CR denoting the ratio of strength after soaking in sterilized tap water to strength after six months of soaking in dry indoor air, index CR_1 denoting the ratio of strength after soaking in sterilized liquids to strength after soaking in tap water, index CR_2 denoting the ratio of strength after exposure to bacteria to strength after soaking in sterilized tap water, and $CR_3 = CR_2 - CR_1$. The results of these tests indicate a beneficial effect of all three surface-active additives on finish hydration of the binder. The effect of Catamine AB was found to raise the stability of all mortars during exposure to ammonifiers and thiosulfate oxidizers but to lower it during exposure to sulfate reducers, both Catapin KB and Polydim P raising the stability of the denser mortars (0.4-0.6 water-to-cement ratios) during exposure to ammonifiers and thiosulfate oxidizers more than during exposure to sulfate reducers. While both Catamine AB and Catapin KB were found to protect all mortars about equally well against corrosive action by ammonifiers and thiosulfate oxidizers respectively, of both groups of bacteria producing acids, Polydim P was found to protect especially well the thinner and thus more porous mortar (0.8 water-to-cement ratio) against corrosive action by ammonifiers. Figures 1; references 3.

Life Expectancy of Reinforced-Concrete Cover Plates for Railroad Buildings

927D0227D Moscow *BETON I ZHELEZOBETON* in Russian No 5, May 92 pp 25-27

[Article by V.P. Chirkov, doctor of technical sciences, professor, and A.N. Kardangushev, engineer, Moscow Institute of Railroad Transportation Engineers; UDC 624.012.45]

[Abstract] A set of formulas is proposed for predicting the useful service life of reinforced-concrete cover plates for railroad buildings; corrosion of their steel rods under tension has been found to be the principal cause of failure. These formulas include one for the corrosion index as a function of time in service after corrosion has begun, with mechanical failure due to corrosion treated as a multicycle process, one for the corrosion rate, and one for the degree of accumulated defectiveness. Taken into account is the variance of stresses in the steel rods under load. The time in service after corrosion has begun is then calculated on the basis of these formulas, and the life expectancy based on the corrosion criterion alone becomes equal to the difference $T_r - T_c$ (T_r —minimum actual time of retention of protective passivation effect, T_c —time in service after corrosion has begun). Numerical estimates based on data pertaining to plates, which

cover "Stenkino" washing-steaming depots, yield for these plates a 32 years long life expectancy. Figures 4; references 5.

Electrical Resistance of Oxide Film Coatings on Glass

927D0260A Moscow *STEKLO I KERAMIKA* in Russian No 5, May 92 p 16

[Article by A.B. Atkarskaya, V.I. Borulko, V.Yu. Goykhan, G.V. Zhmykhov, T.A. Dudnik, L.I. Maricheva, and S.A. Popovich, Scientific Research Institute of Automotive Glass; UDC 666.11.01:537.311.3:621.315.612]

[Abstract] An experimental study of oxide film coatings on glass was made concerning the dependence of their electrical resistance and the film composition and deposition process. Film forming water-alcohol solutions of In, Sb, La, Bi oxides and Fe, Co chlorides dissolved in HCl, of zirconium chloroxyl, tetraethoxysilane, tetraethoxytitan, and also of $AgNO_3$ were prepared for hydrolysis with HCl serving as catalyst (HNO_3 as catalyst for hydrolysis of $AgNO_3$). The films were deposited on sheet glass by extraction from the respective solutions, the glass surface having been polished by heat treatment. They were extracted at a rate of 1 mm/s, to form 5 mm thick coatings covering a 100 mm square area. Subsequent heat treatment took place in a silite furnace at temperatures of 350-550°C for 0.5-1 hour at each. The electrical surface resistance was then measured with a bridge. The results reveal a correlation between the electrical resistance of these films and the electronegativity of elements contained in the film-forming solutions: the more electronegative an element is, the lower is the electrical resistance of the film containing the cation of this element. A coating with a higher concentration of oxides has accordingly a lower electrical resistance, but addition of iron or cobalt (say 0.5 wt. percent) will raise it. Also longer heat treatment was found to lower the electrical resistance of these coatings. Tables 1; references 1

Elasticity of Si_3N_4 -Base Ceramic

927K0260B Moscow *STEKLO I KERAMIKA* in Russian No 5, May 92 pp 19-20

[Article by V.N. Yakovkin and V.A. Kuzmenko, Institute of Problems in Materials Science at Ukrainian Academy of Sciences]

[Abstract] The elasticity characteristics of $Si_3N_4 + 2$ percent MgO (grades MK-2,3) and $Si_3N_4 + 40$ percent SiC (grade NKM-2) ceramic were measured in an experimental study, these materials being produced by the Makeyev branch of the Institute. Their modulus of elasticity in bending and Young's modulus were measured by the resonance method, by determining the resonance frequencies of flexural and longitudinal vibrations respectively. Their modulus of elasticity in shear and Poisson's ratio were measured by the ultrasonic

method, by determining the propagation velocities of surface acoustic and longitudinal volume acoustic pulses respectively. The density of these materials was measured by hydrostatic weighing, the difference between theoretical density and measured density then yielding the porosity of these materials. All measurements were performed on 5 mm thick rectangular bars with a 27×131 mm² cross-section and on 3.5 mm thick rectangular bars with a 5×51 mm² cross-section. The data on both Si_3N_4 + 2 percent MgO grades revealed an only linear rather than superlinear power-law dependence of their average Young's modulus E and average Poisson's ratio μ on their porosity θ as the latter varied from 0.17 to 0.01 with improvement of the ceramic production process: $E = 330(1 - 3\theta)$ GPa and $\mu = 0.25(1 - 3.2\theta)$. These unexpected relations indicate simultaneous involvement of two processes in the bonding of particles and an excessive defectiveness of low-porosity materials. The average modulus of elasticity in bending, measured over the 0-1500°C temperature range, was found to be linearly dependent on the temperature: the modulus of Si_3N_4 + MgO ceramic decreasing from 220 GPa at 0°C to 210 GPa at 750°C (less than 5 percent) and then to 170 GPa at 1500°C (almost 25 percent), the modulus of Si_3N_4 + SiC ceramic decreasing from 155 GPa at 0°C to 130 GPa at 1500°C (about 16 percent). Figures 2; tables 1; references 1.

Some Technological Problems in Enamel-Coating of Cast Iron Products

927D0260C Moscow STEKLO I KERAMIKA in Russian
No 5, May 92 pp 21-25

[Article by P.G. Pauksch, Riga Technical University; UDC 666.293]

[Abstract] The technology of enamel-coating of cast iron products is reviewed, taking into account phase transformations of cast iron and of quartz during the heating and cooling cycle. While pearlite forms when cast iron is cooled from a temperature above 860°C, graphitic ferrite forms when cast iron has been heated to temperatures not higher than 780°C. Sintering of sand-borax primers in pots at temperatures above 1100°C, meanwhile, requires regeneration of quartz into cristobalite and this gives rise to large compressive stresses during cooling of enameled parts to temperatures within 230-180°C. Inasmuch as the primer bonds much better to cast iron with a finer-grain structure than to cast iron with a coarser one, the main problem is to determine the optimum annealing temperature and time for maximum iron-primer bond strength. One not yet resolved other problem is whether the porosity of the primer should be maintained or allowed to decrease during deposition of the coating. Dilatometric and hydrogen absorption tests were performed on six primers: 1) raw (borax only); 2) industrial-grade fritted primer containing SiO_2 , B_2O_3 , Na_2O , Al_2O_3 , K_2O , CaF_2 , CaO , MgO ; 3) and 4) industrial-grade fused primers with and without 3.2 percent K_2O + 0.5 percent Pb_2O_3 respectively; 5) sintered primer

without K_2O , CaF_2 , Pb_2O_3 ; 6) primer with TiO_2 (without CaO , MgO , K_2O , CaF_2 , Pb_2O_3). On the basis of the results and their analysis are recommended composite frits: two frits with an interlayer in which structural and chemical changes taking place during annealing of the primer will gradually increase the viscosity of the melt and widen the degasability range. Figures 6; tables 2; references 18.

Crystallization of "Biosital" Glass-Ceramic during Radiation Heating

927D0260D Moscow STEKLO I KERAMIKA in Russian
No 5, May 92 pp 26-27

[Article by S.T. Suleymenov, A.A. Mirzakhodzhaev, A.P. Yumankov, and V.V. Kravchenko, Scientific Research and Planning Institute of Structural Materials, Alma-Ata; UDC 666.263.2:6215.464]

[Abstract] An experimental study of a stomatological glass-ceramic ("biosital") for artificial bone tissue was made in which it was heated by radiation during its crystallization, such a treatment being known to increase the mechanical strength of this type of glass-ceramic. Used as a radiation source was a bank of halogen lamps with a total power of 7.5 kW and a power supply built on thyristors with voltage control over the 30-200 V range. A uniform temperature distribution inside the radiation heat chamber was attained by lining its walls with kersile (reflection coefficient $R = 0.80$). Specimens of "biosital" placed inside this chamber were 1-2.5 mm thick, up to 12 mm wide, and up to 70 mm long or up to 10 mm high. Preheating of a specimen by multiple passage of radiation through it was followed by its additional heating to 850°C after the temperature of the kersile lining had reached 800°C, "biosital" heating up much faster than the kersile. As any glass melt, "biosital" melt is an electrolyte consisting of charged and neutral particles, its crystallization being governed principally by diffusion of these particles and the orientation of crystal blocks in absence of external action depending mainly on the state of the glass matrix. External action therefore may be used for controlling both speed and direction of movement of microparticles so that the orientation of crystal blocks will be determined by the resultant action of internal and external forces. The purpose of conventional heat treatment at 840-860°C for 2.5 h optionally followed by soaking at 550-600degC is to produce lithium metasilicate as the seeding phase and subsequently synthesize lithium bisilicate as the principal crystalline phase. In the process, articles made of a stomatological glass-ceramic acquire the appropriate color as well as a high mechanical strength. By radiation heat treatment at 900°C, this is accomplished in 10 min and thus about 15 times faster than by conventional heat treatment in a muffle furnace. Stomatological articles produced from "biosital" by this method have a temperature coefficient of linear expansion within the $(110-115) \times 10^{-6}$ range and remain heat-resistant at 200-220°C, a 50-60 μm thick glass-like coating formed on the

their surface making them also resistant to chemically aggressive media. Tables 1; references 2

Stability of Quartz Glass Slurries

927D0260E Moscow STEKLO I KERAMIKA in Russian No 5, May 92 pp 27-29

[Article by A.M. Akhyan, Scientific-Industrial Association "Kvarts"; UDC 66.192:666.3.022.66]

[Abstract] An experimental study of quartz ceramic slurries was made concerning their stabilization by stirring in a grinding mill without abraders prior to casting. Regularly crushed slurry of amorphous clay was so treated in a porcelain mill for 72-120 h. The slurry, with a 17-18 percent moisture content and a 8-10 percent mesh size 006 residue, had been split into two batches: one of them remaining unstabilized. After having been calcined at 1200°C, specimens of both batches were tested not only for tensile strength and flexural strength but also for fatigue strength and water absorption. Analogous tests were performed on: 1) synthetic amorphous clay with a 20-22 percent moisture content and a 8-10 percent mesh size 006 residue; 2) slurry of transparent quartz glass collet with a 16.8 percent moisture content and a 25 percent mesh size 006 residue. The results confirm that such a treatment of quartz ceramic slurry increases both its fluidity and the strength of articles made from it. The drawbacks are a 2-3 times longer slurry preparation time, slower thickening of the suspension, and most importantly a longer pottery buildup time. Stabilized slurry thus requires 2-3 times more processing capacity, a slurry with a higher moisture content, and high-quality gypsum molds. It is from very difficult to impossible to cast large articles in the 25-250 kg range from stabilized slurry without loss of homogeneity, but the pottery buildup time can be shortened and the homogeneity of the cast material can be improved by preparation of a slurry with a high disperse-phase content, an effective way to achieve this being 2-stage crushing with addition of a filler. Tables 3; references 5

Use of Porcelain Collet as Filler Material

927D0260F Moscow STEKLO I KERAMIKA in Russian No 5, May 92 p 29

[Article by B.U. Barshchevskiy, Industrial Association "Gzhel", and V.M. Loginov, Institute of General and Inorganic Chemistry at Russian Academy of Sciences; UDC 666.5.004.8]

[Abstract] A preliminary experimental study was made concerning utilization of porcelain collet and tailings. Porcelain collet was crushed and then sifted into batches of various grain size fractions from 0.1-7.0 mm granules to 1-50 μ m "porcelain flour". Irregular shape and rough surface of these grains facilitate extraction of suspended impurity particles from water and thus enhance their filtering action. Porcelain collet of the 2-7 mm grain size fractions can also be used for filtration and purification of

fluids containing large particles of inorganic or organic material, but are best when formed into a layer supplementing a fine-grain (0.05-0.25 mm) porcelain layer. The performance of such filters was measured by the optical method with a SPEKORD UV-ViS instrument in terms of transparency of the fluid, namely its increase from before to after filtration. The results indicate that the thicker filter layer is more effective, but also less productive. Porcelain collet can be used for filtration of natural waters and for production of drinking water as well as for industrial applications, waters with large impurity particles requiring multilayer filters with grains of different sizes in each layer: coarse-grain layers on top of fine-grain layers for downward flowing water. Such an arrangement lengthens the time between shutdowns for filter wash or replacement. As filter material, porcelain collet is more economical than sand. Another favorable feature of this material is its being ecologically clean.

Effect of Pressing Force on $\text{YBa}_2\text{Cu}_3\text{O}_{7-x}$ Powder Structure and T_c

937D0008K Moscow FIZIKA I KHIMIYA OBRABOTKI MATERIALOV in Russian No 4, Jul-Aug 92 pp 122-127

[Article by V.F. Shamray, Yu.V. Yefimov, V.F. Choporov, Ye.A. Myasnikova, A.M. Postnikov, T.M. Frolova, Moscow; UDC 621.762:537.312.62]

[Abstract] The stability of the high- T_c (VTSP) structure as a function of process factors is an important parameter necessary for understanding the origin of HTSC and producing materials with reproducible properties. The need to examine the effect of mechanical stresses and strain on the structure and properties of HTSC materials prompted an investigation of the effect of the pressing force and subsequent annealing in the air or oxygen on the structure and T_c of the orthorhombic phase of $\text{YBa}_2\text{Cu}_3\text{O}_{7-x}$ powders (the 123 phase). The study is carried out using commercial Y-HTSC powders containing 90-95 percent of 123 orthorhombic phase with clearly allowed reflexes. To this end, Y-HTSC powder is compressed in molds at a force within a 200-1,000 MPa range. The phase composition, HTSC phase structure, and sample texture is examined by X-ray analyses; X-ray diffraction patterns are recorded by a DRON-2.0 diffractometer in FeK radiation. T_c is measured by the variable induction method at a ≥ 77 K temperature. The samples are annealed at 450-930°C for 1-6 h with a subsequent slow cooling at a 20-50°C/h rate. The principal 123 phase reflexes at 88.5K in the initial state and after one-sided pressing at a 710 MPa force, the reflex position shift under one-sided pressing, the effect of the pressing force on lattice constants and 123 phase cell volume, the effect of the pressing force on the 123 phase T_c , and the principal 123 phase reflexes of uniformly strained and annealed samples are plotted. Pressing at a ≥ 200 MPa pressure causes a basal texture formation and a change in the substructural state, a partial 123 phase decay, and as a consequence, a decrease in the critical temperature and an expansion of the critical temperature range; the initial equilibrium structure can be fully restored after double annealing with an intermediate

grinding or by thermal cycling without grinding. The reproducibility of the results suggests that straining and subsequent annealing are not related to surface phenomena. Annealing in O₂ speeds up the restoration of the HTSC structure and T_c without a change in the degradation and recovery mechanisms. Figures 5; references 4.

Fibers and Fibrous Materials for Reinforcing Composites With Extreme Characteristics

937D0009A Riga MEKHANIKA KOMPOSITNYKH MATERIALOV in Russian No 3, May-Jun 92
pp 291-306

[Article by K.Ye. Perepelkin, St. Petersburg Textile and Light Industry Institute; UDC 539.2:677.4]

[Abstract] Scientific and technical progress brought about the development of new reinforcing fibers and fibrous materials for composites with such extreme characteristics as superhigh strength, superhigh modulus, heat resistance and refractory, inflammable and fire, chemi- and bioresistant, etc. In this context, the physical principles of producing fibers and fibrous materials with extreme characteristics are considered, and their structure and properties are examined. The structural conditionality of the mechanical and thermal properties of materials and the effect of such environmental factors as the temperature and corrosive media are analyzed and the theoretical and maximum feasible properties are determined. The most promising types of reinforcing fibers and fiber materials are identified and their likely uses are suggested. The structural and temperature characteristics of several polymer fiber-forming materials and graphite, methods of normal life analysis, principal properties of highly oriented fibers and filaments, and the main characteristics of chemi-, bio-, and fire-resistant and refractory fibers are summarized. The morphological and energy characteristics which determine the stability and resistance of reinforcing fibers are examined at molecular, epimolecular, and microlevels and it is shown that the utmost mechanical properties are attained in fiber-forming polymers with a high dissociation energy of the skeletal bonds at a high orientational and coordinational structure ordering. The high thermal properties are attained in cross-linked polymers and fibers with the highest dissociation energy while the chemical resistance is determined by both high chemical bond energies and the minimum reactivity for various agents. Tables 11; references 66: 46 Russian, 20 Western.

Mechanical Properties of Polyethylene- and Thermally Exfoliated Graphite-Based Composite Materials

937D0009B Riga MEKHANIKA KOMPOSITNYKH MATERIALOV in Russian No 3, May-Jun 92
pp 307-314

[Article by L.S. Semko, I.G. Chernysh, S.L. Revo, N.N. Dashevskiy, Surface Chemistry Institute at the Ukrainian Academy of Sciences, Kiev, and Kiev State University imeni T.G. Shevchenko; UDC 678.742:546.26-162:620.17]

[Abstract] The scarcity of data on the physical-mechanical properties of polymer- and thermally exfoliated graphite (TRG)-based composite materials (KM) prompted an experimental investigation into the physical and mechanical properties of polyethylene (PE) and exfoliated graphite-based composites and thermal phenomena observed under adiabatic tension in composite samples. To this end, composite samples containing 0-0.31 percent by volume (0-50 percent by mass) of GAKV-2 exfoliated graphite in a 10803-020 high-pressure polyethylene matrix are examined. The mechanical tests are carried out in an Instron machine under uniaxial tension at a 0.01-2.0 mm/s rate while the mechanical properties are assessed by the yield stress, tensile strength, elongation at rupture, and the modulus of elasticity. The dependence of the yield point, tensile strength, and logarithm of elongation on the exfoliated graphite concentration at various straining rates for intact and notched samples, the dependence of the elasticity modulus on the exfoliated graphite concentration of intact and notched samples, the dependence of the sample temperature on the tension duration at various exfoliated graphite contents, the dependence of the elongation integrals on the exfoliated graphite content, and the dependence of the temperature drop on the exfoliated graphite content are plotted. The curves show that virtually all mechanical characteristics change sharply within a 0.075-0.16 EG volume range which is referred to as the critical range where continuous spatial structures develop from EG particles while the critical ranges coincide for electrical and mechanical tests. An analysis demonstrates that the percolation behavior of composites and their critical indices are universal under both the electrical and mechanical tests and that at a critical filler content in the composite, critical phenomena similar to second-kind phase transitions occur. It is shown for the first time that as the tension rate increases, the threshold of these transitions shifts to higher EG concentrations. Figures 5; references 19: 16 Russian, 3 Western.

Stressed State of Polycrystalline Diamond Compacts Under Thermal and Force Load in High Pressure Machines

937D0011A Kiev SVERKHTVERDYIE MATERIALY in Russian No 2 (77), Mar-Apr 92 pp 7-11

[Article by A.M. Anisin, Superhard Materials Institute at the Ukrainian Academy of Sciences, Kiev; UDC 539.3/4:621.9.025.77.02]

[Abstract] Sintering of polycrystalline diamond compacts (ATP) and their subsequent soldering to holders in high pressure machines (AVD) is accompanied by changes in the thermal and pressure loads of up to 8 GPa and 1,200°C and may lead to considerable process stresses in the composite cutting insert and its eventual failure. This prompted a review of published data on the polycrystalline diamond compact stress and an attempt to examine the stressed state in such inserts. To this end,

a procedure for analyzing the stressed state of polycrystalline diamond compacts is proposed on the basis of known data allowing for the external hydrostatic pressure realized during the cutting tip soldering to the high pressure machine holder. Expressions are derived for crude estimates of the stressed state; for simplicity's sake, the temperature and pressure gradients within the high pressure machine are ignored. The behavior of the stress levels on the lateral surface of the diamond-bearing layer and the hard alloy base during the thermal-force loading is plotted, and the strength of polycrystalline diamond compact cutting inserts is examined within the temperature and pressure range under study. A study of the compact strength during diffusion soldering shows that the highest stress intensity is developed on the lateral surfaces of the diamond-bearing layer and hard-alloy base where axial, tangential, and radial stress components are at work. The external pressure factor is shown to increase the plastic deformation probability in the polycrystalline diamond compact and thus worsen its performance. Subsequent cutting tip heating has a stabilizing effect and compensates for the tension strain between the adamantine layer and the hard alloy base. It is noted that although from the viewpoint of stressed state, the pressure-temperature loading curve is not optimal, the polycrystalline diamond compact tip's margin of strength has not been exhausted. Figures 2; references 3.

Determining Wear Resistance of Polycrystalline Diamond Compacts by Acoustic Emission Method

937D0011B Kiev *SVERKHTVERDYIE MATERIALY* in Russian No 2 (77), Mar-Apr 92 pp 11-15

[Article by S.L. Udovik, B.A. Oleynikov, B.B. Mina-sevich, Superhard Materials Institute at the Ukrainian Academy of Sciences, Kiev; UDC 620.179.14:621.9.025]

[Abstract] The importance of on-line wear resistance diagnostics of structural composite materials for enhancing their development and improvement and the shortcomings of existing wear resistance diagnostic methods prompted the development of a new technique which is more adaptable to streamlined production and is characterized by high precision within a broad resistance range. According to the proposed method, the acoustic emission signal parameters are recorded during transverse cutting to a specified depth at a constant force. The polycrystalline diamond compact tip wear resistance is determined by a criterion which incorporates these parameters. To this end, a 24A 251 ST2 7K5 grinding wheel from synthetic corundum (GOST 2424-750) with rather uniform physical properties spinning at a 1,000 RPM speed is used as a cutting blank. The blank is cut to a 400 μ m depth at a 100 N load. The design of a test bench for measuring the wear resistance of 64 polycrystalline diamond compact tips divided into five batches is described, and its block diagram is cited. The dependence of the criterion K , which is the ratio of the peak acoustic emission (AE) signal amplitude to its duration at a given level, on wear resistance is plotted,

and the averaged acoustic emission signal parameters are summarized for five polycrystalline diamond compact tip groups with different wear resistance. The method is proven to be effective in monitoring cutting tips with an elevated wear resistance and can be used for on-line monitoring of polycrystalline diamond compact tips during their production and operation. It is suggested that measurements be taken at two to three points for estimating the polycrystalline diamond compact tip wear resistance. The method can be used for through on-line production control; since the wear resulting from the test is insignificant, the method may be characterized as nondestructive testing. Figures 2; tables 1; references 10.

Structure Formation in Diamond-Bearing Foil

937D0011C Kiev *SVERKHTVERDYIE MATERIALY* in Russian No 2 (77), Mar-Apr 92 pp 22-26

[Article by O.A. Katrus, E.E. Mitrova, A.V. Belyankina, Superhard Materials Institute at the Ukrainian Academy of Sciences, Kiev; UDC 621.922:666.233]

[Abstract] The structure formation in diamond-bearing rolled foil blanks is examined, and the multiple rolling and annealing process of making foil from loose materials is outlined. The structure formation in the foil is studied mostly by X-ray diffraction analyses using a DRON-2.0' diffractometer in CuK radiation and by metallographic and electron diffraction analyses. Formulae are derived for calculating microdistortions and the dislocation density. The effect of the production process factors on the structure formation in each binder is considered in detail. In examining the MD copper-based matrix, MM1 bronze-base matrix, and MM20 nickel-based matrix, the line width is measured both before and after rolling. The MD and MM1 binder substructure characteristics both in the burden before rolling and in nonsintered rolled stock and the structural characteristics of the Fe-Ni composite in the charge before rolling, in rolled nonsintered stock, after sintering, and after heat treatment are summarized. An analysis of the findings shows that the structure formation and diffusion annealing of the matrix material are completed after the first two heat treatment and rolling cycles. It is speculated that the cold diffusion mechanism has a considerable effect on the structure formation whereby an equilibrium state is developed in the area of low heat treatment temperatures. It is noted that diamond grains contained in the foil remain unchanged after rolling and sintering. The composite compaction is due to the plastic component deformation. Tables 2; references 9.

TiB₂ Structural Transformations at High Pressures and Temperatures

937D0011D Kiev *SVERKHTVERDYIE MATERIALY* in Russian No 2 (77), Mar-Apr 92 pp 26-31

[Article by G.S. Oleynik, Yu.I. Lezhnenko, V.F. Britun, N.P. Semenenko, Institute of Materials Science Problems at the Ukrainian Academy of Sciences, Kiev; UDC 669.018.45:539.5]

[Abstract] The mechanism of plastic deformation in TiB_2 —a superhard material used as a composite binder—and its role in the granular and subgranular structure formation in polycrystalline samples are discussed, and both of these issues are examined by thin foil transmission electron microscopy and carbon replicas of the natural fracture surfaces. To this end, polycrystalline samples produced in toroidal chambers and sintered at a 2.5, 4.0, and 7.7 GPa pressure within a 1,000-2,200°C temperature range for 60 s are used. The study reveals a high dislocation density accumulation in the grains, the formation of various disordering boundaries in the grains with subsequent grain fragmentation, and primary recrystallization. A change in the mean grain size of TiB_2 samples produced at a 7.7 GPa pressure with an increase in the sintering temperature is plotted. An analysis shows that plastic deformation is realized by the slip mechanism with a partial role of rotational plasticity. The substructural grain transformations are due to the development of the defect structure found in the microscopy study; primary recrystallization occurs by the grain boundary mechanism whereby the initial process stage shifts to the lower temperature area. The effect of plastic grain fragmentation and recrystallization on the grain structure development is discussed. Figures 5; references 6: 4 Russian, 2 Western.

Effect of Static Magnetic Field on Electrodeposition of Diamond-Bearing Composite Coats

937D0011E Kiev SVERKHTVERDYE MATERIALY in Russian No 2 (77), Mar-Apr 92 pp 38-41

[Article by G.N. Znamenskiy, I.A. Tsisar, L.A. Lobodzinskiy, Vinnitsa Polytechnic Institute; UDC 621.922.025:621.357.7]

[Abstract] The effect of the diamond powder concentration in tools with an electrodeposited diamond-bearing coat and the physical and mechanical properties of the matrix on the tool performance is discussed, and the effect of the static magnetic field on the hardness of the electrolytically deposited matrix and the diamond powder concentration in the coat is examined. To this end, Fe, Ni, Zn, Cu, and Ni-Zn alloy coats are electrodeposited from acid electrolytes with and without the ASM 3/2 diamond powder at a volume content of 25 carat/dm³. The coats are deposited in a specially designed cell without and with a static magnetic field at a 0.1-0.5 T induction in the gap between the permanent magnet poles while the mutual electric and magnetic field orientation is manipulated. The coat microhardness is measured by a PMT-3 gauge, the surface diamond powder concentration is measured by an Orim-1 metallographic microscope, and polarization curves are recorded by a PI-50-1.1 potentiostat. The dependence of the coat microhardness on the mutual magnetic and electric field orientation and the effect of the magnetic field on the Ni polarization curves in coats with and without the ASM 3/2 diamond powder are plotted. The findings shown that under the effect of a static magnetic field, the

ferromagnetic's (especially Fe) hardness decreases due to a decrease in the hydroxide concentration in the coat. The diamond powder concentration in the coat increases with magnetic field induction, especially in vertical iron matrices. The hard particle concentration rise on vertical cathodes is attributed to the electrolyte and charged diamond particle movement under the combined effect of electric current and magnetic field and due to Lorentz's forces. It is recommended that the findings be utilized for developing the process of electrolytic deposition on both sides of vertical cathodes simultaneously. Figures 2; references 8: 5 Russian, 3 Western.

Formation of Graphite With Corrugated Layers During Diamond Graphitization

937D0012A Kiev SVERKHTVERDYE MATERIALY in Russian No 3 (78), May-Jun 92 pp 7-10

[Article by V.D. Andreyev, Yu.I. Sozin, A.F. Goncharov, Superhard Materials Institute at the Ukrainian Academy of Sciences, Kiev, and Crystallography Institute at Russia's Academy of Sciences, Moscow; UDC 538.69:539.121.14:666.233]

[Abstract] The formation of "crumpled" graphite with corrugated layers inside the crystals during partial diamond graphitization and the results of an observation of the phenomena occurring during the diamond graphitization are presented. The study is carried out by X-ray diffraction analyses and Raman scattering (KRS) using the ASM 28/20 graphitized powder after its isothermal annealing in a resistance vacuum furnace at a 1,900°C temperature for 30 min. The diffraction patterns of the ASM 28/20 powder after annealing and Raman spectra of the ASM 28/20 powder and single crystal graphite after annealing are plotted. In addition to the reflexes which characterize the adamantane and graphite phases, a (110) line satellite is discovered on the graphite diffraction pattern. Raman spectra show a drop in the graphite's fundamental 1,581 cm⁻¹ line frequency. These findings are attributed to the residual intraplanar graphite layer corrugation which may remain even after the total interplanar bond relaxation. A formula is derived to calculate the dependence of the graphite's dominant mode on the C-C interatomic bond rotation angle and its straining. Figures 2; references 8: 4 Russian, 4 Western.

Effect of Glow Discharge Parameters and Heat Treatment on Synthetic Diamond Single Crystal Metallization

937D0012B Kiev SVERKHTVERDYE MATERIALY in Russian No 3 (78), May-Jun 92 pp 17-20

[Article by Ya.L. Potapenko, N.A. Paskal, A.A. Paskal, V.N. Myslina, Odessa Agricultural Institute and Odessa State University; UDC 620.179.4:621.791.35:621.922]

[Abstract] Extensive uses of diamonds in the electronics industry call for additional studies of diamond metallization (i.e., bonding) and the effect of various factors on

this process. To this end, diamond metallization is carried out by cathode sputtering of metals in an Ar medium by the triode procedure using a UVN-R unit which ensures an up to 200 mA current in the glow discharge plasma at an up to 2 kV sputtering voltage and makes it possible to maintain the base temperature within 200-1,000°C. The dependence of the metallization and adhesion force of Ti, Cr, and Ni films on synthetic diamond single crystals on the glow discharge parameters is examined. The samples are heat treated in order to break old adhesion bonds before the new ones are formed. The dependence of the metal film thickness on the sputtering duration, voltage, and current density is plotted. The study makes it possible to identify the following optimum process parameters: a 4-5 mA/cm² current density and a 1,600 V sputtering potential. It is suggested that after the bonding, the metal films be heat treated (annealed) in a vacuum at a 500-600°C temperature for at least 20 min. Figures 1; references 9.

Wear Resistance of Si₃N₄-TiN Ceramics Under Friction Against Diamond Abrasive

937D0012C Kiev *SVERKHTVERDYIE MATERIALY* in Russian No 3 (78), May-Jun 92 pp 20-25

[Article by Yu.G. Gogotsi, A.M. Kovalchenko, I.I. Osipova, V.P. Yaroshenko, V.A. Goncharuk, Institute of Materials Science Problems at the Ukrainian Academy of Sciences, Kiev; UDC 621.922.025.004.6:666.3/.7:621.921.34:666.233]

[Abstract] The effect of TiN additions to silicon nitride ceramics on their properties and the correlation between the physical and mechanical properties, structure, and wear resistance of ceramic-based composites are discussed, and the abrasive wear of Si₃N₄-TiN ceramics is examined. To this end, a silicon nitride powder with 90 percent of α -phase and no more than 2.5 percent of impurities with sintering activator powders as well as TiN powder separated into three fractions by sedimentation are used for making the test samples. Wear resistance under friction against a fixed abrasive particle is the fundamental strength characteristic of refractory ceramic materials. Consequently, the dependence of the volumetric sample wear under friction against a shaft with diamond grains on the TiN concentration in the ceramics at various loads; the dependence of the volumetric wear on the load under varying Ti concentrations; the concentration dependence of the crack resistance, hardness, bending strength, and relative wear resistance of ceramics with various TiN fractions; and the dependence of the relative wear resistance on the strength, hardness, and crack resistance are plotted. A study of the fractured surface with the help of a profile gauge shows that roughness increases slightly with an increase in the load while the diamond grit and ceramic composition have the dominant effect on the relief. The findings also show that the wear resistance, strength, hardness, and crack resistance of hot compacted ceramics depend on the TiN addition dispersivity and amount. The best properties are found in composites with a rough TiN

fraction of less than 40 percent while all parameters peak in materials with 20 percent of fine fractions. A correlation between the properties except for the crack resistance is established for all materials. It is shown that brittle failure is the dominant abrasive wear mechanism. Figures 5; references 11: 8 Russian, 3 Western.

Effect of Nickel and Manganese Sulfates on Chromium Sulfate Solution Recovery in Synthetic Diamond Production

937D0012D Kiev *SVERKHTVERDYIE MATERIALY* in Russian No 3 (78), May-Jun 92 pp 30-34

[Article by V.V. Putivskiy, A.A. Milner, A.K. Zapolskiy, Colloidal Chemistry and Water Chemistry Institute at the Ukrainian Academy of Sciences, Kiev; UDC 666.233:546/547.05]

[Abstract] The shortcomings of the method of nonadamantine carbon removal by selective oxidation with chromic acid in synthetic diamond production, particularly its high cost and the difficulty of spent solution recovery, prompted an investigation into the polymer chromosulfuric acid breakdown in the presence of nickel and manganese sulfates in the solution. A solution with 10.94 percent chromium sulfate and 71.86 percent sulfuric acid is used in the experiment whereby the effect of nickel and manganese sulfates on the chromosulfuric acid breakdown is examined at a 190°C temperature (which corresponds to the maximum process rate) with subsequent heat treatment. The solid phase forming due to the acid breakdown is examined by chemical and thermogravimetric analyses. The dependence of the acid solution breakdown degree on the heat treatment duration and initial solution composition and the dependence of the solid phase composition on the initial solution content are summarized. Data from chemical and thermogravimetric analysis of the solid phases are compared to the thermograms of the nickel and manganese sulfates used as additions. The findings indicate that the presence of metal sulfates in the spent solutions facilitates the chromium precipitation into the solid phase and the production of a pure circulating sulfuric acid solution. The optimum $\text{MeSO}_4:\text{Cr}_2(\text{SO}_4)_3$ ratio is within (0.1-0.2):1. Figures 1; tables 2; references 6.

Selecting Methods of Efficient Nonfired High-Alumina Ceramic Product Machining

937D0012E Kiev *SVERKHTVERDYIE MATERIALY* in Russian No 3 (78), May-Jun 92 pp 49-53

[Article by V.P. Lepetukha, I.M. Sova, Slavyansk Branch of the Kharkov Engineers Teaching Institute and Slavyansk Branch of the All-Union Scientific Research Institute of Synthetic Ceramics; UDC 621.923]

[Abstract] Intensive cutting tip wear during the machining of high alumina ceramics used in the electronics industry, particularly the VK 94-1 alloy containing about 98 percent of aluminum oxide and having

a specific gravity of 2.8-3.4 g/cm³ and a Mohs hardness of 9 and the lack of sufficient published data on the selection of machine tools for hard materials prompted a study of the possibility of the machining to size of compacted nonfired high alumina ceramics using cutting inserts made from various superhard materials (STM). To this end, an experiment is conducted using cutters equipped with a cutting insert from the VK6M alloy. In the tests, compacted washer- and bushing-shaped blanks from the VK 94-1 nonfired ceramics are machined in a special arbor with elastic elements in a 1K62 lathe without coolant lubricants at a 70 m/min cutting speed and a 0.7 mm/turn feed. The wear time is measured by a stopwatch, and wear is measured by an MPB-2 microscope. The dependence of the cutter wear on the machining duration is plotted for two types of cutters. The possibility of machining high alumina ceramics with diamond grinding wheels is also examined. An analysis of the curves shows that as the machining duration increases to 45 min, the cutter wear increases to almost 2 mm while the machined surface roughness increases sharply and the total cutter service life is shortened to 45-90 min with 1-2 resharpening procedures. The diamond grinding-wheel test data are summarized for in-feed grinding by conventional and special wheels. An analysis demonstrates that nonfired high alumina ceramic products can be efficiently machined by turning, drilling, and grinding whereby the use of superhard material tools, especially diamond grinding wheels with a special profile, is preferable. The optimum in-feed grinding feed is 0.25-0.50 mm/turn and the optimum turning parameters for elbor-R and geksanit-R borazon cutters are as follows: a 180-260 m/min cutting speed, a 0.4-0.6 mm/turn feed, and a 1.5 mm cutting depth per pass without the lubricant coolant (SOZh). The above recommendations have been implemented in the industry and resulted in a saving of over 90 thousand rubles per year. Figures 2; tables 1; references 5.

Superfinishing of Carbide- and Nitride-Based Engineering Ceramics

937D0012F Kiev *SVERKHTVERDYIE MATERIALY*
in Russian No 3 (78), May-Jun 92 pp 54-57

[Article by A.A. Orap, Ya.A. Kryl, A.V. Galkov, A.A. Ivanenko, Superhard Materials Institute at the Ukrainian Academy of Sciences, Kiev; UDC 621.923.5]

[Abstract] The advantages of low-temperature superfinishing and its effect on the development of excellent surface properties of materials and their service life prompted a study of superfinishing of silicon and boron carbide- and silicon, titanium, and aluminum nitride-based engineering ceramic samples shaped as cylindrical bushings. To this end, samples are prepared at the Superhard Materials Institute at the Ukrainian Academy of Sciences in Kiev by hot compaction in graphite attachments using induction heating in the air; the samples are subsequently ground by diamond wheels. The tests are carried out using 10x10 square bars at a 200 RPM sample rotation speed, a 1,400 stroke/min bar

vibration frequency, a 0.6 MPa clamping pressure, a 3 mm bar stroke, and a 60 s machining time. Superfinishing is performed in a 1K62 lathe with an SFG-100 head; a mixture of kerosene and oil in a 7:3 mass ratio is used for cooling. For comparison, ASM and ASMK diamond grain bars with an M2-08 metal matrix and K3-02-k ceramic polymer binder are also tested. The dependence of the tool wear, machining allowance removal, and machined surface roughness of various samples on the diamond concentration and bar porosity is plotted. The conclusion is drawn that superfinishing tools from synthetic diamond with a low-temperature K3-01 ceramic binder is suitable for blanks from high-temperature structural ceramics, including carbide and nitride ceramics. Effective superfinishing is possible using bars with a relatively low diamond concentration and low porosity. The use of bars with a diamond content of >75 percent is inefficient since it increases the bar wear without improving the removal and roughness indicators. Figures 1; references 6: 2 Russian, 4 Western.

Electric Conductivity of BN_{sp} Polycrystals Produced by Direct Phase Transition From Pyrolytic BN

937D0017B Kiev *POROSHKOVAYA METALLURGIYA*
in Russian No 8 (356), Aug 92 pp 14-18

[Article by N.A. Shishonok, V.B. Shipilo, Solid State and Semiconductor Physics Institute at the Belarussian Academy of Sciences, Minsk; UDC 621.762]

[Abstract] Wide-ranging uses of sphalerite boron nitride are hindered by the lack of data on its electric properties; this prompted an investigation into the temperature dependence of electric conductivity of high-density (3.47 g/cm³) polycrystalline BN_{sp} produced by direct phase transition at a 7-8 GPa pressure and a 2,800K temperature from pyrolytic BN by linearly raising the temperature at a 0.04°/s rate in a nitrogen medium to various final temperatures. The initial resistivity of the samples at room temperature in about 10¹⁰ Ω x cm. The temperature dependence of electric conductivity of a nonannealed sphalerite sample, the temperature dependence of conductivity of samples annealed at different temperatures, the dependence of the conductivity on the annealing temperature, and the temperature dependence of conductivity of a sample annealed at 920°C are plotted. Thermal cycling under 700K is shown to have little effect on the shape curves. The curves display a peak in the area of 710K and a departure from linear behavior with an increase in the annealing temperature to 770K; the oscillating behavior of electric conductivity on the annealing temperature and a change in the shape of the lgσ(1/T) curve under thermal cycling is attributed to the sphalerite boron nitride defect structure transformation under the effect of temperature; this conclusion is consistent with other data. The formation of acceptor-like traps capturing the charge carriers is speculated. Figures 4; references 8: 7 Russian, 1 Western.

β -BN Oxidation Mechanism

937D0017D Kiev POROSHKOVAYA METALLURGIYA
in Russian No 8 (356), Aug 92 pp 22-27

[Article by A.P. Garshin, V.Ye. Shvayko-Shvaykovskiy,
St. Petersburg Polytechnic Institute; UDC 621.762]

[Abstract] The lack of reliable data on the chemical behavior features of boron nitrides which hinder their practical applications despite their unique combination of low density and high melting point and reports of accelerated sintering at elevated partial nitrogen pressures prompted a study of the behavior of cubic boron nitride during heating under various oxygen and nitrogen partial pressures. This method is selected because β -BN tools are usually used in an air medium at high temperatures. The LM7 commercial β -BN with a 7 μ m grain and a 0.5 m²/g specific surface and β -BN single crystals with a 200-300 μ m size as well as cylindrical samples from elbor-R borazon material are tested. To this end, the samples are polished by a diamond tool and washed in alcohol. The β -BN behavior is examined in a precision thermal mass gravimetric unit which makes it possible to measure the mass variation of the samples in any gaseous medium within wide temperature and pressure ranges. The gas desorption curve of β -BN heated in a vacuum, the mass change of the β -BN micropowder during oxidation as a function of temperature under heating-cooling, the dependence of the β -BN micropowder mass change on temperature, the mass change curve of nonstoichiometric β -BN micropowder as a function of the partial nitrogen pressure, and the dependence of the mass change of a monolithic polycrystalline sample on temperature are plotted. An analysis of the curves and oxidation and nitriding models makes it possible to suggest that nonstoichiometric defects in the anion sublattice affect the oxidation process, plot a hypothetical defect map, and develop an oxidation model of nonstoichiometric β -BN. Oxidation commences at a 573K temperature and the mass behavior process is divided into four stages. Figures 7; references 9.

Postirradiation Defects in Neutron-Irradiated Pyrolytic BN

937D0017E Kiev POROSHKOVAYA METALLURGIYA
in Russian No 8 (356), Aug 92 pp 27-31

[Article by A.V. Kabyshev, V.M. Ketskalo, Yu.P. Surov,
L.V. Serikov, L.N. Shiyan, High Tension Scientific
Research Institute, Tomsk; UDC 620.22.538.95]

[Abstract] Extensive uses of pyrolytic boron nitride (PNB) for making fusion reactor discharge chambers prompted a study of the origin of postirradiation defects in neutron-irradiated pyrolytic boron nitride. An attempt is made to check the Kinchin-Pease model according to which the recoil nuclei concentration per fluence unit for the fission neutron spectrum depends little on the pyrolytic boron nitride thickness. To this end, pyrolytic boron nitride samples with a 2.05×10^3 g/cm³ density are irradiated in water-filled vertical channels of a fission reactor whereby some samples are filtered by a 1 mm thick Cd filter and others are irradiated with the reactor spectrum neutrons in order to simulate the fission spectrum neutron effect. The vacancy defects and their local environment resulting from the shift cascade generation are examined by electron-positron annihilation (EPA) and electron paramagnetic resonance (EPR) while angular distributions of annihilation photons (URAF) are measured by a spectrometer with a 0.8 mrad resolution. The URAF is expanded into components using PAACFIT or PARAFIT routines. The angular distributions and EPR spectra are plotted. The URAF half-width increases after irradiation with both fast and reactor spectrum neutrons. An analysis of URAF parameters points toward a decrease in the positron-sensitive defect (PChD) concentration. A comparison of the electron-positron annihilation and electron paramagnetic resonance data indicates that under irradiation, deep acceptor centers are injected into the forbidden gap of graphite-like BN crystal grains. This causes a decrease in the positron-sensitive defect concentration and oxidation which is manifested by abnormal magnetic extinction. A positron-sensitive defect concentration recovery after annealing at 1,300°C is accompanied by the triboron center (TBTs) development which attests to a defect redistribution which favors populated donor levels. Figures 2; references 7: 2 Russian, 5 Western.

Higher Strength and Cold Resistance of Structural Steels Will Advance Machine Building and Construction

927D0244A Moscow STAL in Russian No 5, May 92
pp 5-9

[Article by N. P. Lyakishev and S. I. Tishayev, Institute of Metallurgy imeni Baykov, Russian Academy of Sciences]

[Abstract] Ways are suggested for increasing the strength and cold resistance of general-purpose carbon, low-alloy and alloy structural steels, which account for approximately 80 percent of all rolled steel products.

For carbon structural steels, instead of the classical heat treatment from a separate heat, combined strain and heat treatment using the heat of rolling has been shown to be more effective and to require far less energy. Combined strain and heat treatment of the common St3 brand of carbon steel increases its yield stress and cold resistance to a level equal to the requirements for hot-rolled products made of low-alloy steels of the type 09G2S. Use of this method, however, is not widespread due to economic conditions forestalling the modification and modernization of rolling mills. A more immediate solution lies in microalloying with carbonitride-forming elements. Trials on existing mills have proven that rolled products with increased strength and cold resistance can be produced from St3 steel microalloyed with vanadium, titanium and nitrogen and rolled at high temperature with complete recrystallization of austenite.

Increased strength and cold resistance for low-alloy structural steels can also be achieved, as with St3 carbon steel, by controlled rolling or combined strain and heat treatment in the mill. Also, as with St3 steel, increased strength and cold resistance are achieved in 09G2S low-alloy steel by high-temperature rolling and microalloying with carbonitride phases to produce fine-grain recrystallized austenite. Another important factor for both carbon and low-alloy steels is said to be the use of new processes in steelmaking that reduce sulfur content (0.02 percent and less) and oxide inclusions and ensure uniform chemical composition from melt to melt.

For alloy structural steels, two institutes have demonstrated good results with microalloyed steel plate with bainite structure which undergoes controlled rolling at 760-780 degrees C, and with rolled coil steel which undergoes rapid cooling after the finishing stands. Also, good prospects have been demonstrated for low-carbon alloy steels of the martensite class which when air-cooled after hot rolling possess a fine-grained structure with small amounts of bainite and residual austenite. Subsequent tempering at 600-680 degrees adds high cold resistance to high strength.

Ways of Saving Titanium in Alloying of Converter Steel

927D0244B Moscow STAL in Russian No 5, May 92
pp 28-29

[Article by V. P. Kirilenko, P. I. Yugov, V. M. Zhuravlev, V. M. Kukartsev, and F. V. Fedosenko, Central Research Institute of Ferrous Metallurgy and Novolipetsk Metallurgical Combine; UDC 669.184.244.66]

[Abstract] A process was developed for microalloying steel with titanium by reduction of titanium oxides in synthetic slag, which results in a Ti content of 0.015-0.04 percent in the finished steel. To increase the Ti content to 0.05-0.09 percent, it was necessary to determine the effect of the main process parameters on the effectiveness of titanium reduction from synthetic slag for a prescribed Ti content in the steel. In the process, synthetic slag (30-50 kg per ton of steel) containing 2.5-4.5 percent titanium oxide is poured into the ladle before the molten steel is discharged from the converter, and then aluminum is added. In the tests, 16 process parameters which vary in the course of a heat were selected to study their controllability within certain bounds. The sample comprised 80 heats.

It was determined that the introduction of titanium should be spread out and its content monitored after each addition. Considering that there is a statistically significant connection between the titanium and aluminum contents, it is advisable to develop a way of monitoring them during the process using instruments that record the degree of oxidation of the metal. Titanium's high affinity to oxygen and nitrogen requires that the metal's oxygen content not exceed 0.0015 percent and that the metal be totally shielded from contact with the air, including by vacuum treatment.

Modernization of a Converter Automated Control System

927D0244C Moscow STAL in Russian No 5, May 92
pp 30-31

[Article by S. M. Chumakov, V. D. Kuleshov, Yu. A. Romanov, G. S. Novozhilov, and V. I. Baulin, Cherepovets Metallurgical Combine and Central Research Institute of Ferrous Metallurgy; UDC 669.184.244.66:65.011.56]

[Abstract] A multiple-parameter control system which has been introduced in the converter shop of the Cherepovets Metallurgical Combine is described. The system includes a FTIAN-3 gas analyzer unit. For different types of heats for different brands of steel, conditions for conducting the heats have been plotted according to the necessary changes in oxygen consumption, position of the tuyere, and addition of material, and the information is programmed into a control computer. Algorithms of control of slag conditions are based on a dynamic assessment of the melting process which is performed

using pre-programmed oblique parameters. Such parameters may include any parameter that may be known to characterize the condition of slag in the converter.

The control system is said to have stabilized the steel-making process and improved the technical-economic indicators of converter production.

Silicon in Low-Carbon Rimmed and Semikilled Steel

927D0244D Moscow *STAL* in Russian No 5, May 92 pp 31-32

[Article by B. A. Burdonov, I. K. Ibrayev, V. P. Tsymbal, V. I. German, and V. I. Bogomyakov, Central Research Institute of Ferrous Metallurgy and Karaganda Metallurgical Combine; UDC 669.184.244]

[Abstract] In production of low-carbon rimmed and semikilled steel with silicon content of not more than 0.01-0.03 percent, the question of the residual Si concentration and its behavior in the process of deoxidation and blowing of the metal with an inert gas has special importance. Studies were performed at the converter shop of the Karaganda Metallurgical Combine. Phosphorous cast iron with 0.7-1.1 percent Si was used for steelmaking; samples were deoxidized with primary aluminum, and the Si content in samples was determined by the photometric method.

It was found that in making low-carbon steel, the residual Si concentration at the end of blowing of the metal in the converter is 0.006-0.008 percent. In low-carbon rimmed steel even small concentrations (0.006-0.010 percent) of silicon impede the start of the decarburization reaction, and consequently it is necessary to use ferromanganese with up to 1.0 percent Si for deoxidation, and the phosphorus concentration in this ferromanganese may be increased in comparison with requirements of the existing industry standard GOST 4755-80. In melting low-carbon semikilled steel the highest quality indicators are achieved with a Si content below the requirements of the industry standard GOST 1050-74. In this case the chemical composition and mechanical properties are identical to those of rimmed steel.

Higher Assimilation of Titanium in Ladle Treatment and Teeming of Corrosion-Resistant Chromium-Nickel Steel

927D0244E Moscow *STAL* in Russian No 5, May 92 pp 35-37

[Article by M. A. Filimonov, A. F. Kolosov, Yu. I. Utochkin, R. V. Kakabadze, and N. N. Perevalov, "Serp i molot" Plant and Moscow Institute of Steel and Alloys; UDC 669.14.018.8]

[Abstract] On the basis of data on different processes for preparing and teeming corrosion-resistant steel of the austenite class, studies were performed to determine the

effect of different metallurgical factors on the degree of assimilation of titanium in steel. As a result of observations of titanium's behavior during ladle treatment and teeming of corrosion-resistant steel, the extent of the effect of the steel's temperature, processes of secondary oxidation, and the metal's interaction with slag and refractory materials on assimilation of titanium was determined. This permits optimization of teeming in continuous casting machines and makes it possible to obtain a uniform Ti content over the length of continuously cast billets.

It was established that as the metal's temperature increases, the degree of assimilation of Ti decreases and instability of assimilation increases. This is associated with extra oxidation of Ti by the silica in slag and refractory linings which break down under high temperatures. As a result of argon blowing of steel in the ladle, up to 60 percent of Ti (overall loss) is removed in the form of nitrides and up to 40 percent in the form of oxides. In teeming of the steel on continuous casting machines, Ti losses amount to 30 percent, the result of secondary oxidation and interaction of the steel with the lining and slag of the intermediate ladle.

It may be concluded that higher assimilation of Ti can be achieved by using basic ladle linings, lowering the steel's temperature out of the furnace, and reducing the silicon oxide content of slag.

Production of White Synthetic Corundum Powders With Isometric Grit Shape

927D0247F Kiev *SVERKHTVERDYE MATERIALY* in Russian No 4 (79), Jul-Aug 92 pp 32-35

[Article by S.M. Uman, Yu.N. Nikitin, A.N. Bakalenko, O.A. Zaritskaya, Superhard Materials Institute at the Ukrainian Academy of Sciences, Kiev; UDC 621.921.33:666.232.2]

[Abstract] The efficiency of aluminum oxide abrasive powders and its relationship to the grit size, shape, and roughness and the advantages and shortcomings of isometric grains are discussed. An attempt is made to produce powders with an isometric grain shape and a rigid grain composition from white synthetic corundum and estimate the efficiency of using such powders in certain types of specialty tools. To this end, 25A aluminum oxide abrasive powders with a 12, 8, 6, and 4 grit commercially produced by the domestic industry with a 40-55 percent principal fraction content are used as the initial product. The integral grain size distribution of white synthetic corundum is plotted on the basis of sieve tests using a method developed at the Superhard Materials Institute (ISM). The characteristics of the A25 synthetic corundum powders with various grits are summarized; an analysis shows that powders with an elevated isometric grit concentration have a higher apparent density (by 15 to 18 percent). The efficiency of abrasive powders is estimated by grinding tests using wheels with a ceramic binder. The tests demonstrate the

expediency of using abrasive powders with an elevated concentration of isometric grains despite their high cost due to their higher machining stability and surface quality. Highly efficient machines developed at the ISM are recommended for making such abrasive powders. Figures 2; tables 2; references 5.

Optimization of Diamond and Mechanochemical Polishing of Semiconductor Wafers

927D0247G Kiev *SVERKHTVERDYIE MATERIALY* in Russian No 4 (79), Jul-Aug 92 pp 50-53

[Article by B.G. Zakharov, V.V. Rogov, P.N. Kiyko, N.I. Zabolotskaya, Kaluga Department of the Crystallography Institute at Russia's Academy of Sciences and Pulsar Scientific Research Institute; UDC 621.923.7:666.652]

[Abstract] Mechanochemical polishing (KhMP) practices are considered as complex systems of interacting factors, i.e., pressure, tool rotation speed, temperature, pH, etc., and mechanochemical polishing optimization trends are examined. The issues of increasing the stability of mechanochemical polishing and automating the process by maintaining a constant rotation speed ratio of the polishing tool and the block with semiconductor wafers glued to it are addressed and it is suggested that this parameter be used as the controlled variable. The dependence of the rotation speed ratio on pressure for diamond polishing vs. mechanochemical polishing and the dependence of the rotation speed ratio on the polishing composition viscosity and content at an 8 kPa pressure are plotted. The spread of wafer thickness values and deviation from planeness as a function of the

rotation speed ratio is examined. The findings show that at a ratio of unity, the best planeness and thickness spread are attained, thus attesting to the fact that the mechanochemical polishing process and wafer parameters can be controlled by manipulating the unit pressure and rotation speed ratio. A 0.92-1.09 speed ratio and a 4 kPa pressure are recommended for the process. Figures 5; references 2.

Standardization Principles of Complex Shaped Items Made by Powder Metallurgy Methods

937D0017G Kiev *POROSHKOVAYA METALLURGIYA* in Russian No 8 (356), Aug 92 pp 97-104

[Article by Yu.G. Dorofeyev, A.Ye. Kushchevskiy, G.G. Lvova, V.I. Miroshnikov, G.G. Serdyuk, L.I. Svistun, Institute of Materials Science Problems at the Ukrainian Academy of Sciences, Kiev; UDC 621.81:621.762]

[Abstract] The lack of world-wide standards governing the design and fabrication of items by powder metallurgy methods and the obsolescence of the standards used in the USSR until recently prompted the development of a standard and specifications for structural members produced by the most common methods used in powder metallurgy, i.e., compaction at regular temperatures and cold and hot forging. All specifications are unified and are both unique and optimal. Branch-wide specifications are incorporated in the standard which is based on an existing classification. All structural members are taken into account in developing standards for complex shaped items. The standard was approved by the USSR Gosstandart and will become effective on 1 January 1993 as GOST 29278-92. Tables 1.

Stressed State of Thin-Walled Tubes During Multicycle Deformation by Drawing

927D0246C Kiev PROBLEMY PROCHNOSTI in Russian No 6, Jun 92 (manuscript received 10 Dec 90) pp 33-38

[Article by Yu.A. Tsekhanov, Voronezh Polytechnic Institute; UDC 539.4]

[Abstract] Processing of tube blanks by multicycle drawing is considered, an experimental study having established that only the stress intensity distribution in the direction normal to the surface within the contact zone changes as a result of attendant strain hardening and that open cracks appearing on the surface are indicative of axial tensile stresses. While a mathematical solution of the stress analysis problem for tubes made of a homogeneous ideally plastic material yields only compressive stresses within the contact zone, this is evidently not consistent with the real situation and experimental data must be differently interpreted. As the basis for such an interpretation considered are the gradient of strain hardening, constant along the tube axis (x -axis), and the results of hardness tests. Such tests were performed specifically on thick-walled tubes of grade-45 carbon steel with 36 mm and 108 mm initial inside and outside diameters respectively, these tubes having been deformed in successive passes by rings with a 5° cone angle and a 1.2 mm per diameter constant interference fit. The microhardness at points within the plastic region was measured under a 200 g load, whereupon the distribution of stress intensity σ_i was calculated with the aid of the $H_{200}-\sigma_i$ calibration curve according to G.D. Del. Calculations made for successive deformation cycles, with the function $k = \sigma_i^{1/2}$ evaluated by approximation of the original σ_i readings on a rectangular grid have yielded the following stress distribution over the contact zone ($\theta = \tan^{-1} dy/dx$ - slope angle of α -slip line relative to tube x -axis x): $\sigma_x = \sigma - k \sin 2\theta$, $\sigma_y = \sigma + k \sin 2\theta$, $\tau_{xy} = k \cos 2\theta$. For a nonhomogeneous ideally plastic material then $k = by + c$, $\delta k/\delta x = 0$ and $\delta k/\delta y = b$. The system of differential equations for both α -slip and β -slip lines slip is then $d\sigma - 2k d\theta = -b dx$ and $d\sigma + 2k d\theta = b dx$. Taking into account hydrostatic compression as well as the gradient of strain hardening, the axial stress is shown to be $\sigma_x = \sigma + k_{max} = -k_{max} \pi + 16^{1/2} \Delta k_x / l_k$. Figures 4; references 5.

A Process for Producing Getter Powders for Ultrapurification of Gases

927D0248C Moscow VYSOKOCHISTYYE VESHCHESTVA in Russian No 4, Jul-Aug 92 (manuscript received 20 Mar 92) pp 108-109

[Article by M.L. Kotsar, V.M. Azhazha, M.I. Borisov, P.N. Vyugov, A.N. Ivanov, Yu.F. Korovin, S.S. Krivulya, A.M. Lakhov, A.P. Mukhachev, and V.G. Chuprinko, Chemical Technology Scientific Research Institute, Moscow; UDC 669.296+533.583]

[Abstract] The authors of this concise report have described a process for producing getter powders for use in gas ultrapurification. The getter material is an alloy of zirconium with 16 percent aluminum by mass (TsA-16). The process entails four principal stages: smelting the alloy, crushing the ingot, grinding the coarsely crushed grains, and activating the powder. The getter alloy is smelted by self-propagating calcium-thermal reduction of zirconium tetrafluoride in the presence of aluminum. The reduction melting is implemented in an argon atmosphere in graphite, steel, or copper water-cooled crucibles loaded with a total of 70 to 150 kg of the components. The result is ingots in a yield of 95 to 99 percent. The composition of the getter alloy is as follows (percent by mass): aluminum, 16 +/- 1.0; nitrogen, 0.004 to 0.02; calcium, 0.01 to 0.1; oxygen, 0.06 to 0.2; carbon, 0.003 to 0.03; and fluorine, 0.003 to 0.05. The calcium-thermal reduction results in an alloy with a more uniform chemical and phase composition than is obtained by the conventional method of producing TsA-16 by alloying zirconium and aluminum, which in turn results in a better powder. The crushing and grinding stages result in grains and powders measuring +1, -1, +0.2, and -0.2 mm. The first two fractions are used in systems for purifying inert gases and hydrogen. The powder with a grain size of -0.2 mm is pressed into products for evacuation systems. The powder is activated at a temperature of 800°C at a residual pressure of 10^{-2} Pa for 30 minutes, during which time the getter's surface is purified thanks to dissolution of the oxygen and nitrogen in its crystalline lattice and the elimination of hydrogen from the powder. The activated powder is used in portions weighing 300 g to purify inert gas. The most complete purification of inert gases on the getter is achieved when the getter is heated to 150-350°C. Table 1; reference 1: Russian

Neutron Effect and Environmental Aspects of Using Iron in Nuclear Fission and Fusion Reactors

937D0008A Moscow FIZIKA I KHIMIYA OBRABOTKI MATERIALOV in Russian No 4, Jul-Aug 92 pp 5-9

[Article by Ye.V. Demina, V.V. Ivanov, L.I. Ivashin, V.P. Kolotov, Yu.M. Platov, Moscow; UDC 669.017.3:539.1.043]

[Abstract] Increased interest in induced radioactivity in the structural materials used in nuclear fusion and fission reactors—primarily steel—is due to the fact that many structures are nearing the end of their useful life and may pose a potentially greater problem than radioactive waste disposal due to their enormous weight and dimensions. Consequently, the characteristics of radio-nuclides forming in Fe are considered from the viewpoint of modern environmental requirements using an ACTIVA computer routine which is a part of the ENDF/B database. The induced radioactivity decay kinetics in Fe in three operating reactors and in hypothetical ^{54}Fe and ^{56}Fe isotopes and natural nickel after irradiation in

water moderated water cooled power reactor and fusion reactor, respectively, are plotted and the reactions of the dominant radionuclide formation are examined. Safe concentrations of Ni, Co, and Cu impurities under varying irradiation conditions are summarized, and the conclusion is drawn that structural steels with a minimum cool down period of 50 years after 10 years of irradiation in fusion and fast neutron reactors can be created by using iron consisting of the stable natural isotope ^{56}Fe . Experimental studies demonstrate that in order to meet existing environmental requirements imposed on the nuclear power industry, direct-reduction iron produced by the Tula Chermet scientific production association and K1 iron made by Metallurgy Institute at Russia's Academy of Sciences should be used for making structural steels. Figures 2; tables 1; references 8: 7 Russian, 1 Western.

Graphite Materials' Size Behavior Under Irradiation and Their Serviceability Criterion

937D0008B Moscow FIZIKA I KHIMIYA OBRABOTKI MATERIALOV in Russian No 4, Jul-Aug 92 pp 10-17

[Article by Yu.S. Virgilyev, Moscow; UDC 621.039.532.21]

[Abstract] The relationship between the size behavior of graphite structural members of reactors under irradiation and their porosity and the effect of porosity on the compressive strength, dynamic modulus of elasticity, hardness, thermal conductivity, and electric resistivity are discussed, and the correlation between the radiation-induced growth of graphite material samples and the strength of graphite is considered. To this end, the strength and its behavior are assessed by nondestructive testing by measuring the dynamic modulus of elasticity. The dependence of the pore volume behavior on the neutron fluence in various types of reactor graphites under varying doses, the correlation of the compressive strength and dynamic elasticity modulus behavior in reactor graphite, the correlation of the electric resistivity and dynamic elasticity modulus behavior, and the dependence of the sample volume, length, and dynamic elasticity modulus behavior on the neutron fluence are plotted. An analysis of the graphite material behavior within a 320 to 1,500°C temperature range under a fluence of up to 1.6×10^{22} neutrons/cm² reveals an increase in porosity leading to a drop in the strength characteristics and performance. A decrease in the dynamic modulus of elasticity has a linear relationship to an increase in the sample volume in semilogarithmic coordinates. It is shown that a more monolithic graphite microstructure reduces the loss of strength. It is suggested that the compressive-strength-to-bending-strength ratio be used as a serviceability criterion of reactor graphite. An increase in the ratio is the best indicator of radiation-induced graphite structure degradation. Figures 8; references 11: 10 Russian, 1 Western.

Structure and Property Behavior of Carbon Fibers Under High-Temperature Neutron Irradiation

937D0008C Moscow FIZIKA I KHIMIYA OBRABOTKI MATERIALOV in Russian No 4, Jul-Aug 92 pp 18-21

[Article by Ye.N. Kurolenkin, Yu.S. Virgilyev, D.A. Kuznetsov, Moscow; UDC 662.039.21]

[Abstract] Graphitization or three-dimensional ordering—one of the most important operations in making artificial graphite—cannot be accelerated by neutron irradiation due to the structural changes in the material under the neutron flux. Consequently, the effect of neutron irradiation on the behavior of carbon material structure and properties at high temperatures typical of nuclear reactors is examined. To this end, VPR-19 carbon fibers are annealed beforehand at a 2,300, 2,700, and 3,100K temperature; the crystal lattice and crystal grain parameters as well as compressive strength, density, dynamic modulus of elasticity, and electric resistivity of the fibers are summarized; the dependence of the structural characteristics of the VPR-19 fibers on the annealing temperature and the correlation between the dynamic elasticity modulus and resistivity behavior and the volume behavior as well as between the tensile strength and fiber length behavior are plotted. The 7-10 μm thick, 30 mm long fibers are irradiated in the high-temperature channel of the VVR-SM reactor in a He atmosphere at a 2,100-2,200K temperature and a neutron fluence of 10^{20} cm⁻². The percentage change in fiber weight after irradiation is calculated and a loss of mass is noted in the sample treated at 2,300K while the most perfect sample gained weight. An analysis shows that after irradiation, the fibers display an improvement in their crystal structure: the lower the heat treatment temperature, the more noticeable the improvement. The change in the fiber resistivity and elasticity modulus are attributed to a change in the fiber density and its crystal grain diameter. The tensile strength which depends on the fiber shrinkage decreases. Carbon ablation and redistribution are noted. Figures 2; tables 2; references 8.

Investigation of Martensitic Steels' Temperature Conditions Under High-Fluence Ion Implantation

937D0008D Moscow FIZIKA I KHIMIYA OBRABOTKI MATERIALOV in Russian No 4, Jul-Aug 92 pp 22-27

[Article by V.G. Abdrashitov, V.V. Ryzhov, V.P. Sergeyev, V.P. Yanovskiy, Tomsk; UDC 537.534]

[Abstract] The effect of high-fluence ion implantation (VII) on the tribological properties of structural materials and the effect of the metal surface modification under high-dosage ion irradiation are discussed. The temperature conditions of high-fluence ion implantation carried out in a Diana unit are studied theoretically and experimentally and an attempt is made to find the optimum martensitic steel treatment conditions in these units. The implantation unit operates at a 100 kV

current with an ion pulse density of 0.1-1.0 mA/cm² and can treat a 300 cm² surface with 300 μ s pulses at a 1-50 Hz repetition frequency. The heating model of metal samples under ion irradiation is developed, and the added energy distribution in α -Fe under implantation of 100 keV tungsten ions is plotted. The heat conduction equation is derived and the surface temperature of a 1 cm thick plate as a function of the irradiation dose at various current densities and as a function of the mean current density in the saturation condition are plotted. An electron microscopy analysis reveals that in order to preserve the original martensite structure of the ShKh-15 martensitic bearing steel after high-fluence irradiation, it is necessary to adhere to the tempering conditions by manipulating the current density. A comparison of CW and pulse irradiation shows that the mean current density is the principal factor which affects the temperature conditions. The following optimum irradiation parameters are suggested for pulse-periodic Diana units at a 100 keV ion energy: a current density of 0.1 mA/cm² and a pulse repetition frequency of 50 Hz or a current density of 0.2 mA/cm² at a pulse repetition frequency of 25 Hz. Figures 5; references 12: 11 Russian, 1 Western.

Radiation-Induced Insulator Electrization for Fusion Reactor's Superconducting Magnetic System

937D0008E Moscow FIZIKA I KHIMIYA OBRABOTKI MATERIALOV in Russian No 4, Jul-Aug 92 pp 28-31

[Article by A.I. Akishin, A.I. Tyutrin, E.A. Vitoshkin, Moscow; UDC 573.226:539.1.043]

[Abstract] Electrization of such composite insulating materials as polyimide and epoxy resin with glass fiber as a dielectric filler, used in fusion reactors (TYaR) under design, under the effect of irradiation is discussed, and the factors which affect the radiation-induced electrization (RE) are addressed. Radiation-induced electrization, conductivity, and electric breakdown of composite and model insulators under varying temperature conditions of irradiation with accelerated electrons simulating the effect of γ -radiation in fusion reactors are examined, and the electric field and charge distribution and relaxation under various conditions are investigated experimentally. To this end soda lime glass and polymethylmethacrylate (PMMA) are used as model dielectrics. The dependence of the critical fluence on the electron energy in PMMA, the dependence of the critical fluence on the electron flux density in PMMA, and the electric field strength magnitude at a 1.5 mm distance from the irradiated borosilicate glass face as a function of the 2 MeV electron fluence are plotted. It is speculated that excess electric charge accumulation under irradiation is due to the particle thermalization in the forbidden gap traps. The radiation-induced and natural conductivity components of polyethylene, PMMA, and a composite material are summarized, and the PMMA breakdown under uniaxial compression and in an unloaded state are examined. The findings point toward the possibility of

electric breakdown failure of composites under radiation-induced conductivity. An analysis of the experimental results indicates that uniaxial compression of insulators to a 20 MPa pressure lowers the critical fluence at which an electric breakdown failure occurs due to the electron charge implanted in the material by irradiation. Figures 4; tables 1; references 3.

Interaction of Thin Copper Films With Sulfur Under Pulse Laser Irradiation

937D0008F Moscow FIZIKA I KHIMIYA OBRABOTKI MATERIALOV in Russian No 4, Jul-Aug 92 pp 43-45

[Article by F.A. Piskunov, A.S. Podoltsev, M.I. Markevich, Minsk; UDC 621.785.3:621.373.826:539.216.2:546.56.221]

[Abstract] The lack of consistent data on the interaction of metals with chalcogenides under laser irradiation—an important part of metal treatment by laser radiation in active media—prompted a study of copper sulfidation during the interaction of elementary sulfur with copper under laser heat treatment; the study involves a computational experiment and an examination under an electron microscope. To this end, copper sulfidation by elementary sulfur is carried out by using 1,000 angstrom thick Cu films produced by thermal vacuum deposition on a polikor substrate and then depositing a 0.5 μ m thick sulfur layer by atomizing a sulfur solution in CS₂ with subsequent drying in the air at room temperature. The bilayer structures are then exposed to 1.06 μ m YAG laser radiation for 3 s which under the experiment conditions, simulates exposure to a train of quasi-CW pulses for 1 ms. The energy density is controlled within 1.5-2.2 J/cm². The principal purpose of the experiment is to examine the interaction mechanism and process kinetics. The resulting structure is examined under an EMR-103 electron microscope and a mathematical model is developed for analyzing the temperature in the system under study in the form of a two-dimensional axisymmetric transient heat conduction equation of a multilayer medium with a distributed heat source and relevant initial and boundary value conditions. The experimental and theoretical electron diffraction patterns are summarized and analyzed, showing the presence of a single CuS phase; no additional copper oxide or lower sulfide lines are detected. The conclusion is drawn that during the interaction of this Cu and S layers under pulse laser irradiation, the chemical relaxation process is delayed, leading to the development of copper sulfide corresponding to covellite. Tables 1; references 8: 5 Russian, 3 Western.

Decomposition and Property Behavior of α -Al₂O₃ Single Crystals Under Multiple Exposure to 1.06 μ m Pulse Laser Radiation

937D0008G Moscow FIZIKA I KHIMIYA OBRABOTKI MATERIALOV in Russian No 4, Jul-Aug 92 pp 46-51

[Article by A. Chmel, S.B. Yeronko, S.A. Knyazev, A.M. Kondyrev, Yu.V. Tarasova, St. Petersburg; UDC 535.211:539.4:549.517.1]

[Abstract] The role of the corundum sample behavior under "subthreshold" laser irradiation is discussed, and a study of the effect of laser radiation on single crystal corundum which began in the May-June 1991 issue of this journal is continued. In particular, the issue of the radiation-induced change in the properties of crystals not subjected to machining is addressed. To this end, α - Al_2O_3 single crystals synthesized by Kyrospoulos's modified method developed at the Vavilov Institute are used. In addition, some crystals grown by Verneuil's method are also examined. YAG:Nd lasers are used to irradiate the corundum samples under various conditions. Infrared studies are conducted by a DS-403G diffraction spectrometer and slow electron diffraction (DME) studies are carried out using a Varian diffractometer. The natural growth surface decay probability of α - Al_2O_3 single crystals as a function of the laser radiation power density at a 120 μm effective spot diameter, the dependence of the number of pulses to failure on the electric field strength in the pulse, and infrared reflection spectra and the resulting dielectric functions before and after irradiation are plotted. An analysis of the optical strength or the number of pulses to failure shows that the spread of the surface data is smaller than that of bulk data, probably due to a smaller interaction volume in the formed case; under subthreshold ("safe") irradiation, the number of pulses to failure increases with a decrease in the power density. Under subthreshold irradiation with nanosecond pulses, the crystal structure becomes ordered while multiple exposure eventually leads to a dielectric breakdown, i.e., an accumulation of irreversible defects which competes with the structural improvement or perfection process. The role of extraneous inclusions in synthetic corundum is stressed. Figures 4; references 6: 4 Russian, 2 Western.

Reversible and Irreversible Structure Defect Formation on Silicon Surface Under Laser Pulse Effect

937D0008H Moscow FIZIKA I KHIMIYA OBRABOTKI MATERIALOV in Russian No 4, Jul-Aug 92 pp 55-58

[Article by A.F. Banishev, L.V. Novikova, Shatura; UDC 532.311.322]

[Abstract] The possibility of selectively controlling the physical and chemical characteristics of the surface layer of semiconductors and dielectrics by laser pulse irradiation and the development of a high defect concentration under irradiation prompted the development of surface modification diagnostics and a search for methods of controlling the defect formation process on the surface. To this end, single crystal silicon wafers with a (100) surface orientation are exposed to p -polarized solid state laser radiation at a 3 J energy, a 1.06 μm wavelength, and a 1.6 ms pulse duration whereby the energy density is manipulated within a 5-60 J/cm^2 range. The crystals are irradiated in the air and in an etchant. Three irradiation conditions are studied: in the air; in the air with subsequent etching; and

in the etchant. After the exposure the samples are examined under a microscope and roughness gauge. The experiments confirm that the dislocation and dislocation structure formation processes starts at lower pulse energy densities than local fusion and that local fusion craters are generated on the dislocation clustering lines. The defect formation process under millisecond laser pulses has a threshold of approximately 7.5 J/cm^2 . Under the threshold, unstable defects (dislocations) form on the surface and relax quickly after the end of the laser pulse. Above the threshold, the defects are irreversible. The findings are important for laser microtechnology applications and microelectronics. Figures 3; references 8: 7 Russian, 1 Western.

Al-Cu Alloy Zone Melting Experiment Under Normal Gravity and in Weightlessness Using Mirror-Beam Furnace' Unit

937D0008I Moscow FIZIKA I KHIMIYA OBRABOTKI MATERIALOV in Russian No 4, Jul-Aug 92 pp 64-71

[Article by S.A. Maslyayev, V.N. Pimenov, I.P. Sasinovskaya, S.Ya. Betsofen, V.L. Levtoy, V.V. Romanov, Moscow; UDC 621.315.3:669.715.3]

[Abstract] Heightened interest in zone melting (ZP) in space under zero gravity prompted an investigation into the characteristic features of zone melting and solidification of Al-Cu alloys both in earth and space experiments using mirror beam heating of samples dragged through the heating zone. To this end, alloy samples with a 2, 5, and 10 percent Cu concentration are prepared in the form of cylindrical ingots with a 40 mm length and 6 mm diameter; then the sample surface is machined by a lathe. The ingot zone melting is carried out in a mirror beam furnace which is a component of the Pion-M experimental complex. The space experiment is conducted on-board the Mir orbital space station. The CuK X-ray intensity distribution in the alloy grain after zone remelting at zero gravity and the radial and axial Cu concentration distribution of the ground- and space-melted samples are plotted. The sample speed, temperature, angular velocity, and pulling duration in three tests are summarized. An analysis of the distribution curves and alloy microstructure shows that a much more nonuniform impurity component distribution is realized under zero gravity; it is characterized by a noticeable increase in the copper concentration in the melt zone movement direction. The oxide film on the melt surface also has a significant effect under zero gravity and plays the role of a crucible which stabilizes the free surface and helps to preserve the original ingot shape. The use of the mirror beam furnace in space makes it possible to control the surface layer microstructure and component distribution along the cylinder length. Figures 7; tables 1; references 9: 7 Russian, 2 Western.

Structural Characteristics of Laser-Doped Layers on VT-6 Alloy Produced Using Boron Powder Injection

937D0008L Moscow FIZIKA I KHIMIYA OBRABOTKI MATERIALOV in Russian No 4, Jul-Aug 92 pp 152-154

[Article by A.M. Bernshteyn, Ye.M. Yandimirkin, Moscow; UDC 669.14:621.785]

[Abstract] The tendency of high-strength titanium alloys toward contact seizure and galling which hinders their use in tribological joints prompted an attempt to dope the surface of the VT-6 titanium alloy by B powder injection in order to determine the possibility of increasing its wear resistance. To this end, a 30-40 kW/cm² LT1-2 CW CO₂ is used whereby a B₄C boron carbide powder with a 20-80 μm dispersivity is injected in a He jet into the melt pool moving on the VT-6 alloy sample. An X-ray diffraction analysis of the sample surface shows that laser irradiation leads to the development of 2-2.5 mm wide and 1.5 mm deep tracks without pores or cracks with α- and β-Ti solid solutions and oxides with a cryolite crystal lattice. The surface oxidized despite the use of the shielding gas in the process. The surface is saturated with B, C, and O simultaneously as a result of laser doping. Laser remelting of the doped layer leads to a total dissolution of boron carbide particles and the development of a more uniform structure. The study confirms the expediency of laser doping for producing defect-free layers with a uniform microhardness and increasing the alloy's wear resistance by 1.5-2 times. Figures 1.

Protecting YBa₂Cu₃O_{7-δ} Ceramics From Degradation in Water Vapors

937D0008M Moscow FIZIKA I KHIMIYA OBRABOTKI MATERIALOV in Russian No 4, Jul-Aug 92 pp 154-156

[Article by V.L. Arbuzov, O.M. Bakunin, V.B. Vykhodets, B.A. Glazer, A.D. Levin, V.R. Poskrebysheva, A.F. Reyderman, I.Sh. Trakhtenberg, Yekaterinburg; UDC 620.193.2:537.312.69]

[Abstract] The urgency of protecting high-*T_c* YBa₂Cu₃O_{7-δ} superconductor ceramics from degradation under the effect of water vapors prompted an examination of the degradation mechanism and a search for ways of preventing it. The chemical reactions describing the HTSC property degradation are formulated and it is assumed that the reaction kinetics may depend of whether liquid or gaseous water attacks the ceramics. As a result, the experimental study is carried out in a bounded volume where water access is opened only after the samples are heated to the operating temperature. The dependence of the relative magnetic susceptibility on the temperature of dimethyldiethoxysilane (DMDEOS) protected and unprotected samples subjected to degradation treatment in saturated water vapors at 333K, the dependence of the critical temperature range during the transition to the superconducting state on the exposure of DMDEOS protected and unprotected samples to saturated steam at 333K, and the dependence of remanent magnetization on the external magnetic field of DMDEOS protected and unprotected samples exposed to saturated steam at 333K for four hours are plotted. Magnetic measurements are taken by two different methods. The findings indicate that under the rather stringent experimental conditions, dimethyldiethoxysilane prevents the water penetration and thus

considerably retards the Y-Ba-Cu-O HTSC ceramic degradation and it therefore a promising agent for stabilizing the HTSC properties of products operating under moist conditions. Figures 3; References: 6 Western.

Effect of High Pressure on Hard Alloy Properties

937D0011F Kiev SVERKHTVERDYIE MATERIALY in Russian No 2 (77), Mar-Apr 92 pp 77

[Article by A.V. Gerasimovich, N.M. Grigoryev]

[Abstract] The effect of pressure on the strength of the VK3 and VK6 hard alloys produced by cementing titanium carbides is examined using the modified high pressure method developed by the authors. A 1.9 GPa lateral alloy binding pressure was attained by a block of fastening rings and by sectioning the outside part of the samples. The total radial pressure in the maximum equivalent stress area reached -3.3 to -3.9 GPa and the mean hydrostatic pressure reached -4.3 to -5.3 GPa. The study demonstrates that high pressure has no effect on the difference between the limits of elasticity and yield points and the lateral binding pressure within a -1.5 to -3.9 GPa pressure range. It is suggested that the analysis procedure be used for studying the mechanical properties of high-strength and superhard materials. Figures 7; references 11.

Laser Heat Treatment of Powder Iron-Graphite Materials

937D0017F Kiev POROSHKOVAYA METALLURGIYA in Russian No 8 (356), Aug 92 pp 54-56

[Article by P.A. Vityaz, V.S. Ivashko, S.A. Chernousova, Yu.N. Zubrinovich, Belarussian Republican Scientific Production Association of Powder Metallurgy, Minsk; UDC 669.019.9:535.211]

[Abstract] The need for a wide range of antifriction powder materials capable of operating under diverse conditions and the high porosity of the iron-graphite composites traditionally used for this purpose, as well as the scarcity of data on the effect of laser heat treatment on the properties of porous powder composites, prompted a study of the effect of discrete laser treatment of powder antifriction materials on the surface layer structure and its physical and mechanical characteristics. To this end, ZhGr3Tss4 iron graphite composites produced by single compaction at 400 MPa and sintering in a continuous SK3-2140 furnace in a dissociated ammonia medium at 1,050°C with a 3 hours exposure are examined. The samples have a 15 percent porosity and a ferrographite structure with a 0.9-1.0 GPa microhardness. Discrete laser fusing is performed by a 2 kW CW CO₂ laser. An X-ray diffraction analysis is carried out in a DRON-3 diffractometer in monochromatic CuK radiation, the microstructure is examined under a Polivar optical microscope, the microhardness is measured by a Micromet-II gauge at a 0.5 N load, and the

phase and structural analysis are conducted on metallographic sections in a Protonpress unit. Friction characteristics are measured by an MT-2 friction machine. The microhardness variation in the sample depth after the laser treatment is plotted, and the structural and physical and mechanical characteristics of the composite are summarized. An analysis of the findings shows that high-speed discrete laser hardening of 3.5 mm radial bands (50 percent of the friction surface) leads to the

formation of a virtually pore-free iron graphite surface layer while the fused zone structure consists of martensite with retained austenite whose microhardness is 5-7 times higher than that of the nonfused sections. The wear resistance is higher by 3.5-4 times than that after sintering. Discrete laser treatment is the most efficient under boundary lubrication conditions when it utilizes most fully the advantages of the porous structure. Figures 2; tables 1; references 3.

Long-Term Strength and Creep of Molybdenum Alloy Welds at High Temperatures

927D0249A Kiev AVTOMATICHESKAYA SVARKA in Russian No 2 (467), Feb 92 pp 15-20

[Article by V.V. Bukhanovskiy, V.K. Kharchenko, Ye.P. Polishchuk, G.N. Alekseyenko, V.S. Kravchenko, A.V. Perepelkin, Strength Problems Institute, Electric Welding Institute imeni Ye.O. Paton, and Materials Science Institute at the Ukrainian Academy of Sciences; UDC [621.791.754'291:669.285]:[539.4+539.376]]

[Abstract] The properties of welds on the TsM-6 and TsM-10 molybdenum alloys with Zr and B or Al and B, respectively, which have a broad range of physical, mechanical, and performance characteristics are discussed, and the short-term creep and long-term strength of the weld and welded joint metal on TsM-6 and TsM-10 molybdenum alloys at temperatures of 1,500 and 1,750°C are investigated. To this end, welds are made by nonconsumable electrode helium arc welding on 1 and 2 mm thick sheets with 90 and 80 percent straining, respectively. The chemical composition and mechanical properties of the weld and welded joints are determined within a 20-2,000°C range under active static tension at a $2.2 \times 10^{-3} \text{ s}^{-1}$ rate while creep and long-term strength tests are performed in a VTU-2V unit in a vacuum. The characteristic creep curves, the dependence of the steady-state creep rate on the stress level, and long-term weld, welded joint, and base metal strength diagrams are plotted. The findings indicate that under an extended high-temperature load, the base metal, joint, and weld have an almost identical strength in the TsM-6 alloy while in the TsM-10 alloy the weld metal has a tenfold lower high-temperature resistance. Zirconium in the amount of up to 0.2 percent significantly increases the high-temperature strength, decreases anisotropy, and stabilizes the physical and mechanical properties under static loading; this makes the TsM-6 alloy preferable. In addition to the plastic deformation of the weld grains, the "grain boundary" processes play a dominant role in the failure of welded joints under long-term static loading. Figures 5; tables 3; references 22.

On Mechanism of Heat Affected Zone Crack Prevention During Hardenable Steel Welding Using Austenitic Materials

927D0249B Kiev AVTOMATICHESKAYA SVARKA in Russian No 2 (467), Feb 92 pp 21-25

[Article by Yu.N. Gotalskiy, D.P. Novikova, Electric Welding Institute imeni Ye.O. Paton at the Ukrainian Academy of Sciences; UDC [621.791.75.052:669.15.018.298]:620.192.46.001.5]

[Abstract] The mechanism of heat affected zone (ZTV) cracking during the welding of hardenable steels and methods of preventing this phenomenon as well as the mechanisms suggested for explaining it are discussed. The shortcomings of additional heating, both before, during, and after the welding operation, are outlined, the positive impact of the austenitic weld metal on preventing HAZ

cracks is noted, and a new theory is proposed for explaining HAZ cracking: the formation of martensite with a high degree of tetragonality. Thus, a new HAZ crack prevention mechanism of austenitic materials is proposed whereby a different stressed state forms during the welding of hardenable steels with austenitic materials (from that of welding with ferritic-pearlitic materials) and the martensitic transformation shifts to the area of higher temperatures where it occurs with self-tempering, thus preventing cracking. Numerous published data dealing with this issue are reviewed; the deformation degree (or the HAZ width variations) during the cooling of welds with austenite and with ferrite and pearlite and the HAZ metal hardness in hardenable steel 30KhGSN2A welded by austenitic and ferritic + pearlitic wires are plotted. An analysis of experimental data confirms the theory of different stress mechanisms and self-tempering as well as the high tetragonality degree of the martensite forming in the weld. It is noted that the above mechanism does not rule out the effect of hydrogen on HAZ cracking, but it is speculated that this effect is not dominant. Figures 6; tables 1; references 15: 13 Russian, 2 Western.

Narrow Gap Welding of Steels and Alloys Sensitive to Thermal Cycle

927D0249C Kiev AVTOMATICHESKAYA SVARKA in Russian No 2 (467), Feb 92 pp 30-32

[Article by V.I. Kulik, V.A. Kazakov, O.Ye. Ostrovskiy, Central Scientific Research Institute of Mechanical Engineering Technology, Moscow; UDC 621.791.754'29.021:669.15-194.3]

[Abstract] The shortcomings of inert gas consumable electrode arc welding for making thick-walled power units from the KhN62MTYuL or VZhL-14 nickel alloys which are sensitive to the thermal cycle and the resulting defects, such as incomplete fusion and crystallization cracks in the heat affected zone (ZTV), prompted the development of narrow gap welding with thin wires using one or two electrodes located along the longitudinal axis of the weld and installed at a small angle to the opposite edges. Yet this method is also characterized by insufficient stability and poor penetration, so it is modified by using strained wire electrodes, thus making it possible to control its position in the gap. The narrow gap welding specifications are cited, and the typical geometrical parameters of consumable strained electrode welding are depicted. During the procedure, the heat contribution is controlled by manipulating the welding current, arc voltage, and welding rate as well as the geometrical parameters. The welding head makes it possible to manipulate the curvature radius of the bent wire as a function of the metal yield point and the wire and roller diameters. The use of the new technology and equipment for making high-alloy steel units sensitive to the thermal cycle makes it possible to eliminate poor penetration and HAZ macrocracks, increase the welding material utilization, and lower labor and material outlays. Figures 2; tables 2; references 6: 5 Russian, 1 Western.

Electron Beam Control in Electron Beam Vaporization and Remelting Units

927D0249D Kiev AVTOMATICHESKAYA SVARKA
in Russian No 2 (467), Feb 92 pp 39-41

[Article by V.P. Mishchenko (deceased), Electric Welding Institute imeni Ye.O. Paton at the Ukrainian Academy of Sciences; UDC 621.793.14:621.9.048.7-52+669.187.526-52]

[Abstract] The additional requirements for the precision and speed of local automation devices being imposed by improvements in the electron beam melting and vaporization practices and a gradual transition to comprehensive computer-aided process automation prompted increased interest in automatic control of the electron beam gun emission current, focusing, and spatial position. The operating characteristics of a planar beam electron gun used in a production system are analyzed, and the principal requirements for modern electron beam control devices are formulated on this basis; in addition, the function of beam control devices is defined, and a standard electron beam control device design is suggested. In particular, the static characteristics of the P112 and P103 straight-channel electron guns is plotted, and the beam focusing behavior as a function of the beam current and filament current fluctuations is depicted. The electron guns capable of generating 10-100 kW beams are developed at the Paton Institute; the electron beam control devices consist of regulators which automatically stabilize the beam current and deflection current in two mutually perpendicular directions; the beam current controller can operate in the beam current and filament current regulation modes. In electron guns with a linear cathode, the effect of filament current fluctuations on the beam focusing can be lowered substantially by adding a signal proportionate to the instantaneous filament current to the electromagnetic deflection system. Figures 3; references 4.

Electron Beam Sweep Generators for Welding and Heat Treatment

927D0249E Kiev AVTOMATICHESKAYA SVARKA
in Russian No 2 (467), Feb 92 pp 43-45

[Article by Yu.N. Lankin, Ye.N. Bayshtuk, Electric Welding Institute imeni Ye.O. Paton at the Ukrainian Academy of Sciences; UDC 621.791.72.03-52]

[Abstract] The instant response of electron beams and their broad power control range, which make it possible to produce welding current sources with a random spatial power distribution and ensure an almost unlimited variety of welding, heat treatment, and scanning conditions, cannot be fully utilized due to the low accuracy and stability of existing analog electronic beam control devices and their complexity and limitations. This prompted the development of digital beam deflection systems where periodic voltages of a special shape are formed by a stored program or electronically. The latter possibility is considered in detail and a block diagram of an electron beam

sweep generator is cited, and its operating principle is described. The use of different electron beam variation laws and deflection coil current oscillograms are plotted. The principal element is a clock pulse oscillator which generates square pulses converted into analog voltage for the deflection coils. The variation law is ROM-controlled. A program device is developed for deflecting the beam according to a specified law, making it possible to form a surface heating source along a 1-m-long weld with a random power distribution across a 20-mm-wide weld. Tests of the new devices reveal their high reliability and efficiency in electron beam heat treatment and welding machines. The emergence of fast single-chip computers will make it possible to develop a new generation of electron beam devices. Figures 4; references 4.

Capacitor Discharge Stud Welding Under Water

927D0249F Kiev AVTOMATICHESKAYA SVARKA
in Russian No 2 (467), Feb 92 pp 50-51

[Article by D.M. Kaleko, N.A. Chvertko, L.I. Podolyan, Electric Welding Institute imeni Ye.O. Paton at the Ukrainian Academy of Sciences; UDC 621.791.75.053.97(204)]

[Abstract] The advantages of percussive capacitor discharge welding are discussed, and its specific uses for welding fasteners with a diameter of up to 8 mm to the ship hulls or other structures during repair and erection work under water are considered. An experiment to refine such welding technology conducted at the Paton Institute is described, and special equipment developed for this purpose is examined. The stages of percussive capacitor discharge welding of studs with a collar on the welded end are plotted, and a schematic diagram of the welding head of the underwater percussive capacitor discharge stud welding device is shown. The dependence of the strength of samples produced by percussive capacitor discharge welding on the hydrostatic pressure under tensile tests is measured. An analysis of underwater welding of low carbon steel studs to low carbon steel sheets and mechanical tests of various welded joints reveal that as the hydrostatic pressure increases, the mean breaking strength drops from 11 kN in the air to 1 kN at a 1 MPa pressure while the curve displays a sharp break at a 0.4-0.5 MPa pressure. Thus, the method is recommended for a depth of no more than 40-50 m. Figures 3; references 2.

Low-Temperature Vacuum Soldering Practices of Lattice Girder Structure Joints From Aluminum Alloys

927D0249G Kiev AVTOMATICHESKAYA SVARKA
in Russian No 2 (467), Feb 92 pp 52-53

[Article by V.F. Khorunov, V.F. Lapchinskiy, V.I. Shvets, V.F. Shulym, Electric Welding Institute imeni Ye.O. Paton at the Ukrainian Academy of Sciences; UDC [621.791.3.05:66.085:669.715].001.5]

[Abstract] Advances in space exploration necessitated the development of practices for making permanent joints in orbit under ultralow temperatures in a vacuum; the specific spacecraft conditions require that the new technology provide for the maximum number of operations to be performed on the ground and also be simple and not energy-intensive. An electron beam soldering system for making permanent joints of lattice girders from aluminum alloys in space in a vacuum at ultralow temperatures is proposed. The system requires the use of a low-temperature solder and

a layer which is applied to the surface beforehand and maintains its properties for a long time. The Ni, Ni-Cu, and Ni-Sn alloys are suggested, and Ni-Cu and Ni-Sn coats are tested in a lab using heating by a defocused electron beam. An analysis of the microstructure and element distribution in the welded joints in a Camebax unit and under a JSM-840 scanning electron microscope with a Link Systems analyzer shows that the microstructure is nonuniform while the weld is a tin-based matrix containing inclusions. The need for further studies is stressed. Figures 3; references 3.

Radiometric Ore Enrichment

927D0231A Moscow RAZVEDKA I OKHRANA NEDR
in Russian No 4, Apr 92 pp 11-12

[Article by V.A. Mokrousov, All-Union Institute of Mineral Raw Materials; UDC 550.835:622.7]

[Abstract] The two radiometric ore enrichment technologies, fast rough sorting into batches with different concentrations of the key components and fine separation of ore fractions preclassified with respect to lump size, are reviewed with emphasis on two new methods of separation developed at the Institute of Mineral Raw Materials. The neutron-absorption method (V.A. Mokrousov, V.A. Lilejev; 1975) facilitates extraction of clean concentrates containing 80-90 percent of the boron trioxide residing in undressed eluvial borate ores. The photoabsorption method (Ye.N. Gulin, E.G. Litvintsev; 1983) facilitates direct separation of quartz fractions on the basis of their transparency. Both methods are efficient and suitable for a large variety of respective raw material. While designed to increase the concentration of the key component in a raw mineral, they are also designed to include granulometric analysis of the raw mineral and to establish its contrast range for a determination of the appropriate radiometric treatment. Tables 1; references 7.

Quantitative Rock and Ore Analysis for Mineral Content

927D0231B Moscow RAZVEDKA I OKHRANA NEDR
in Russian No 4, Apr 92 pp 16-17

[Article by V.S. Gaydukova, V.V. Golubnichiy, and O.O. Chekinova, All-Union Institute of Mineral Raw Materials; UDC 622.7.016.34]

[Abstract] A semiautomatic rock and ore analyzer MIU-5 with computer-aided data processing only has been developed in the applied mineralogy laboratory at the Institute of Mineral Raw Materials for quantitative determination of the mineral content much better than is now possible with both MIU-1 and MIU-3 analyzers built by the Leningrad Optical-Mechanical Association since the 1970's. This analyzer operates by the optogeometrical method in either the line mode or the point mode. Measurements in the point mode yield only the phase composition. In the line mode, are measured chords of random grain intersections, which yield not only the phase composition, but also a set of structural parameters and coefficients. The analyzer has been checked for reliability and accuracy by comparison of its readings with those of the British "Magiscan-2" image analyzer. With the grid of scan lines properly selected to match the granulometric composition of a specimen, the MIU-5 instrument operating with a scan speed of 200 $\mu\text{m/s}$ or slower performs quantitative phase analysis with class-III accuracy. The accuracy can be improved by performing two or more simultaneous measurements on the same specimen. Tables 2; references 4.

Protection of Environment During Preparation of Hydrogenous Mineral Deposits for Industrial Utilization by Underground Leaching Ore Deposits in Preparation for Industrial Processing

927D0231C Moscow RAZVEDKA I OKHRANA NEDR
in Russian No 4, Apr 92 pp 26-29

[Article by K.G. Brovin, Hydrogeological Post "Krasnokholmsk Geologiya"; UDC 502:622.839.43]

[Abstract] Underground leaching of hydrogenous mineral deposits in preparation for their exploration and subsequent industrial utilization is examined from the standpoint of the effectiveness of this process in protecting the environment, this process having been designed to minimize contamination of the ground and the air basin above during the procedure. Extensive field and scale-up studies conducted for about 40 years have established that hydrogenous uranium ore deposits exist in artesian basins with up to 1 g/l impurities, low-salinity (3 g/l), or rarer high-salinity impurities with saline groundwater, ecologically most critical being regions where fresh water sources are developing. The specifics of exogenic epigenic ore formation are, moreover, an important factor to be considered in underground leaching, just as it has been in the layout of supply routes for drinkable water through oxidized rocks at least 10 km away from ore sites and upstream relative to the direction of groundwater flow. This is crucial, inasmuch as groundwater in these regions may contain up to 10-100 times more Se, 2-5 times more Ra, also much more Fe and Mn than their respective maximum permissible concentrations. Underground leaching is designed to reduce the actual concentrations of these impurities, the residual solutions then being demineralized and neutralized by purification either above ground or underground so that they become reusable. Field studies conducted for 13 years have revealed that, after leaching of uranium ore deposits, the overall salt concentration in the residual leaching solutions could over this period be decreased by a factor of four (concentration of sulfates by a factor of 3.7, concentration of nitrates by a factor of 16) with an attendant decrease of the contaminated area by a factor of 3.7 and with the pH shifting from 2 into the 3.5-8 range. An important role was found to be played by self-purification. Further laboratory tests concerning adaptation of sulfate-reducing microflora in high-acidity media have just been completed by G.A. Shugin and field tests concerning this problem are now under preparation, the object being to raise the pH so that the concentrations of contaminator elements will be lowered: Sr and Ba by a factor of four to five each, Be by a factor of 12, Na + K by a factor of 20, Mg by a factor of three, Al by a factor of 50, P by a factor of five, Ti by a factor of seven, V by a factor of 70, Cr by a factor of 11, Mn by a factor of four, Ni + Cu by a factor of six, and Th by a factor of 23, while the uranium concentration will be lowered by a factor of 50 owing to reduction during precipitation. These laboratory tests together with earlier field tests have already demonstrated the feasibility, in principle, of completely eliminating contamination of

the environment at the sources of contamination by underground leaching. References 5.

Principles of Developing and Results of Testing BS20 and BS36 Diamond Drill Bits

927D0231D Moscow RAZVEDKA I OKHRANA NEDR in Russian No 4, Apr 92 pp 29-30

[Article by V.I. Opolskiy, R.K. Bogdanov, and A.A. Bugayev, Institute of Superhard Materials; UDC 622.24.031.71]

[Abstract] Research and development concerning further improvement of impregnated bits with size AS80-AS125 synthetic diamond single crystals and with inserts of superhard diamond-base composite materials for rock blasting drills continues as an ongoing project at the Institute of Superhard Materials. Considering that such a drill operates with a small clearance between its matrix and the rock, the two key factors affecting the conditions in the contact zone are the concentration of rock particles in the sludge passing through this clearance and the dependence of the rate of matrix wear on that concentration. A theoretical analysis of the problem has revealed that less sludge will pass through this clearance as the bit is split into a larger number of segments. Two series of three drill bits each have been designed on this premise for strongest possible bonding of the bit segments to the ring in core drills with single-tube barrels 59 mm in diameter (16-segment bit), 76 mm in diameter (20-segment bit), 93 mm in diameter (24-segment bit); the BS20 bits with a 1.29 ratio and the BS36 bits with a 1.00 ratio of cutting length on the addendum circle to cutting length on the dedendum circle. Both series are designed for 20-60 m deep drilling into various slightly cracked quartzites, shales, acidic lavatic breccia, gabbros, granites, and jaspilite of 9-12 drillability class at mechanical speeds from 12 m/h to 60 m/h depending on the rock composition. Tables 2.

Drill Bits With Tungstenless Matrix for Effective Rock Blasting

927D0231E Moscow RAZVEDKA I OKHRANA NEDR in Russian No 4, Apr 92 p 32

[Article by A.M. Isonkin, Institute of Superhard Materials; UDC 622.24.051.71]

[Abstract] Drill bits of the two BA24 and BA30 types have been developed for high-speed rock drilling, their matrix being made of a tungstenless synthetic diamond base and impregnated with a special binder material featuring strong adhesion to diamond. Impregnation with such a binder material ensures excellent coverage of the working bit surface with diamond crystals and makes the binder hardness a controllable factor during the drill manufacturing process. The bits were tested and found to be suitable for drilling rocks covering a wide range of abrasiveness, up to a 3.6 index, and impact strength: the BA24 bit for drilling 43.7 m deep into Class 9.7 rocks at

a mechanical speed of 3.24 m/h (576-780 rpm) with 15-19 l/min of wash fluid, the BA30 bit 59 mm in diameter for drilling 28.8 m deep into Class 9.2 rocks (gneisses, gabbros, granite-gneiss) at a mechanical speed of 4.03 m/h (637-710 rpm) with 19-40 l/min of wash fluid. Tables 1.

The Experience of Operating a Dump Leaching Shop at the Kounradskiy Ore Mine

927D0232A Moscow TSVETNYYE METALLY in Russian No 4, Apr 92 pp 10-12

[Article by M.Yu. Radzhibayev, N.Ye. Plaksa, L.D. Sheveleva, G.I. Karavayko, M.R. Kamalov, and V.V. Bubnov, Balkhashmed Production Association, Unipromed, Microbiology Institute of the Russian Academy of Sciences, IMiO of the Kazakhstan Academy of Sciences, and Tselinnyy Mining and Chemical Combine; UDC 669.34]

[Abstract] The dump leaching shop at the Kounradskiy Ore Mine has been in operation since 1987. From 1987 through 1990 the leaching shop recovered more than 6,000 tons of copper from cementation sediment. The main result of the shop's operation has been the development of a technology that has made it possible to advance the production of copper by the method of bacterial-chemical leaching to implementation on a commercial scale. The experience that has been gained in the leaching shop has also helped accelerate the development of analogous enterprises at other mines and ore deposits. Included among the shop's equipment are four drum separators with a capacity of 300 to 320 m³/h, thus resulting in the recovery of up to 400,000 tons of copper from sediment in a season of above-zero temperatures. The experience accrued at the shop has demonstrated that the acidity of the solutions diverted to cementation should be maintained between 1.75 and 1.8 and that the scrap feed rate should be kept between 2.0 and 2.2 tons per ton of precipitated copper. The content of primary metal in the cementation sediment has been found to fluctuate from 60 to 85 percent. The cementation copper is separated from the solution by successive settling, thickening, and decantation operations. The wet product is air-dried to its finished state and then sent on for metallurgical processing at the production association or else to outside clients. During the years of the leaching shop's existence covered herein, improvements in the process made it possible to reduce the cost of obtaining 1 ton of copper in cementation sediment from 606 to 229 rubles (in 1989 prices). Analysis has indicated that the yield of copper recovered by the process may be increased dramatically (from 2,400 tons in a season to 5,000-7,000 tons yearly provided that sufficient iron scrap is available) by switching to a year-round leaching regimen incorporating jetpoint irrigation. Figure 1.

Conditioning Copper Heap Leaching Solutions From Oxidized Ore of the Kounradskiy Ore Mine Deposit

927D0252B Moscow TSVETNYYE METALLY in Russian No 4, Apr 92 pp 12-14

[Article by A.V. Shubinok, Balkhashmed Production Association; UDC 669.334.081.243]

[Abstract] In 1990 the copper heap leaching section at the Kounradskiy Ore Mine recovered the following along with 2,975 tons of sulfuric acid: 1,269 tons of copper, 554 tons of nickel, and 516 tons of arsenic. According to the process that is currently used in the shop, the copper is precipitated from the leaching solutions by iron chips. The nickel and arsenic are not recovered but are instead lost as a result of infiltration of a portion of the process solution into the soil. The iron passes into the solution in the amount of two to three tons per ton of copper, and 70 to 75 percent of the copper is extracted. According to data collected from multiyear observations, the iron concentration has been stabilized at the level of 15 to 25 g/l. A new process has been developed for conditioning copper heap leaching bypass solutions of oxidized ore from the Kounradskiy Ore Mine. The process was developed for use with the averaged solutions available for cementation at the mine, which contain 1.58 to 2.1 g/l Cu, 4.51 to 6.14 g/l Ni; 0.7 to 0.8 g/l As, 18.99 to 22.78 g/l Fe (II), and 0.8 to 1.1 g/l Fe (III) along with various background components (Na, K, NH_4 , Ca, Mg, Al, Cl, and Si). The metal ions are sorbed by KU sulfo cation exchanger in a steel column with a layer height of H-form sorbent of four m. At the outlet from the ion exchange layer, H-cationized filtrate containing 41.1 to 53.3 g/l H_2SO_4 and 0.6 to 0.7 g/l As is collected. The arsenic is precipitated by hydrogen sulfide in a leaktight intermittent-type reactor, and the sediment is separated out and then dried and prepared either for burial or processing into antiseptic preparations. After the arsenic sulfide solution has been separated from it, the mother liquor, which has a residual content of 0.06-0.07 g/l As, is returned to the leaching stage. The residual hydrogen sulfide is removed by blasting with air. Solutions of 300 to 315 g/l H_2SO_4 are used for desorption of the metal from the cation exchanger. The eluate at the outlet from the column is separated into three nearly equal fractions that are then processed into green vitriol suitable for use in agriculture. Further processing results in yellow and red pigment corresponding to the condition required for merchant products. The mother liquor remaining after extraction of the green vitriol is returned to the starting stock of mother liquor for repeated use. Tests of the new process have confirmed its feasibility, and the test results were used as a basis for developing regulations for designing movable and stationary ion-exchange units for periodic (once yearly) neutralization and conditioning of solutions. It is anticipated that besides improving the ecological situation at the Kounradskiy Ore Mine, the new conditioning equipment and process will result in a

yearly economic gain of 850,000 rubles as a result of the green vitriol produced. Figures 2, table 1; references 4: Russian

Change in the Material Composition of Balanced Copper-Porphyrific Ores of the Dumps of the Kounradskiy Ore Mine During the Leaching Process

927D0252C Moscow TSVETNYYE METALLY in Russian No 4, Apr 92 pp 14-17

[Article by S.I. Druzhinina, L.D. Sheveleva, D.P. Khramenkova, Yu.P. Krayeva, and M.R. Kamalov, Unipromed, Geology and Geochemistry Institute, Ural Department, Russian Academy of Sciences, Metallurgy and Enrichment Institute, Kazakhstan Academy of Sciences; UDC 622.791]

[Abstract] The dumps of the eastern group of balanced copper-porphyrific ores of the Kounradskiy Ore Mine are the basis of the first phase of the pilot-commercial bacterial-chemical leaching section. They were formed during the period between 1940 and 1965 during stripping operations and direct working of the ore body by selective recovery. Oxidized and depleted sulfide ore that does not lend itself to flotation has also found its way into the dumps. The ore in the dumps is from different sections of the open-pit mine and has undergone extensive weathering. A series of studies were performed to determine the change in the material composition of the balanced copper-porphyrific ores in the dump during the course of the natural leaching and weathering to which they have been exposed since the dump was originally formed. The mineralogic, petrographic, and x-ray structural analyses performed on samples of the balanced ores from the No. 9 and No. 10 dumps established that the ore-forming minerals present in the dumps have undergone only a slight degree of transformation and have, by and large, maintained properties conducive to infiltration and filtration of process solutions through the dumps' mass. The qualitative and quantitative changes that have occurred in the ore minerals illustrate the stage of the bacterial-chemical mechanism of the leaching out of copper. It should be noted, however, that the copper sulfides that have been finely and dispersely embedded in dense rock that remains inert when exposed to sulfuric acid solutions have been left largely unchanged and are thus not likely to undergo bacterial-chemical transformation. In view of these findings, further studies were conducted to determine the possibility of regeneration and purification of the circulating solution on the surface and in the body of the leached block. The researchers concluded that removing the surface layer in which nickel and arsenic impurities accumulate and renewing the sedimented layer when necessary by sending off the pulverized rock mass or clay-sand mixture might be an effective way of regulating the depth of purification of the circulating solutions in the process of bacterial-chemical leaching under the

specific operating conditions of the Balkhashmed Production Association. Figures 4, table 1; references 4: 2 Russian, 2 Western.

The Potentials of Geotechnology in Processing Oxidized Copper Ores

927D0252D Moscow TSVETNYYE METALLY in Russian No 4, Apr 92 pp 17-20

[Article by G.A. Pavlichenko, B.M. Rogov, and D.A. Pirmagomedov, Unipromed; UDC 669.334.12]

[Abstract] In view of the increasing need for nonferrous metals, a study was conducted to determine the possibility of processing clayey oxidized ores from the Kalmarkyrskiy and Boshchekulskiy deposits by means of geotechnology methods. (The Kalmarkyrskiy contains deposits with a 0.3-0.4 percent copper content along with agrillaceous minerals, and the Boshchekulskiy deposit contains copper in a concentration of 0.05 to 0.3 percent). Samples of natural atacaminte were taken from both deposits for the studies. The samples contained the following (percent): Cu, 50.31; SiO₂, 2.18; CaO, 0.116; MgO, 0.35; Al₂O₃, 4.24; and Cl, 16.0. The tests were performed on an experimental unit described elsewhere based on the rotating disk specimen method (duration, 6 hours; volume of sulfuric acid solution, 2 dm³; volume of samples used for the analysis, 0.025 dm³). The stirring intensity was varied from 20.9 to 104.6 radians/s, the temperature was varied from 283 to 303 K, and the acid concentration was varied from 5 to 400 g/dm³. The studies performed established that geotechnology-based methods are not effective for use in processing the ores from the Boshchekulskiy mines because of the large amounts of acid required and because of the intensive decomposition of the rock component. Geotechnology-based techniques were, however, found to be suitable for use with the Kalmarkyrskiy mine ores. Seasonal tests conducted over the course of three years established that the type of ore present in the Kalmarkyrskiy mines could be processed at a filtration rate of 0.5 m/d and with a concentration of productive element between 0.35 and 0.5 g/dm³. Figures 4; references 4: Russian

Mechanism of the Bacterial-Chemical Leaching of Pyritic Ores

927D0252E Moscow TSVETNYYE METALLY in Russian No 4, Apr 92 pp 20-23

[Article by L.D. Sheveleva, O.B. Krushkol, V.V. Abakumov, D.P. Khramenkova, M.P. Petrov, and L.S. Smolskaya, Unipromet and Mekhanobr; UDC 669.334:622.34]

[Abstract] In an effort to learn more about the pyritic ores present in the Ural region, the authors of the study reported herein studied the mechanism of bacterial-chemical leaching of pyritic ores. Specifically, they study the degree to which copper passes from ore samples prepared in the form of disks and into a solution per unit

of time. The leaching was conducted both with and without the use of a biomass that had been specially prepared in a KB-8M4 electrochemical propagator designed at the Biophysics Institute of the Siberian Department of the USSR Academy of Sciences. The changes in the concentration of copper, *Th. fer.* cells, and the pH of the solution over time were monitored. The starting parameters were as follows: volume of solution, 2 dm³; pH = 1.9 to 2.0; Fe (II), 4.5 g/dm³; Fe (III), 0.5 g/dm³; temperature, 305 K; disk specimen rotation speed, 7.91 radians^{1/2}/s^{1/2}; and air flow rate for purposes of aeration, 15 dm³/dm³ solution. The concentration of *Th. fer.* cells was varied at 0, 10⁴, and 10⁸ cells/cm³. Pyrite was the predominant mineral in the ore specimens (from 47 to 57 percent in samples from the Blyavinskiy and Karabashskiy deposits and from 80 to 85 percent in the specimens from the Degtyarskiy deposits). Chalcopyrite was present in amounts ranging from 10 to 15 percent. The studies performed established that the intensity at which metals are leached from pyritic ores of the Ural region are commensurate with the rates obtained for the copper of copper-porphyrific, mixed, and even oxide ore deposits. The ores of the Karabashskiy deposit were found to be the most predisposed to processes of copper and zinc leaching. The relatively poor ore samples from the Degtyarskiy and Safyanofskiy deposits were found to be especially receptive to the intensifying effect of *Th. fer.* Specifically, the use of *Th. fer.* resulted in a tripling of the yield as compared with the yield from purely chemical leaching over a 120-day period. The use of *Th. fer.* proved less effective with the samples from the Blyavinskiy deposit and even less effective with the samples from the Karabashskiy deposit. The studies further established that passivation of the surface of the dissolved minerals by products of an active bacterial-chemical mechanism may be eliminated by varying the concentration of acid to dissolve the blocking formations. Figures 3, tables 5; references 8: 7 Russian, 1 Western.

Preparing an Ore Mass for Underground Copper Leaching by the Hole-Slit Method

927D0252F Moscow TSVETNYYE METALLY in Russian No 4, Apr 92 pp 23-25

[Article by B.V. Dyakov, S.N. Popov, Yu.S. Chekhanov, I.V. Brezgulevskiy, V.I. Fominykh, and A.A. Abroskin, Mining Institute, Siberian Department, Russian Academy of Sciences, Unipromed, Blyavinskiy Ore Mine; UDC 669.334]

[Abstract] Geotechnological techniques appear to be a promising way of meeting the ever-increasing demand for nonferrous and noble metals in the face of the increasing difficulty of recovering metals of suitable quality or in suitable quantity. In an effort to solve this dilemma, the authors of the study reported herein worked to develop a new method of preparing an ore mass for underground copper leaching by the hole-slit method. The study was a joint multiyear effort of researchers from the Unipromed, Mining Institute of the

Siberian Department of the Russian Academy of Sciences, Applied Geophysics Special Design Office of the Siberian Department of the Russian Academy of Sciences, and the Mednogorsk Copper and Sulfur Combine. The process developed was designed for use in preparing blocks of poorly permeable ores with a tendency toward suffusion due to underground workings by the hole-slit. The new process entails the use of head leaching with acidified solutions, with periodic forced aeration of the ore mass, and with the possibility of changing the direction of the motion of the productive solutions in the block. After a given block has been thus prepared, it is worked in one of two ways depending on the results of the preparation process. If rich productive solutions form during the head leaching and suffusion proceeds so intensively as to result in filtration of the working solution throughout the entire volume of the ore body, the block is worked in a head leaching regimen. Otherwise, the block is worked in accordance with a plan developed at the Unipromed Institute. In accordance with the said plan, explosives are used to crush the ore into a compensating space, and leaching is implemented in an infiltration regimen. A plan for testing the new head leaching technique was developed for use at the Blyavisnkiy Ore Mine. A technical and economic comparison of the two methods of working the ore block after the initial head leaching established that, assuming identical costs of the processes of processing productive solutions to the copper cementation stage, the costs of preparing a block by using the slit-hole method and head leaching are less (by a factor of 2.4) than the costs incurred when the base technology of preparing the block by creating a compensating space is used. Figure 1; references 4: Russian

The Possibility of Geotechnological Extraction of Molybdenum Based on Hypochlorite and Sulfuric Acid Leaching

927D0252A Moscow TSVETNYYE METALLY in Russian No 4, Apr 92 pp 25-27

[Article by G.M. Yashina, Unipromed; UDC 669.283]

[Abstract] At the present time, more than 60 percent of all molybdenum is obtained as a by-product of copper production. The large stores of unconditioned molybdenum ores that do not lend themselves to processing by conventional schemes at domestic enterprises have necessitated the development of new processes for obtaining molybdenum from sulfide, oxidized, and mixed (sulfide-oxide) ores. One benefit of incorporating geotechnology techniques into the molybdenum recovery and production process is that such methods would permit the selective transfer of molybdenum into soluble compounds so that it could be subsequently extracted by the ion-exchange method to produce commercial salts. The ore mine Vostochnyy Kounrad is one ore mine in the former Soviet Union where effective geotechnological recovery of molybdenum is possible. Preliminary analysis has demonstrated that sodium hypochlorite is the most effective alkaline solution for

use as a reagent in molybdenum extraction. The advantages of sodium hypochlorite include its high selectivity, ability to become activated at low temperatures and concentrations, and ease of regeneration by electrolyte methods. In view of these facts, the Unipromed, VNI-IKhT [not further identified], and Balkhshmed Production Association have developed a process for leaching molybdenum. The process, which was tested under laboratory conditions (on percolator models), entails sorption separation of molybdenum (in columns with a barrier layer based on AM-P anion exchanger) from hypochlorite solutions. The new process results in a higher once-through extraction of molybdenum (62 percent as compared with 45 percent when the conventional process of recovery and transport to an enrichment plant for processing is used) and, as a result, in lower capital and operating costs. The new process also requires less land use and, hence, less extensive land reclamation operations. Furthermore, the productive hypochlorite solutions may be regenerated by electrolysis after the molybdenum-containing ore has been leached out. The drawbacks of the new process include the need to recycle or neutralize the spent hypochlorite solutions, the higher requirements of the process regarding the material used to manufacture the process equipment, more stringent labor safety requirements, and the fact that hypochlorite is harsher on the environment than sulfuric acid. The new hypochlorite-based process is nevertheless superior to sulfuric acid leaching because of the former's higher yields and quicker time until maximum extraction process parameters are reached. Researchers are currently in the process of completing the contractor design of a pilot unit for use in testing the finalized version of the new hypochlorite-based extraction process and to assess the real prospects of using the new process at the Severnyy Kounrad deposit. Figure 1, table 1; references 10: 9 Russian, 1 Western.

A Biohydrometallurgical Process for Processing Gold-Pyrite Concentrate

927D0252H Moscow TSVETNYYE METALLY in Russian No 4, Apr 92 pp 27-29

[Article by R.Ya. Aslanukov, G.V. Sedelnikova, T.A. Pivovarova, G.I. Karavayko, O.B. Voronina, and S.B. Makarov, Microbiology Institute, Russian Academy of Sciences, and Central Scientific Research Institute for Geological Prospecting of Nonferrous and Noble Metals; UDC 669.213]

[Abstract] A study was conducted to determine the role of *Th. fer.* in a new process for extracting noble metals from gold-pyrite concentrates that includes leaching and cyanidation. The studies were performed on concentrate from a Central Asian deposit that contained 39.2 g/t Au and 27.4 g/t Ag along with the following (percent): 18 SiO₂; 5.5 Al₂O₃; 2.4 CaO; 1.5 MgO; 2.0 K₂O; 1.5 Na₂O; 1.5 C (organic); 28.9 Fe_{tot}; 0.3 Σ (Ni, Zn, Pb, Cu, Co); and 30 S_{tot}. From the standpoint of mineral composition, the concentrate consisted primarily of pyrite (56.6 percent). The gold was present in the concentrate in its

elemental stage, and the silver was present in tetrahedrite form. The tests of the new biohydrometallurgical process were conducted at the Tula Affiliate of the Central Scientific Research Institute for Geological Prospecting of Nonferrous and Noble Metals. A test unit operating in a continuous mode was used to process 2.5 tons of concentrate at a rate of 100 kg/d. A *Th. fer.* culture was adapted to the concentrate under conditions of continuous culturing at a temperature of 28 to 35° with a liquid:solid ratio of 1:5. At the outset of the process the pH was maintained between 2.0 and 2.2 and later dropped to 1.5-1.6 by adding lime milk. The concentration of bacterial biomass in the pulp increased sharply during the first three days of the leaching process, after which it changed only slightly. About 40 percent of the bacterial cells were in the solid phase regardless of the concentrate oxidation time. After 110 hours of leaching, the concentration of sulfur sulfide in the concentrate decreased from 31.5 percent to 19.2 percent, resulting in a degree of pyrite oxidation amounting to 39 percent. Cyanidation resulted in the extraction of 94.2 percent of the gold and 91.3 percent of the silver contained in the concentrate. The completeness of the extraction of noble metals was found to be dictated not only by the degree of pyrite oxidation and destruction of its crystalline lattice, but also by the distinctive features of the association of the particles of the noble metals with the pyrite. Microbiological studies of the products of the bacterial leaching process revealed that the pyrite oxidation process developed along the grains' surface, in cracks, around inclusions, and along mineral aggregate boundaries. The new biohydrometallurgical process was thus confirmed to be effective on a semicommercial scale and to be promising for use in processing pyrite concentrates with finely embedded gold. Figures 5; references 5: 2 Russian, 3 Western.

The Use of Bioactive Wastes From Antibiotics Production in Hydrometallurgy

927D0252I Moscow TSVETNYYE METALLY in Russian
No 4, Apr 92 pp

[Article by B.N. Laskorin, G.I. Karavayko, T.V. Molchanova, O.P. Polyakova, V.V. Rodionov, B.N. Sharapov, L.I. Vodolazov, N.A. Sharapova, and L.V. Konopleva, VNIKhT and Microbiology Institute, Russian Academy of Sciences; UDC 66.081+661.863+615.33]

[Abstract] The authors of this communication have previously demonstrated the possibility and promise of using biomass wastes from antibiotics production as a sorbent for uranium and selected rare earth elements. Neomycin and erythromycin were shown to have the best sorption properties. The present study examines the possibility of using bioactive mass from neomycin and lincomycin production as sorbents for extracting selected heavy metals. The biomass was dried at a temperature of 100 to 105° and then used in powder form. Separate solutions containing 2 g/l copper with a pH of 1.5 and 4.0, 1 g/l chromium with a pH of 2.0 and sulfuric acid concentration of 50 g/l, and 1 g/l iron with a pH of 2 and a 5 N concentration of sulfuric, nitric,

hydrochloric, and phosphoric acids were used to determine the biomass' sorption characteristics. The experiments were performed under static conditions with stirring at a sorbent:solution ratio (mass) of 1:250 for the copper and 1:1,000 for the chromium and iron. The phases were kept in contact with one another for 24 hours in all of the experiments performed. The biomasses from the production of the different antibiotics were found to differ greatly from one another with respect to their ability to absorb iron, copper, and chromium. The biomass from the production of lincomycin proved best at absorbing copper at a pH of 1.5, and the biomass from neomycin production proved best at absorbing copper from a solution with a pH of 4.0. Biomass from lincomycin production was best at absorbing chromium at a pH of 2. The biomass from neomycin production also proved effective at absorbing chromium in a sulfuric acid medium. The ion absorption studies conducted demonstrated that biomass origin is not the sole decisive factor but that the specific anions used are also important. Sulfate ions were found to completely suppress iron sorption on biomass from lincomycin production, whereas the same bioactive wastes were found to demonstrate maximum sorption properties in phosphoric acid solutions. Nitrate ions facilitated sorption of iron on bioactive mass from neomycin production but greatly suppressed the extraction of metal on wastes from lincomycin production. Overall, the wastes from neomycin production proved most interesting from the standpoint of their sorption properties. pH was also demonstrated to be important for sorption, with sorption dropping by an order of magnitude at a pH of 1. Further studies were conducted to assess the abilities of the two types of bioactive wastes to desorb three pairs of elements, i.e., yttrium-cerium, yttrium-antimony, and yttrium-erbium, by sulfuric, nitric, and nitrate-nitric acid solutions containing bioactive wastes from the production of lincomycin or kanamycin. When nitric acid or nitrate-nitric acid solutions with additives of the said bioactive wastes were used with the pair yttrium-cerium, the degree of cerium desorption increased dramatically while desorption of yttrium was simultaneously suppressed. The biomass additives resulted in the desorption of primarily antimony from the antimony-yttrium pair tested and primarily yttrium from the erbium-yttrium pair. The basic premise of using bioactive wastes from the production of antibiotics to extract selected rare earth metals was thus confirmed to be feasible. Tables 2; references 6: 5 Russian, 1 Western.

Protecting Underground Waters During the Geotechnological Processing of Nonferrous Metal Ores

927D0252J Moscow TSVETNYYE METALLY in Russian
No 4, Apr 92 pp 32-34

[Article by A.M. Roygbaum, L.D. Sheveleva, V.I. Menzhulin, and S.K. Aytkulov, Unipromed, Karaganda GIZ [not further identified], and Balkhashmed Production Association; UDC 622.7:669.34]

[Abstract] According to estimates made by Yugoslav specialists, the yearly losses of copper from ore dumps owing to climate factors range from 2 to 6 percent.

Geotechnological methods of processing crude minerals is both a way of reducing these losses and a way of helping to improve the ecological situation in the vicinity of ore recovery enterprises. At the same time, however, both heap and underground leaching necessitate the more stringent requirements regarding preliminary operations and selection of rational engineering solutions. In view of these facts, the Balkhash department of the Karaganda GIIZ, the institute Unipromed, and the Balkhashmed Production Association have worked to develop ways of protecting underground waters in and around the Kounradskiy deposit during the geotechnological processing of nonferrous metal ores. This research work has included the following: a study of the spatial structure and flow structure of the underground waters; an investigation of the dynamics of the level and chemical compositions of the underground waters; an estimate of the aquifers' filtration and migration parameters; a compilation of the affected area's water balance; and the discovery of sources of contamination and sections where process solutions are discharged into aquifers (including a study of the scales and dynamics of pollution of the underground waters). On the basis of research conducted to predict the change in

the concentrations of nickel and copper in the aquifer in the 5-year period following the beginning of systematic leaching, the following were formulated as the top-priority environmental protection measures for the area: create a drainage canal 800 m long to intercept the flood waters that are the main source feeding the aquifer; create three water-impermeable curtains (barrages) in areas with elevated permeability; eliminate those ponds located in the group that have elevated filtration parameters and that are not used in the process; and monitor the underground waters along the developing network of observation holes. A 3-year cycle of observations demonstrated that thanks to the self-cleansing of the underground waters and the implementation of environmental protection measures during the rhythmic working of the study sector, the propagation of contamination of the waters by microelements contained in the process solutions should not extend beyond the confines of the industrial site for a rather long period of time. Secondary measures are now being developed that will further protect the area in question in the event that extreme conditions should develop. Efforts are now under way to develop programs to ensure the environmental safety of new mines, including the Boshchekulskiy ore mine.

Decreasing Discharges When Emptying Dust Precipitators

937D0020D Moscow TSVETNYYE METALLY in Russian No 8, Aug 92 pp 26-27

[Article by A.M. Kasimov, Ye.S. Makarenko, A.L. Faynshteyn, Energostal Scientific Production Association; UDC 669.2/.8.015.7.074]

[Abstract] The shortcomings of the dust discharge auger conveyors, e.g., the body and part attrition by abrasive and hot dust, the need to service the device with moving parts, and environmental contamination, prompted a study of the possibility of replacing auger conveyors with sloping gas discharge tubes which, however, are characterized by dust releases into the atmosphere. As a result, variable-diameter gas descent tubes with a constriction are developed at the Energostal Scientific Production Association in order to decrease the gas discharges from the dust precipitators when they are being emptied. The averaged results of the gas suppression efficiency of the dust precipitator discharge through constant- and variable-diameter tubes are summarized showing the advantages of the latter system; in particular, the dust moistening uniformity is increased considerably. Figures 1; tables 1; references 3.

Water Defluorination Electrocoagulation Unit

937D0020E Moscow TSVETNYYE METALLY in Russian No 8, Aug 92 pp 32-34

[Article by B.L. Prisyazhnyuk, Chisinau State Teachers Institute; UDC 628.16.069]

[Abstract] The difficulty of defluorination of waste and natural water with a low fluorine content (3-10 mg/l), especially since fluorine is capable of forming stable complex compounds with some metals, and the shortcomings of electrolytic defluorination prompted the development of electrocoagulators with soluble and insoluble electrode systems. An electrocoagulation unit with a capacity of 3 m³/h with an AL 9 aluminum alloy anode and a graphite cathode and its operating principle are described, and its schematic diagram is cited. To determine the optimum operating parameters, the unit is tested by removing excess fluorine in the 4-15 mg/l amount from natural water. The results of defluorination

as a function of the cathode current density and water pH, process duration and water pH, and cathode density and treatment duration are summarized. The results of computer processing of test data resulting in mathematical models of defluorination are presented. An analysis of the regression equations shows that the degree of defluorination depends on the amount of Al ions passed to the solution and the electrolysis duration. The specific electric power demand for servicing the unit is 2.6 kWh per cubic meter and the graphite and aluminum electrode life is 270 and 160 days, respectively. The optimum operating condition is identified: a cathode current density of 6-8 mA/cm² and an 8-10 treatment duration. Figures 1; tables 6; references 6.

Investigation of Municipal Sewer Sediment Dewatering Using Titanium Production Waste

937D0020F Moscow TSVETNYYE METALLY in Russian No 8, Aug 92 pp 44-46

[Article by V.S. Proshkin, N.N. Stremilova, Titanium Institute; UDC 669.215.054.79+628.4]

[Abstract] The urgency of dewatering municipal waste water and sewer sediments and an increasing volume of waste being generated today necessitated a comparative study of various dewatering methods, including reagent treatment and centrifuging using flocculants. The high cost of flocculants prompted the use of industrial waste and byproducts for this purpose, particularly chloride waste of titanium production. The chemical composition of chloride waste from the Zaporozhye Titanium-Magnesium Smeltery (ZTMK) used as coagulants in waste water treatment at the Navaginsk Treatment Facility in Sochi, the results of lab tests of centrifuged sediments treated with ZTMG waste, and the outcome of centrifuging tests of treatment facility sediments with chloride waste products are summarized. An analysis confirms the efficacy of using chloride waste of titanium production. Given 8 percent chloride and 16 percent lime relative to the dry sediment, the following treatment results are obtained: a suspended matter concentration of 2 g/l vs 12.3 in the initial sediment; a sludge moisture content of 61.25 percent vs. the initial content; and a centrifuging efficiency of 94 percent vs. 63.2 percent without the coagulant. Tables 3; references 1.

END OF

FICHE

DATE FILMED

22 December 1992

31/3